AD NUMBER

AD815389

NEW LIMITATION CHANGE

TO

Approved for public release, distribution unlimited

FROM

Distribution authorized to U.S. Gov't. agencies and their contractors; Administrative/Operational Use; Mar 1967. Other requests shall be referred to Air Force Flight Dynamics Lab., Wright-Patterson AFB, OH 45433.

AUTHORITY

AFFDL ltr, 14 Aug 1974

AFFDL-TR-66-64

OPTIMUM CONTROL OF AIR TO SURFACE MISSILES

L. LEISTIKOW, R. D. McCORKLE, R. W. RISHEL, et al

THE BOEING COMPANY

TECHNICAL REPORT AFFDL-TR-66-64

MARCH 1967

AIR FORCE FLIGHT DYNAMICS LABORATORY
RESEARCH AND TECHNOLOGY DIVISION
AIR FORCE SYSTEMS COMMAND
WRIGHT-PATTERSON AIR FORCE BASE, OHIO

NOTICES

When Government drawings, specifications, or other data are used for any purpose other than in connection with a definitely related Government procurement operation, the United States Government thereby incurs no responsibility nor any obligation whatsoever; and the fact that the Government may have formulated, furnished, or in any way supplied the said drawings, specifications, or other data, is not to be regarded by implication or otherwise as in any manner licensing the holder or any other person or corporation, or conveying any rights or permission to manufacture, use, or sell any patented invention that may in any way be related thereto.

Copies of this report should not be returned to the Research and Technology Division unless return is required by security considerations, contractual obligations, or notice on a specific document.

200 - April 1967 - CO192 - 30-708

PAGES _____

ARE

MISSING

IN

ORIGINAL

DOCUMENT

AFFDL-TR-66-64

OPTIMUM CONTROL OF AIR TO SURFACE MISSILES

L. LEISTIKOW, R. D. McCORKLE, R. W. RISHEL, et al

FOREWORD

This final report, which concludes the work on Contract AF33(615)-2409, was prepared by The Boeing Company, Aerospace Group, Seattle, Washington, under Project No. 8219, Task No. 821904, "Flight Control Optimization Techniques." This volume of the report contains the program description and results. The classified missile configuration details which were used in the programs and a limited amount of homing sensor state-of-the-art details are available through the Air Force project office, with proper justification. The work was administered under the direction of the Flight Control Division, AF Flight Dynamics Laboratory, Research and Technology Division. Mr. Frank George was the project engineer for the laboratory.

The study presented here began in March 1965, was concluded in March 1966, and represents the joint efforts of the Missiles Flight Technology and Computing and Analysis Departments. The program was under the direction of Messrs. Richard D. McCorkle and LaVern E. Leistikow of the Flight Technology Flight Controls Group. The principal investigator was Dr. Raymond W. Rishel of Computing and Analysis, Mathematical Analysis Staff, who conducted the linearized guidance comparison and the implementation of the optimal guidance law. The normal acceleration autopilot studies and the analog guidance simulations were conducted by Messrs. Joseph M. Hall and W. Dean Clingman.

This report was submitted by the authors September 1966.

This technical report has been reviewed and is approved.

C. B. Westbrook
Chief, Control Criteria Branch
Flight Control Division
AF Flight Dynamics Laboratory

ABSTRACT

Design guidelines were developed to provide a basis for conducting design trades for a homing type air to surface missile (ASM) with high terminal accuracy. Three basic homing guidance concepts: proportional, pursuit, and optimal guidance were evaluated on the basis of impact error. Two nominal trajectories were investigated.

An optimal guidance law was developed for an ASM with realistic aerodynamic and sensor characteristics. This guidance law was based on the use of a Kalman filter to obtain best estimates of the ASM state variable errors, and a control criterion that minimizes the sum of the mean square impact error and the integral of a quadratic form of the autopilot control variables.

A linearized differential equation program that computed the mean square impact error in the form of a covariance matrix deviation perpendicular to the nominal trajectory was used for comparison of the guidance laws.

A normal acceleration autopilot was designed to meet the mission requirements, and advanced bistable controller techniques were applied to obtain a quasiadaptive autopilot that required no gain changes throughout the ASM midcourse and terminal phases.

A limited state-of-the-art survey was conducted of homing and inertial sensors and on-board digital computers suitable for a homing ASM.

CONTENTS

FIGURES

FIGURES (Cont.)

FIGURES (Cont.)

TABLES

DEFINITION OF SYMBOLS

A_f	ft^2	Missile control fin reference area
$A_1(t)$, $A_X(t)$		Coefficients of linearized LOS angles
A^T		The transpose of a Matrix A
$B_1(t)$, $B_2(t)$, $B_3(t)$		Coefficients of linearized LOS angles
B_{BS}		Autopilot bistable loop gain
C		Matrix in Section V
C_N		Aerodynamic normal force coefficient
$C_{N\alpha}$		Normal force coefficient slope
$C_{N\alpha^3}$		Nonlinear normal force coefficient derivative
$C_{N\delta}$		Fin normal force coefficient effectiveness
C_L		Aerodynamic lift coefficient
C_D		Aerodynamic drag coefficient
C_1, C_2, C_3, C_4		Integration constants
		Autopilot normal acceleration constant in the bistable relay drive circuit
$C_{\dot{\theta}}$		Autopilot missile body angle time rate of change constant in the bistable relay drive circuit
D (α, V, Z)	lb	Drag
D(t), F(t), G(t), R(t), S(t)		Matrices of influence coefficients of linearized ASM equations
E		Operation of taking the expected value of a quantity
F_N		Guidance equation normal force command
GHz	10^9 cycles/sec	Gigahertz
H(t)		Matrix relating linearized LOS angles with position deviations and LOS biases
I	ft-lb-sec^2	Missile moment of inertia
K_1, K_2		Proportional and pursuit guidance gains
K(t)		Weighting matrix of optimal filter

$K_6(t)$		Submatrix of Matrix K(t)
K_I		Integral gain constant in autopilot compensation circuit
$K_{\ddot{z}}$		Gain in autopilot normal acceleration loop
$K_{\dot{\theta}}$		Gain in autopilot missile body angle time rate of change loop
L (α, V, Z)	lb	Lift
M		Matrix of quatratic form in the control variables involved in performance criteria
M_α	ft-lb	Missile pitching moment
N_1, N_2	deg	Noises in LOS angles measurements
N_δ	lb/deg	Fin normal force effectiveness
P		Transfer function poles
R_{sl}		Slant range to target
R		Matrix of scale factor and drift errors of the inertial platform
R(t)		Covariance matrix of N_1 and N_2 (Note: R(t) has been used in two different ways, the meaning will be clear from the context)
$\hat{s}$		Estimate of quantity s
$\bar{S}$	ft^2	Missile body reference area
U		Matrix involved in the optimal feedback control law
V	ft/sec	Velocity of missile
V_s	ft/sec	Velocity of sound
W_V, W_χ, W_γ	ft/sec	System noise due to wind (flight path coordinates)
W_x, W_y, W_z	ft/sec	System noise due to wind (rectangular coordinates)
Z		Transfer function zeros
$\bar{V}$, $\bar{\gamma}$, $\bar{\chi}$, $\bar{x}$, $\bar{y}$, $\bar{z}$		Nominal trajectory coordinate variables

$a_1(t)$, $a_2(t)$, $a_3(t)$	ft/sec^2	Measurements of accelerations by inertial platform
a_c	ft/sec^2	Acceleration command
a_{nc}	ft/sec^2	Acceleration command normal to missile flight path
b_1, b_2, b_3	deg	Biases in LOS angle measurements
g	ft/sec^2	Acceleration due to gravity
ℓ_a	ft	Missile body aerodynamic moment arm
ℓ_c	ft	Missile control moment arm
m	lb sec^2/ft	Mass
q	lb/ft^2	Dynamic pressure
s_1, s_2		State vector in rectangular and flight path coordinates respectively
s		LaPlacian variable
t_1	sec	The time the nominal trajectory hits the target
t	sec	Time
t_o	sec	Initial time
u, v, w	ft/sec	Components of velocity in target-centered rectangular coordinates
x, y, z	ft	Rectangular coordinate distance from target
$y_1(t)$, $y_2(t)$	deg/sec	TV tracker angular rate measurements
$\ddot{z}_c$	ft/sec^2	Missile normal acceleration command
$\ddot{z}_\epsilon$	ft/sec^2	Error in missile normal acceleration
α, β	deg	Control variables: angle of attack and bank angle
γ	deg	Missile flight path angle
δx, δy, δz, δV, $\delta\gamma$, $\delta\chi$		Variations of missile coordinates from nominal values
$\delta\alpha$, $\delta\beta$, $\delta\psi$, $\delta\Phi$	deg	Variations of control variables and LOS angles from nominal values
δc	deg	Missile control deflection command
δ	deg	Missile control deflection

θ	deg	Missile body angle
θ_T	deg	Target elevation angle ($\theta_T = \theta + \eta$)
$\dot{\theta}$	deg/sec	Missile body angle time rate of change
$\dot{\theta}_c$	deg/sec	Commanded missile body angle time rate of change
$\dot{\theta}_\epsilon$	deg/sec	Error in missile body angle time rate of change
ΔV_v, $\Delta\alpha_w$, $\Delta\beta_w$		Change in velocity, angle of attack, and bank angle due to wind
η_1, η_2	deg	Target tracker axis azimuth and elevation
η	deg	Target line of sight angle
$\dot{\eta}$	deg/sec	Target line of sight angular rate
$\Xi(t)$		Matrix relating deviations from the nominal trajectory in rectangular coordinates to deviations in flight path coordinates
Σ		Covariance matrix of optimal filter extimation errors
Φ	deg	Line of sight (LOS) elevation angle
ψ	deg	Line of sight azimuth angle
ρ	Slugs/ft^3	Air density
σ		Standard deviation of a normal distribution
τ_{BS}	sec	Autopilot bistable loop time constant
τ	sec	Fixed time constant
μ		n vector (output from filter of observation vector y(t))
$\zeta(t)$		n vector of Gaussian white noises with zero mean
$\lambda(t)$		Matrix

SECTION I

INTRODUCTION

Recent trends in requirements for high-accuracy air-to-surface missiles (ASM) indicate a need for development of advanced control systems. Even with perfect guidance information, the control task is formidable. Three major control areas and questions of feasibility with regard to high-accuracy ASM's are of immediate concern to the control system designer:

- Flight Path Control: Are conventional techniques such as pursuit (velocity vector aimed toward target) and proportional (normal acceleration proportional to the rate of change of the line of sight) adequate for high-accuracy systems, or are new techniques required?
- Guidance Sensors: What are critical sensor characteristics; what are the effects of bias errors and output noise? What are the best methods for guidance during the final phase of flight where the guidance sensor no longer provides information (i.e., the sensor blind range)?
- Inner-Loop Control: Is the performance of such conventional control techniques as normal acceleration autopilots adequate in the presence of rapidly changing flight conditions and atmospheric disturbances?

The primary objective of this program was to provide answers to some of these questions in the form of control system design guides for ASM's with high terminal accuracy. It was intended that these design guides would delineate those subsystems and components that limit the attainable accuracy of the ASM.

A secondary objective was to test the practicality of using optimal control theory and techniques in solving ASM control problems when practical missile configurations and realistic control subsystems characteristics are specified.

SECTION II

SUMMARY

Design guidelines were developed to provide a basis for conducting the following trades for a homing missile control system:

(1) Selection of the most suitable guidance concept and best gain for that concept;

(2) Selection of homing and inertial sensors;

(3) Selection of autopilot.

Three basic homing guidance concepts — proportional, pursuit, and optimal guidance — were evaluated on the basis of miss distance. Two nominal trajectories: a long-range semiballistic and a low-altitude skip trajectory, were investigated for two homing sensor acquisition slant ranges.

In addition to the design guides, an optimal guidance law was developed based on the use of a Kalman filter to obtain the best estimates of the ASM state variable errors from imperfect sensor information. This guidance law minimizes a performance index that is the sum of the mean square miss distance, plus the integral of a quadratic form of the autopilot control variables. The relative weighting of the two terms is adjusted by a weighting factor on the control integral term. This provides a means for minimizing the miss distance with realistic restraints on control action.

A normal acceleration autopilot was designed to meet the mission requirements and advanced bistable controller techniques were applied to obtain an autopilot with nearly invariant performance without gain changes throughout the ASM midcourse and terminal phases.

Evaluation studies were conducted using two analytical tools: a 3-degree-of-freedom linearized differential equation digital program and a 6-degree-of-freedom analog simulation. The digital program provided a direct computation of the mean square miss distance for optimal, proportional, and pursuit guidance laws. The effects of missile nonlinearities and short-period control dynamics were not considered in the digital program, but tracker dynamics, tracker errors

(noise and bias), and uncertainties in initial position and velocity due to boost and midcourse inertial measurement errors were included. The analog simulation was used primarily to provide a means of determining the effects of guidance gain, missile aerodynamic nonlinearities, atmospheric turbulence, and autopilot characteristics; however, it was also used to obtain additional data for comparison of the proportional and pursuit guidance. Quasistatistical miss distance data were obtained from the analog simulation by conducting several runs and calculating the rms for each data point when stochastic disturbances were investigated. Additional backup studies in the form of root-locus stability studies, time and frequency response analyses, and adaptive autopilot studies provided necessary autopilot design data.

The following information is presented:

(1) Trades for selection of guidance concept;
   (a) Comparison of miss distance for optimal, proportional, and pursuit guidance,
   (b) Effect of guidance gain on miss distance,
   (c) Effect of nominal trajectory on miss distance,
   (d) Effect of atmospheric turbulence on miss distance,

(2) Trades for selection of sensors (inertial and homing);
   (a) Effect of dispersion at acquisition (inertial measurement unit error, IMU error vs cost),
   (b) Effect of homing sensor bias errors and output noise,
   (c) Effect of homing sensor blind range,

(3) Trades for selection of autopilot;
   (a) Effect of short period control dynamics on miss distance,
   (b) Achievement of frequency and time response,
   (c) Achievement of stability.

The results of the guidance law comparisons indicate that all three of the guidance concepts are capable of 1σ miss distance of less than 5 feet with nominal TV tracker bias errors of 1.74 milliradians (0.1 degree) and output noise of 1.0 milliradian rms. These small miss distances can be achieved over a reasonably wide range of guidance gain, which indicates some latitude in the implementation of guidance/autopilot loops.

Miss distance was found to be essentially invariant with both homer acquisition range and nominal trajectory type. Note that miss distance was measured in a plane perpendicular to the trajectory, and therefore, miss distances for the different trajectories will be different when resolved into the ground plane. For example, because of the shallow approach angle of the low-altitude skip trajectory, the miss distances in a direction along the trajectory are approximately ten times those of the semiballistic trajectories that have more nearly vertical approach angles.

Initial dispersion, as a result of inertial sensor errors generated prior to target acquisition, appears to have little effect on miss distance. However, it is possible to have a combination of large initial dispersion and short slant range at acquisition that would affect miss distance (the shortest slant range investigated was 15,000 feet). Initial errors were essentially nulled and the missile velocity vector aligned with the target line of sight with 2000 to 5000 feet of slant range remaining prior to impact. This indicates that the most important aspect of initial dispersion will probably be in considering trades between inertial guidance sensor accuracy and the acquisition capability of the homing sensor. The effects of atmospheric turbulence and gusts were also found to be insignificant. This was not unexpected, because the high missile velocity (1000 - 2500 fps) combined with relatively low gust velocities (< 12 fps rms) result in very small angle-of-attack perturbations. In addition, the guidance loop tends to nullify the effect of these perturbations. However, the effect of the turbulence does become significant for large tracker blind ranges (greater than 1500 feet).

The best estimates of homing sensor (TV tracker) nominal bias and noise level (1.74 milliradians and 1.0 milliradian rms, respectively) had a negligible effect on miss distance. An order of magnitude increase in the nominal noise level increases the miss distance considerably. Pursuit guidance miss distances are proportional to the bias errors. Tracker blind range has very little effect up to about 1500 feet. Returning the acceleration command to the autopilot to zero during blind range, rather than holding the last guidance sensor command value,

reduces the dispersion for large tracker blind ranges. For proportional guidance, the allowable minimum slant range to the target is related to the overall autopilot/guidance stability (and thus directly to the missile short-period response).

Controlled missile short-period response had a definite effect on miss distances. With the detailed autopilot configuration investigated, a sharp increase in miss distance was noted when the equivalent first-order response was lowered below 6 radians per second. The increase in error was caused by an inner-loop stability problem rather than a "looseness" of control problem. Earlier more simplified studies using simplified third order transfer function approximations of controlled missile response indicated that 2 radians per second would be adequate. The results obtained with more detailed analog simulation emphasize the necessity of considering guidance gains, autopilot loops and gains, and body bending together when the homing guidance problem is investigated.

Digital computer programs were developed to determine the coefficients of the optimal feedback control law and the Kalman filter through the solutions of Equations 53 and 54 and Equations 76 and 77, respectively. Programs were also developed for determining the mean square miss distance for an ASM with optimal, proportional, or pursuit guidance. These programs are available in punched card, program listing, or magnetic tape form; however, no user's documentation is available. Requests for information regarding the above programs should be directed to L. E. Leistikow of The Boeing Company, Missile and Information Systems Division. The coefficient matrices (F(t) and G(t) of Equation 49) required as inputs to the optimal feedback control law and Kalman filter programs were determined with an existing program that is documented in Reference 14.

Discussions of the details of conditions investigated and the results obtained are presented in the following sections.

SECTION III

GENERAL DESCRIPTION OF STUDY

The program was aimed at effort prior to the preliminary design stage. That is, the first task was to determine whether control of a highly accurate ASM is even possible considering the various "real world" limitations that must be imposed. When feasibility was established, the task was to develop design guides that could be applied to the design of control systems for this general class of vehicles. The study consisted of four major efforts:

(1) A limited survey was conducted of the current state of the art of ASM's with regard to methods of control, hardware limitations, terminal accuracy, and effects of atmospheric disturbances. The results of the survey are presented in Appendix I. Applications of this information to terminal guidance and autopilot studies are discussed in this section.

(2) Optimal control theory was applied to the development of an optimal control law for the near-impact phase that can be implemented on-board an ASM. The optimal guidance law development is presented in Section V. Steepest descent trajectory optimization techniques were applied to the development of nominal trajectories. The trajectory optimization results are presented in the classified supplement to this report.

(3) The effects of various control laws, control component characteristics, and natural disturbances on terminal accuracy were determined and the results of these studies were used to develop control system design guides for the midcourse and near-impact phases of the ASM mission. These guidelines are presented in Section IV.

(4) A normal acceleration autopilot was designed to meet the mission requirements and advanced bistable controller techniques were applied to obtain a quasi-adaptive autopilot which required no gain changes throughout the midcourse and terminal ASM flight. Autopilot design study results and discussions of other adaptive approaches are presented in Section VI.

Following are descriptions of the baseline missile, control laws, homing sensors, and atmospheric disturbances used in the study.

The baseline ASM configuration used in this study is based on Boeing air-to-surface missile preliminary design studies. As a result, the configuration incorporates typical vehicle design features and subsystem integration characteristics. The assumptions that were made in the analytical description of the missile, its various subsystems, and environment are outlined in this section. Descriptions are provided for the following items:

(1) Missile configuration;

(2) Nominal trajectories;

(3) Homing guidance laws;

(4) Inertial guidance sensor;

(5) Homing sensor;

(6) Autopilot;

(7) Atmospheric disturbances;

(8) Flight simulation and miss distance comparison.

Classified details of the missile configuration and trajectory optimization are presented in the supplement to this report. Separate design studies were made of an optimal guidance law and a normal acceleration autopilot. These are presented in more detail in later sections.

1. Missile Configuration. A missile configuration that was defined in a Boeing ASM program provides realistic characteristics for use in this study. The configuration is capable of a variety of missions through the use of a two-pulse solid-propellant motor. The operational flexibility permits the use of either optical or radar-type homing sensors.

The geometric, inertial, aerodynamic (including roll-yaw coupling effects), and structural bending characteristics of this missile are contained in the supplement to this report. The aerodynamic characteristics used in the study were based on wind tunnel data for this configuration. The data required for the autopilot studies were reduced to transfer function form and are presented in Section VI.

In general, the aerodynamic stability derivatives are nonlinear functions of Mach number and angle of attack. Significant nonlinear characteristics were included in the study. However, certain simplifying assumptions were made in cases where they provided reasonable representation of the wind tunnel data. The body normal force curve slope is strongly dependent on angle of attack and Mach number; the body normal force coefficient is closely approximated by:

$$C_{N_{Body}} = C_{N_{\alpha Body}} \alpha + C_{N_{\alpha^3 Body}} \alpha^3 \qquad (1)$$

This equation was used with $C_{N_{\alpha Body}}$ and $C_{N_{\alpha^3 Body}}$ generated as functions of Mach number. The wind tunnel data indicated that these two contributions to total body normal force may be assumed to act at two distinct centers of pressure, with the location of the cubic term fixed and the location of the linear term a function of Mach number. This assumption was used in the analog simulation.

The body axial force coefficient and the fin normal force curve slope are very weak functions of angle of attack, for angles of attack less than 20 degrees. They were, therefore, assumed to be functions of Mach number only. The aerodynamic center of the control fins varies with angle of attack and Mach number, but since the variation represents a very small percentage of the total lever arm, a constant control arm was assumed.

2. Trajectories. Three reference trajectories, consisting of a "low-altitude skip," a "short-range semiballistic," and a "long-range semiballistic" mission of the form shown in Figure 1 were initially selected for study. This investigation was primarily concerned with the homing (or terminal) phase of the trajectories. This phase was considered for acquisition slant ranges of 15,000 to 30,000 feet to the target.

The low-altitude skip trajectory utilizes a two-pulse mode solid-propellant motor. The short-range semiballistic trajectory and the low-altitude skip trajectory both achieved satisfactory results without violating reasonable angle of attack or minimum dynamic pressure constraints. These trajectories were obtained using conventional open-loop performance evaluation trajectory programs. Study of the short-range semiballistic case was discontinued after preliminary evaluation studies indicated insignificant differences in miss distances.

For the long-range trajectory it was necessary to employ trajectory optimization techniques to provide a flight path with sufficiently large dynamic pressure at apogee so that aerodynamic controls could function to keep the vehicle from tumbling. The optimization was performed with a fixed range requirement using constraints on the minimum dynamic pressure at apogee of 10, 20, 35, and 53 psf. In addition, appropriate constraints were imposed on angle of attack and angle of attack rate

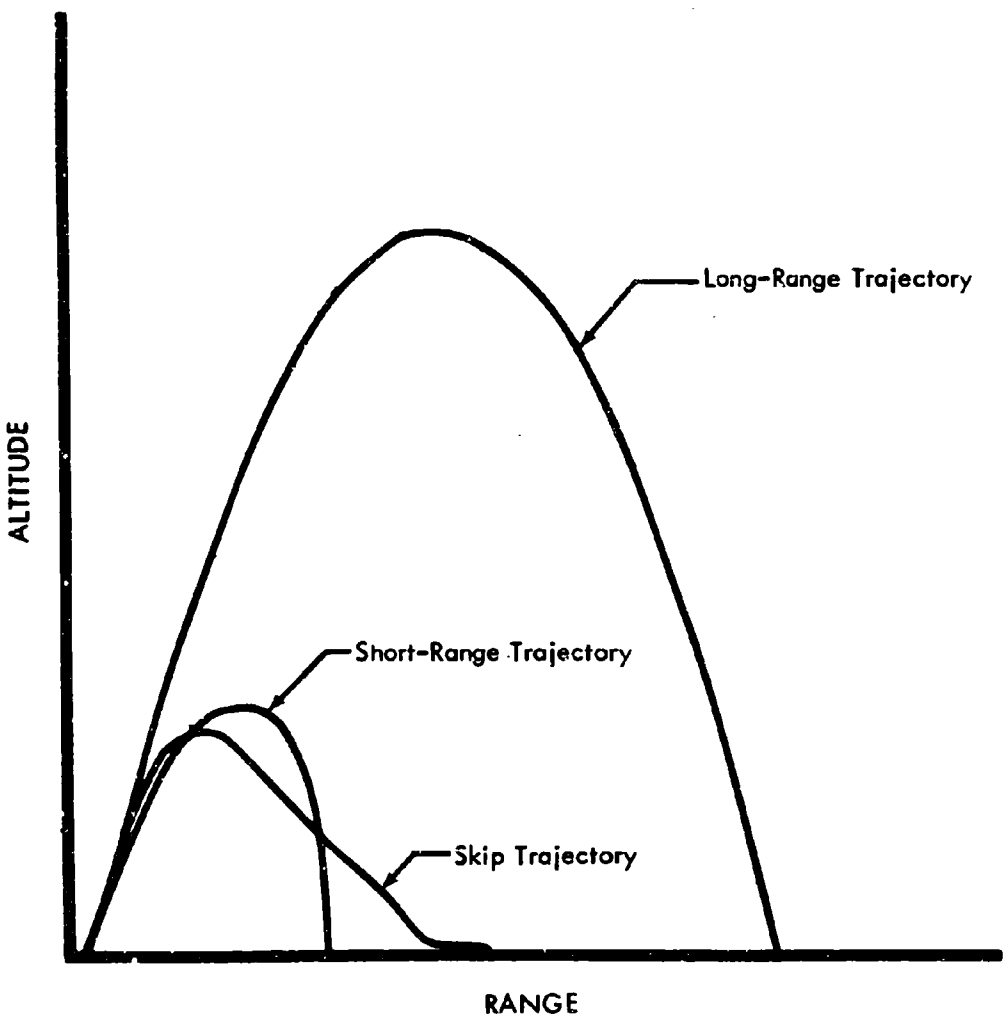

Figure 1: REFERENCE TRAJECTORIES

during the pull-up maneuver after launch from the launch vehicle and the velocity at impact was maximized. The maximization of impact velocity is an important factor for missions involving penetration to defended targets. Data and results regarding this optimization process are shown in Figures 1, 2, and 3 of the supplement.

3. Homing Guidance Laws. Conventional proportional and pursuit homing guidance laws were compared with an "optimal" homing guidance concept. For proportional and pursuit guidance, homing guidance operated in the terminal phase until the ASM reached the homing sensor blind range from the target. At that point options were provided either to zero the guidance commands or to hold the last command value. Optimal guidance used position information from IMU measurements to guide during the blind zone.

The guidance laws are based upon use of a normal acceleration autopilot. For proportional guidance the normal acceleration command, $\ddot{z}_c$, is defined as:

$$\ddot{z}_c = K_1 V \dot{\eta} \tag{2}$$

where K_1 is the guidance gain, V is the missile velocity, and $\dot{\eta}$ is the angular rate of the target line of sight. Another form of the proportional guidance law, which is useful for comparisons with pursuit guidance, can be derived through small angle approximations. This is:

$$\ddot{z}_c = K_1 \frac{V^2}{R_{sl}} (\theta_T - \alpha) \tag{3}$$

where R_{sl} is the slant range to the target. The pursuit guidance law is:

$$\ddot{z}_c = K_2 (\theta_T - \alpha) \tag{4}$$

The basic difference between the two laws is the V^2/R_{sl} term, and the effective pursuit guidance gain remains constant throughout the terminal phase; however, for the proportional guidance law, gain increases as the missile approaches the target (see Figure 2 for definitions).

Proportional guidance can readily be implemented with a gyro-stabilized gimbaled tracker by using the output signals from the rate gyros used in the stabilization

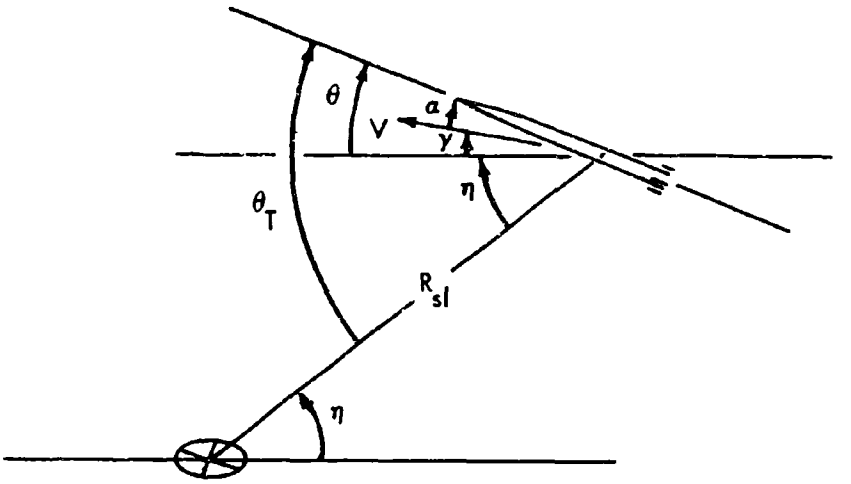

Pursuit guidance:

$$\ddot{Z}_c = K_2 (\eta + \gamma) \tag{5}$$

also

$$\ddot{Z}_c = K_2 (\theta_T - \alpha) \tag{6}$$

Proportional guidance:

$$\ddot{Z}_c = K_1 V \dot{\eta}$$
$$= K_1 V \left[\frac{V(\eta + \gamma)}{R_{sl}} \right], \quad (\eta + \gamma) = \text{small angle} \tag{7}$$

$$\ddot{Z}_c = K_1 \frac{V^2}{R_{sl}} (\eta + \gamma) \tag{8}$$

also

$$\ddot{Z}_c = K_1 \frac{V^2}{R_{sl}} (\theta_T - \alpha) \tag{9}$$

Figure 2: GUIDANCE LAW AND ANGLE DEFINITIONS

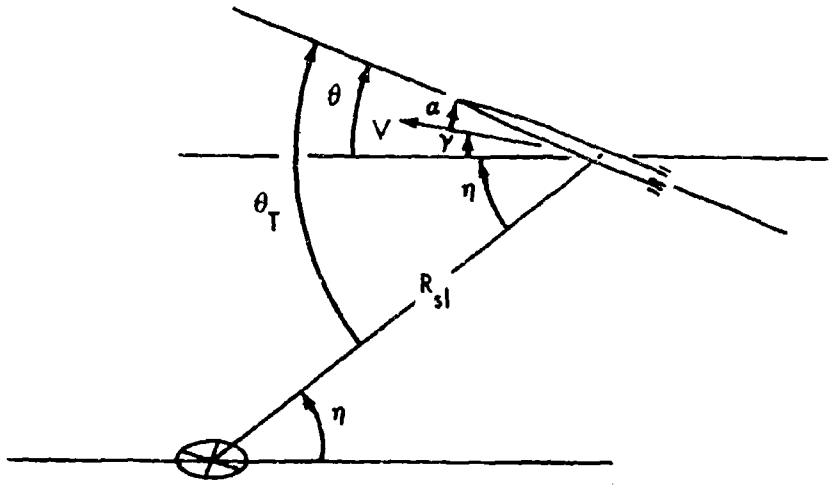

Pursuit guidance:

$$\ddot{Z}_c = K_2 (\eta + \gamma) \tag{5}$$

also

$$\ddot{Z}_c = K_2 (\theta_T - \alpha) \tag{6}$$

Proportional guidance:

$$\ddot{Z}_c = K_1 V \dot{\eta} = K_1 V \left[\frac{V(\eta + \gamma)}{R_{sl}} \right], \quad (\eta + \gamma) = \text{small angle} \tag{7}$$

$$\ddot{Z}_c = K_1 \frac{V^2}{R_{sl}} (\eta + \gamma) \tag{8}$$

also

$$\ddot{Z}_c = K_1 \frac{V^2}{R_{sl}} (\theta_T - \alpha) \tag{9}$$

Figure 2: GUIDANCE LAW AND ANGLE DEFINITIONS

and tracking loops of the tracker. Pursuit guidance is more difficult to implement because it requires a measurement of the target line of sight with respect to the missile velocity vector. This is not a directly measurable quantity since angle of attack must be subtracted from the line-of-sight angles that the sensor measures from the body axes.

The optimal guidance law investigated minimizes the sum of the mean square miss distance plus the integral of a quadratic form of the autopilot control variables. A weighting factor on the integral term allows the relative weighting of the two terms to be adjusted. This provides a means of minimizing the miss distance with realistic restraints on control action. The optimal guidance law is based on the use of a Kalman filter to obtain the best estimates of the ASM state variable errors from imperfect sensor information. Sensor information in the form of accelerations measured with an on-board inertial platform and line-of-sight information from the homing guidance sensor are used in the computation. Details of the development of the optimal control law are presented in Section V.

4. Inertial Guidance Sensors. A conventional gimbaled type of inertial measurement unit (IMU) was chosen for the baseline inertial guidance sensor. This choice was made in part because this was the only type of instrument for which good accuracy and cost information were available. Equipment variations for this type of inertial measurement unit, relating cost to sensor accuracy, were exercised with an upper limit on cost of the inertial platform and associated electronics of $40,000 (excluding the airborne computer). Three gradations of equipment accuracy versus cost were investigated.

The 1σ errors in three inertial position and velocity components were evaluated as measured by the inertial guidance sensor along each of the three reference trajectories. These sets of accuracy data represent the errors generated during midcourse flight and provided the initial errors for the terminal homing phase of flight. A summary of this data in the form of 1σ root sum square position errors is presented in Table I. The data indicates that little accuracy is gained by going beyond the $25,000 IMU. Therefore, this IMU was selected as baseline. Position

fixing and alignment prior to launch were based on low-altitude launch from the launch vehicle. Additional details of the inertial guidance sensor survey and error analysis are presented in Appendix I.

This error data was used in the ASM miss distance studies in two ways. The IMU 1σ errors were used directly in the initial covariance matrix of position and velocity errors for a digital linear error analysis program. In a nonlinear analog study, the IMU 1σ positional errors for each component were used as finite x, y, and z component errors to give a worst-case deviation from the nominal initial conditions. The same set of component errors were used for all the analog studies. For the baseline IMU, inertially referenced angle measurement errors were small (less than 1 degree). However, the position errors result in an initial velocity vector pointing error with respect to the target. This initial angular error was approximately 3.0 to 4.0 degrees for the cases studied.

Table I: INERTIAL MEASUREMENT UNIT 1σ RSS POSITION ERRORS AT TARGET ACQUISITION

	Slant Range (feet)	RSS Errors (~feet)		
		$13,000*	$25,000*	$40,000*
Short-Range Semiballistic Trajectory	15,000	1670	1450	1450
	30,000	1650	1450	1450
	60,000	1620	1450	1450
Low-Altitude Skip Trajectory	15,000	7910	2450	2330
	30,000	6680	2250	2130
	60,000	4740	2000	1770
Long-Range Semiballistic Trajectory	15,000	5210	2850	2730
	30,000	5030	2800	2660
	60,000	4690	2650	2540

* Inertial Measurement Unit Cost.

5. Homing Sensor. Surveys of homing guidance sensors were conducted to obtain operational characteristics of various TV, infrared, and radar-type sensors to determine which of these sensors would be suitable for the study missions. As

a result of these surveys (which are presented in Appendix I), a TV-type homing sensor was selected for the study. Because of a lack of information on the characteristics of wide field of view trackers, and because of the conceptual equivalence of body-fixed and gimbaled sensors as applied to the optimal guidance task (discussed in Section V), the studies were based on the characteristics of narrow field of view, gimbaled TV trackers only. A simplified single axis block diagram representative of this type of tracker is shown in Appendix I.

Bias errors and output noise were considered representative of the types of errors to be encountered in TV trackers. The errors were investigated in parametric form, because detailed performance data were limited. Bias errors typically would result from boresight alignment errors between the TV vidicon tube and its gimbal structure and misalignment between the tracker base and the missile reference axes. Major sources of noise are probably the target background, vidicon tube and its signal processing circuitry, and the rate sensors used to stabilize the tracker gimbals. The noise was considered to be "white noise." In the analog studies the noise was obtained from a low-frequency noise generator with a 30-cps cutoff frequency. The noise generator was scaled to a nominal tracker noise level of 1 milliradian (rms). In the linear analysis, the nominal noise was considered to be "white noise" with a standard deviation of 1.0 milliradian. As long as the response of the ASM system is significantly below the 30-cps cutoff frequency of the noise generator, the two techniques are comparable. Nominal values of 1.74 milliradians (0.1 degree) bias error and 1.0 milliradian (rms) of output noise were assumed. (An experimental program is described in Appendix I in which a centroid tracker was synthesized. This experiment yielded bias error values of less than 1 milliradian.)

Nominal tracker gimbal position dynamics were considered to be a 5-cps, 0.5-damped-quadratic response to line-of-sight errors measured by the optical sensor. Because the program was concerned primarily with the terminal homing phase of flight, investigation of the dynamics and peculiarities of target acquisition were not covered.

6. Autopilot. A normal acceleration autopilot was selected for control of the ASM. This choice was based, primarily, on previous Boeing homing dynamics studies that indicated the desirability of a normal acceleration commanded autopilot because of the simplification (over attitude control) in guidance laws it provides. In addition, the normal acceleration autopilot provides a parameter for limiting command maneuvers to stay within vehicle structural limits.

Autopilot stability and time response studies (discussed in Section VI) resulted in a normal acceleration plus angular rate feedback system with forward loop compensation to reduce steady-state errors. Analog terminal phase studies were conducted to determine the effects of autopilot characteristics on miss distance. These studies used a detailed representation of the autopilot as shown in Figure 3. An idealized version was used in the digital evaluation programs, in which instantaneous response to commanded accelerations was assumed.

7. Atmospheric Disturbances. Two types of atmospheric disturbances were considered in the study. The wind shear profile as shown in Figure 4 was obtained by adding a spike to Figure 9 of Reference 1 and is considered representative of wind shear within a 1% probability. Atmospheric turbulence with a power spectral density described on Page 63 of Reference 1 was added to the analog simulation.

8. Flight Simulation and Miss Distance Comparison. Two approaches were used in evaluating the effects of various system characteristics on miss distance error of the ASM. The effects of proportional and pursuit guidance gain, variations in sensor and autopilot characteristics, and the effects of atmospheric disturbances were determined primarily with an analog simulation of the homing phase. The optimal guidance law is not amenable to simulation on the analog computer; therefore, a digital computer program was developed to permit comparative evaluation of miss distance for all three guidance laws (i.e., pursuit, proportional, and optimal guidance) using a simplified missile representation that assumed an idealized autopilot. The use of the two analysis techniques and the detail considered in each is summarized in Table II.

The analog simulation was previously developed specifically for homing guidance studies (Reference 2). Two automatic scale changes in the three missile-to-target

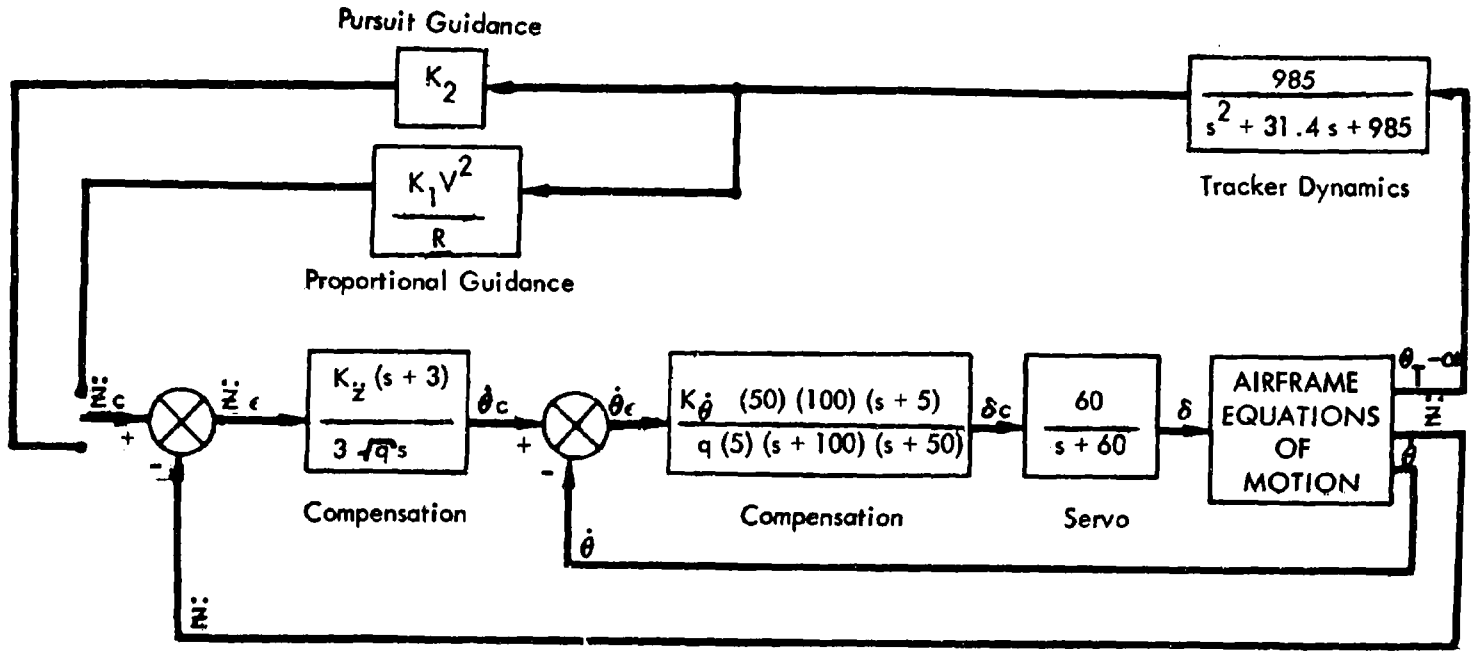

Figure 3: GUIDANCE AND CONTROL SYSTEM - ANALOG

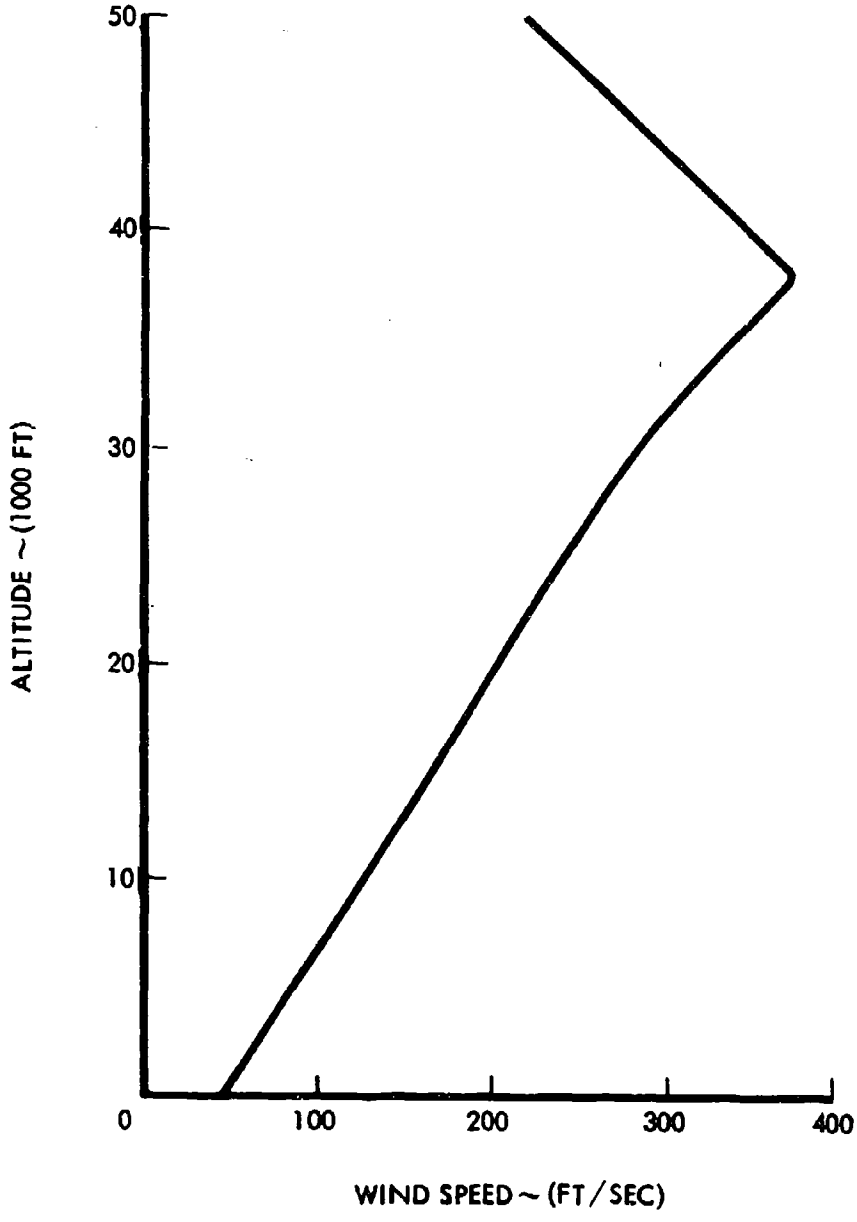

Figure 4: WIND PROFILE

Table II: MISS DISTANCE EVALUATION TECHNIQUES

Purpose	Equations	6DOF	3DOF	Analog	Digital
Guidance Law Comparison	Linearized		X		X
Optimal Guidance	Linearized		X		X
Tracker Errors	Linearized		X		X
	Nonlinear	X		X	
Guidance Gain, Autopilot	Nonlinear	X		X	
Atmospheric Turbulence	Nonlinear	X		X	

displacement components were made to provide satisfactory definition of impact accuracy. Six degrees of freedom were simulated. The equations of motion for pitch and yaw rotations and three translations in a target-centered cartesian coordinate system were solved. The missile roll axis control was considered to be ideal and maintained one pair of the cruciform fins in the vertical plane. Inertial cross-coupling effects were included. Nonlinear aerodynamics, proportional or pursuit guidance, and the autopilot as shown in Figure 3 were included in the simulation. The terminal guidance TV tracker noise and bias, and tracker dynamics as described in 5. Homing Sensor were also included. Provisions were made for atmospheric disturbance simulation in the form of horizontal wind shear profiles and turbulence that acted normal to the missile body axis.

The homing portion of the missile flight was initiated in the analog simulation at a slant range of 15,000 feet (from approximately 1000 to 15,000 feet corresponding altitude) for the three nominal trajectories — long-range semiballistic, short-range semiballistic, and low-altitude skip. Simulation during the region of TV tracker blind range provided the normal acceleration commands from the guidance system to be either set to zero or held at the last commanded value at a preselected range from the target. The simulated autopilot was the normal acceleration plus pitch rate feedback system with forward loop compensation. To obtain adequate and uniform response and stability, the two autopilot gains were

changed continually throughout the flight proportional to the inverse of dynamic pressure and the square root of its inverse. Details of the autopilot characteristics are presented in Section VI.

Comparison data on miss distance for all three guidance concepts (proportional, pursuit, and optimal) were obtained with a digital program for computing the covariance matrix of position and velocity errors from the nominal trajectories. A simplified description of the ASM was used in this program. The missile was considered to be a point mass with lift and drag force coefficients as nonlinear functions of angle of attack and Mach number. An ideal autopilot was assumed (i.e., instantaneous response to commanded accelerations). TV tracker dynamics were included; sensor errors were assumed to consist of random bias plus white noise.

In this approach the equations of motion of the ASM were linearized about a nominal trajectory. The initial conditions for the covariance matrix were the position and velocity errors at target acquisition that were based on the expected dispersions developed during midcourse from inertial instrument errors. The covariance matrix of the state of the linearized missile equations, as a function of time, was then obtained from a numerical solution of the linearized differential equations. The integration was performed on a Sperry Rand 1107 computer. The miss distance was obtained as the value of the covariance matrix at the time the nominal trajectory hits the target. This evaluation technique is described in detail in Appendix II.

Miss distances are defined in a plane passing through the target and normal to the ASM trajectory as shown in Figure 5. These errors are more direct than errors measured in the ground plane, because they are independent of the ASM target approach angle. In the following discussions of results, errors obtained from the linear analysis are presented as 1σ (or standard) deviations about the target as shown in Figure 5.

Miss distances obtained from the analog studies are presented in two forms: an average error and the rms deviation from the average. As discussed previously,

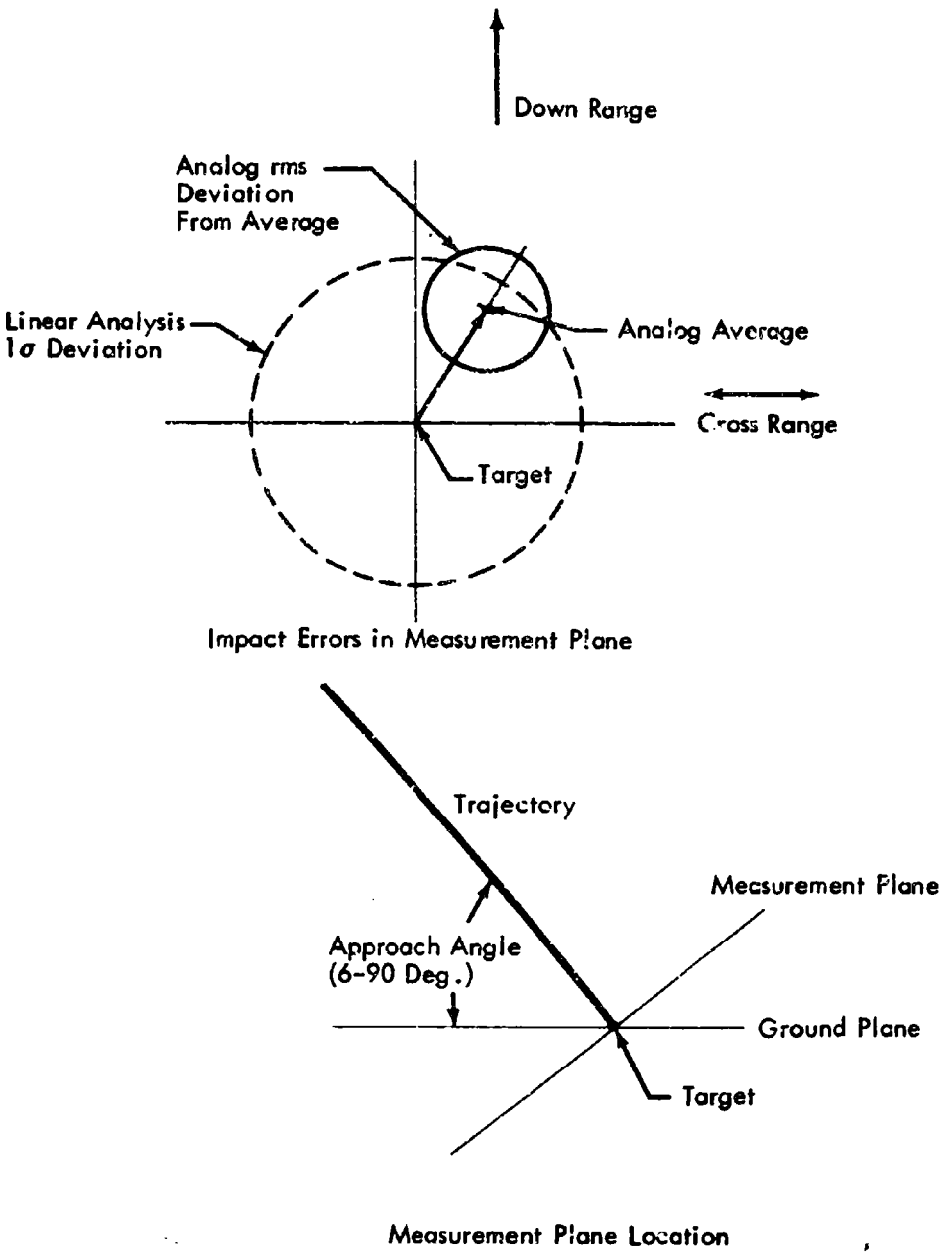

Figure 5: MISS DISTANCE DEFINITION

the initial positional errors were introduced as a finite set of errors from the nominal trajectory. Therefore, the analog miss distances obtained from repeated simulation runs were not centered about the target like those obtained from the linear analysis. This deviation of the center of the group of miss distances from the target is presented as an average (or arithmetic mean) error. With the set of initial position errors used in the analog study, this average error was always positive. Obviously, a different set of initial conditions could have been selected that would have resulted in negative average errors. The analog rms miss distances that are presented are the calculated rms deviations from the average error and represent the effect of stochastic disturbances to the ASM. From 15 to 20 simulation runs were made for each analog rms data point.

SECTION IV

CONTROL SYSTEM DESIGN GUIDES

The control system design guides are presented in three categories:

(1) Selection of Guidance Concepts

These data present a comparison of achievable miss distances for three guidance concepts as a function of nominal trajectories and atmospheric disturbances. The effect of gains for each guidance concept is also discussed.

(2) Selection of Inertial and Homing Sensors

Effects of dispersion at target acquisition, homing sensor bias errors and output noise, and homing sensor blind range are discussed.

(3) Selection of Autopilot

Effects of autopilot short-period control dynamics on miss distance are presented.

Discussion of the details of conditions investigated and the results obtained are presented in the following paragraphs.

1. Selection of Guidance Concept. Three homing guidance concepts (proportional, pursuit, and optimal guidance) were evaluated for impact accuracy. Guidance gains were optimized for proportional and pursuit guidance; the effect of the weighting factor on the integral term of the optimal guidance performance index was explored. (This performance index minimizes the sum of mean square miss distance plus the integral of the quadratic form of the control variables.)

Evaluations were made for two nominal trajectories. Two acquisition slant ranges were evaluated for one of the trajectories. A range of atmospheric turbulence from 0 to 12 fps rms was simulated in the analog computer evaluation of proportional guidance.

a. Comparison of Guidance Concepts. Table III compares the obtainable miss distances for proportional, pursuit, and optimal guidance with the nominal ASM system errors. Guidance gains were set at or near the best values for each guidance technique. Error data is shown only from the linear analysis program and, therefore, represents the 1σ (or standard) deviations about the target (as discussed in Section III). Average error data (as shown in Figures 6 and 7) from

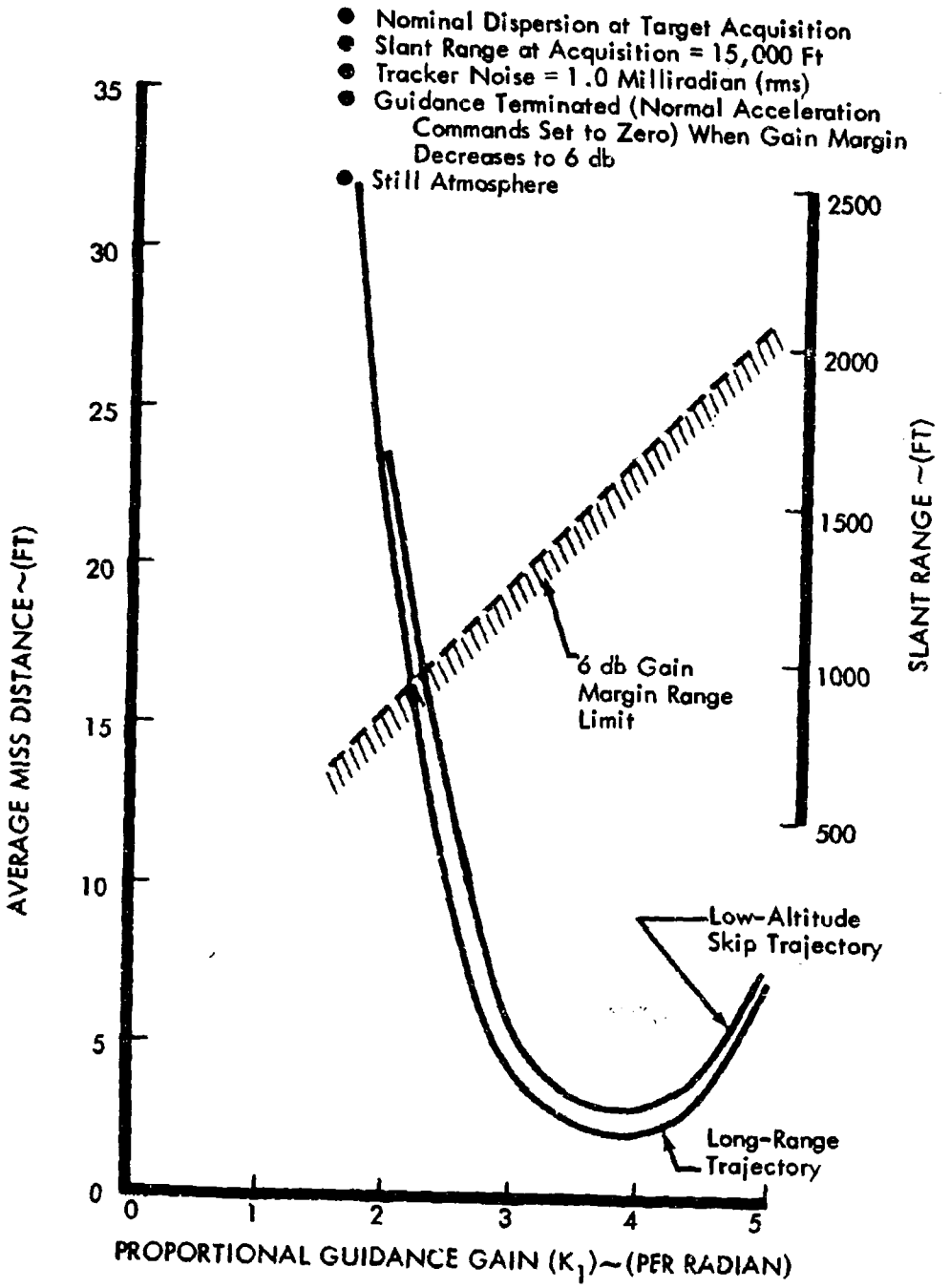

Figure 6: EFFECT OF GUIDANCE GAIN FOR PROPORTIONAL GUIDANCE

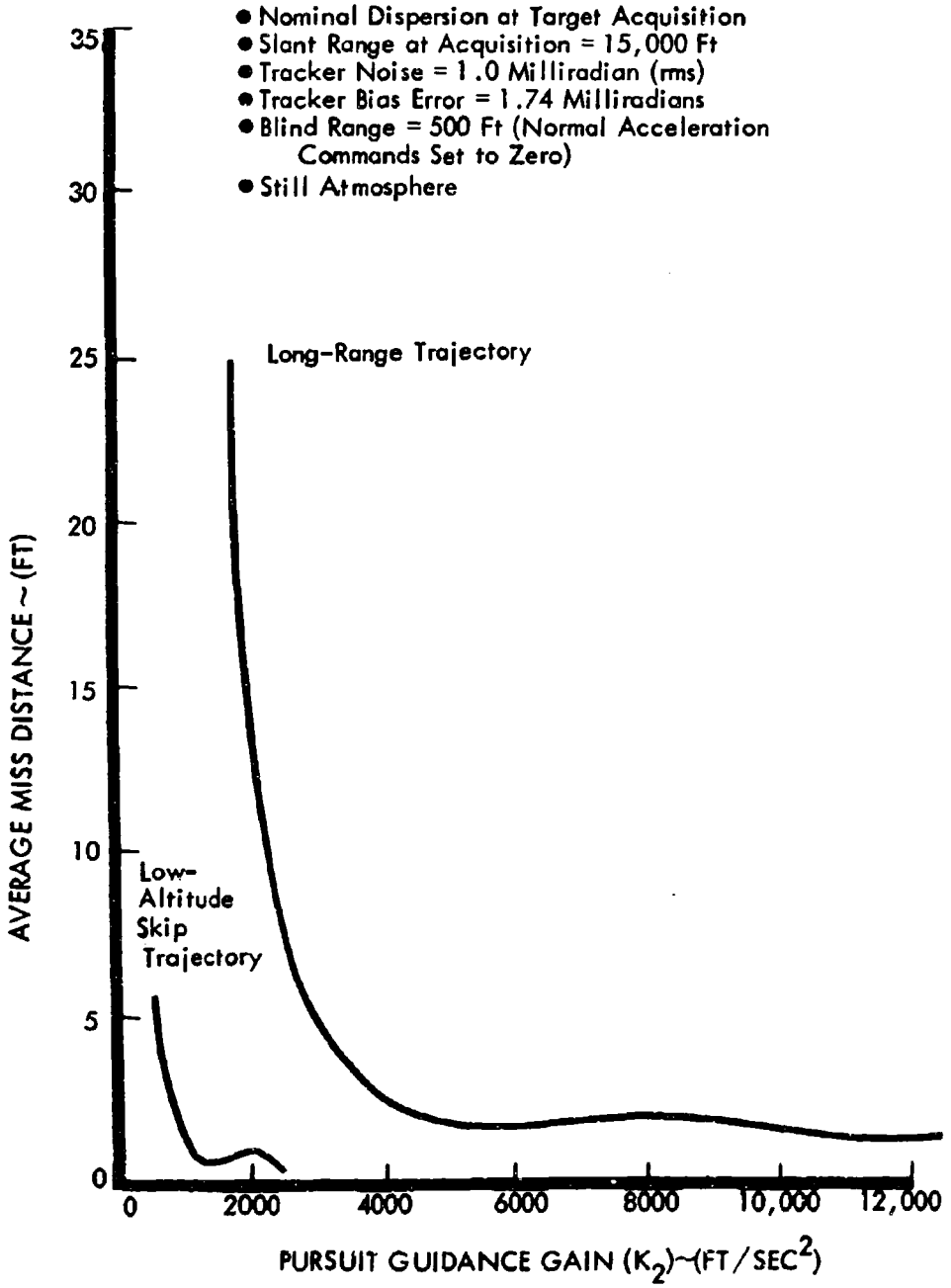

Figure 7: EFFECT OF GUIDANCE GAIN FOR PURSUIT GUIDANCE

the 6-degree-of-freedom analog simulation were reasonably close to the 1σ errors shown in Table III. This indicates that for nominal conditions, the vehicle response is not degrading the ASM performance and the simplified linear analysis is adequate.

Each of the guidance concepts is capable of achieving small miss distances; the spread between minimum and maximum 1σ errors is less than 2 feet. The results show optimal guidance to be better than either proportional or pursuit, and proportional to be slightly better than pursuit.

Table III: GUIDANCE LAW COMPARISON—
MISS DISTANCE MEASURED NORMAL TO TRAJECTORY

Trajectory	1σ Miss Distance (feet)		
	Proportional Guidance	Pursuit Guidance	Optimal Guidance
Long-Range Semiballistic			
Acquisition at:			
30,000-foot Slant Range	2.7	2.9	1.6
15,000-foot Slant Range	3.1	3.3	2.2
Low-Altitude Skip			
Acquisition at:			
15,000-foot Slant Range	---	1.74	1.44

Conditions:

Baseline IMU 1σ dispersion at acquisition
Tracker noise — 1 milliradian
Tracker bias — 1.74 milliradians
Tracker blind range — 500 feet

It can be seen from Table III that the differences in miss distance, as measured perpendicular to the trajectory, between trajectories, and for different slant ranges at target acquisition are very small. A third nominal trajectory (short-range semiballistic) was dropped from evaluation when initial studies indicated

no significant differences between trajectories. When the measured miss distances are resolved into the ground plane through the trajectory approach angle, however, the deviation of impact on the ground for the low-altitude skip trajectory becomes approximately ten times that of the long-range semiballistic trajectory, due to its very shallow target approach angle. For the range of trajectories investigated, the deviation normal to the trajectory can be considered independent of the trajectory. This is significant because it indicates that the ASM performance is not seriously affected by the terminal phase flight conditions. On the two trajectories investigated, terminal velocities are different by approximately a factor of two.

b. Effect of Guidance Gain. Figures 6 and 7 present the effects of guidance gain on proportional and pursuit guidance accuracy with the nominal ASM system errors. As discussed in the presentation of tracker error effects, tracker bias errors were not included in the proportional guidance simulations. These data were obtained from the 6-degree-of-freedom analog simulation described in Section III that included complete autopilot and guidance systems. Only the average error (as described in Section III) is shown for clarity. The rms deviation from the average is less than 0.5 foot for the nominal conditions and best gains. Note that the errors for the best gains are comparable to those shown in Table III for the linear analysis.

The increase in miss distance at low guidance gains for both concepts is the result of inadequate gain to remove the effect of initial position errors (and hence velocity vector pointing errors). At low gains the ASM is essentially operating in an open-loop or unguided condition. As discussed in Section III, the velocity vector pointing error, for the nominal initial position error of approximately 1500 feet, is about 3 to 4 degrees.

The effect of proportional guidance gain, K_1, on miss distance is shown in Figure 6 and indicates that best accuracy is obtained with a guidance gain between 3 and 4. To explain the degradation of performance as the guidance gain is increased beyond 4, remember that the effective proportional guidance gain is $K_1 V^2/R_{sl}$ (shown in Section III). Thus, as the ASM approaches the target the

effective gain increases, and at some range, R_{sl}, stability problems will occur. In Figure 6, the range is shown at which the combined autopilot/guidance gain margin is reduced to 6 db for the ASM configuration studied. In obtaining the data for Figure 6, guidance was terminated ($\dot{z}_c = 0$) at the indicated ranges. The long blind ranges allow insufficient time to remove the effect of initial position errors and large miss distances result. A similar increase in miss distance would be noted at guidance gains beyond 4 or 5 because of decreased stability if guidance was not terminated.

Stability was not a problem for proportional guidance gains less than 4 and slant ranges down to 500 feet, and all remaining data runs were conducted without the 6-db-gain margin restriction. As will be shown later in the discussion of homing sensor blind range effects, long blind ranges are not desirable when atmospheric turbulence is present.

The effect of pursuit guidance gain on missile accuracy is shown in Figure 7. It may be seen that the low-altitude skip trajectory requires less guidance gain than does the long-range trajectory. The reason for this difference is that the velocities for the two trajectories differ. The effective gain for proportional guidance is $K_1 V^2/R_{sl}$. The best K_1 was found to be independent of the missile velocity for the trajectories investigated. Because the effective guidance gain is a constant for pursuit guidance, it follows that for these trajectories the gain for best accuracy will be proportional to the square of the velocity. The ratio of the squares of the initial velocities of the two trajectories is 6 to 1, which coincides very closely to the ratio of the minimal gains for acceptable accuracy as shown in Figure 7.

Because pursuit guidance gain is independent of range, missile stability does not decrease as the missile approaches the target. Therefore, pursuit guidance cutoff range can be selected independent of guidance gain. For the pursuit guidance runs represented by Figure 7, the guidance cutoff slant range (blind range) was set at 500 feet.

The termination of the low-altitude skip trajectory curve at $K_2 = 2500$, as compared to 12,500 for the long-range trajectory, is the result of an instability caused by excessive acceleration commands at acquisition. The problem can probably be overcome with acceleration command and/or acceleration error limiters. However, this extension was not attempted because the terminal gains in each case represent a gain approximately twice the minimum acceptable value. Acceleration command limiting was not required at other times in the trajectory.

The effect of the weighting factor on the control integral term of the optimal control performance index was not investigated in detail. (This term, which is discussed in Section V, essentially limits the ASM maneuver capability.) However, it is believed that considerable latitude is possible in the selection of this factor. Emphasis in this investigation was on obtaining a weighting factor that would provide satisfactory miss distances. As was shown in Table III, this objective was accomplished. The weighting factor that yielded these miss distances was two orders of magnitude below the value of the first factor tried. The larger factor had given completely unsatisfactory errors. Detailed simulation studies of the optimal control concept would be required to compare the optimal guidance maneuver requirements with those of a conventional guidance concept. Studies of this type were beyond the scope of this investigation.

c. Effect of Atmospheric Disturbances. Figure 8 shows the effect of turbulence on impact error for the long-range trajectory, using proportional guidance with a blind range of 500 feet. (The 6-db-gain margin restriction on overall gain was ignored.) The gust characteristics obtained from Reference 1, and discussed in Section III, were applied in the vertical plane. It may be seen that miss distance is insensitive to rms gust velocity for the blind range considered. Although the probability of occurrence is very slight, digital runs were made with approximately 20-fps rms turbulence with no effect on miss distance. This is due primarily to four factors: First, the high missile velocity combined with relatively low gust velocities results in small angle-of-attack perturbations; Second, the random nature of gusts tends to make the average effect on the trajectory small; Third, with a 500-foot blind range, any transient due to gusts existing at the

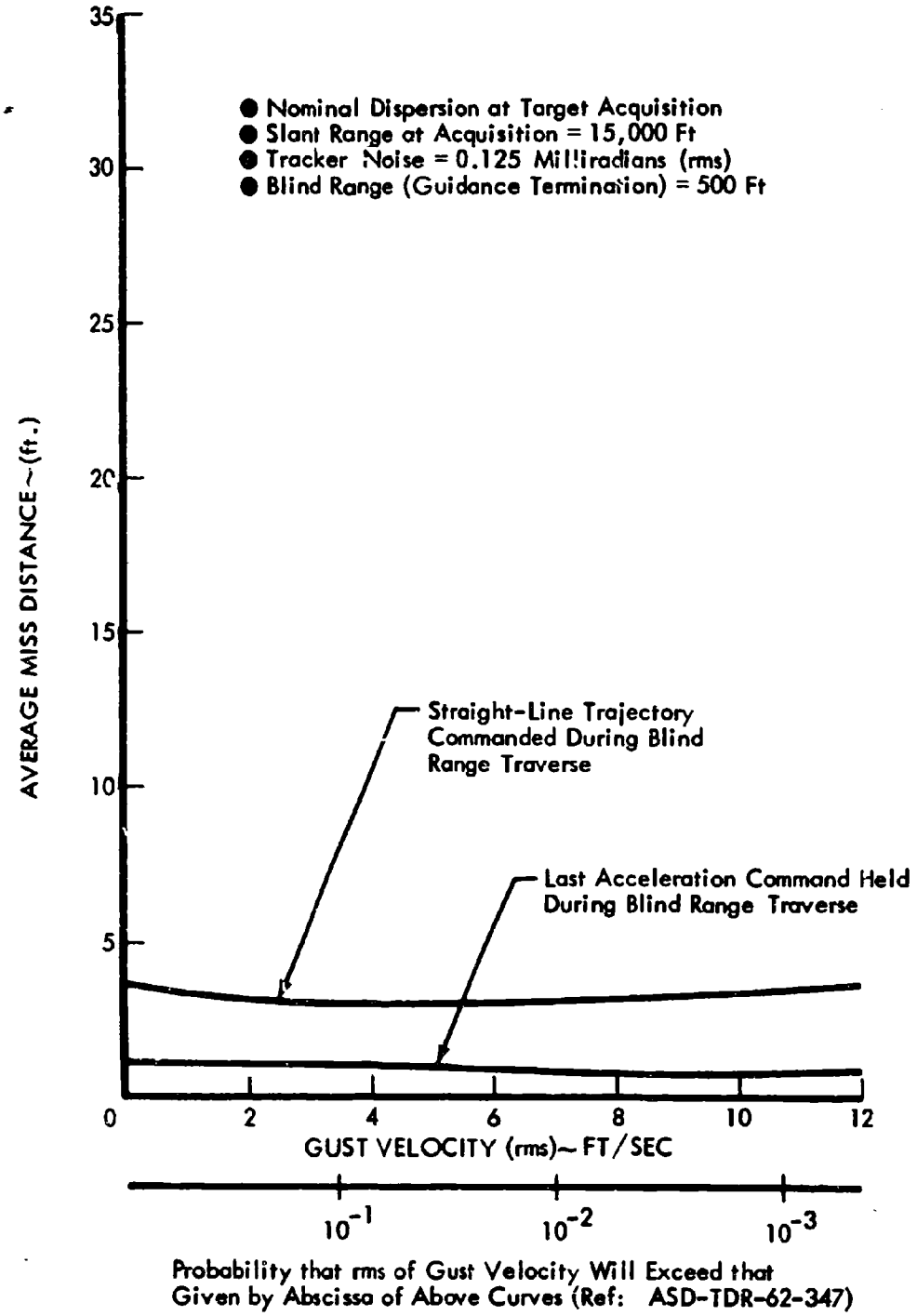

Figure 8: EFFECT OF GUST VELOCITY—PROPORTIONAL GUIDANCE LONG-RANGE TRAJECTORY

time of guidance cutoff has little time (approximately 0.25 second) to affect the impact point; Fourth, the guidance system tends to compensate for gusts.

However, turbulence does contribute to miss distance when blind range is increased, as is shown in the discussion of blind range (Paragraph 2-d of this section).

The wind shear profile shown in Figure 4 was applied in both a head-wind and tail-wind condition in a simplified homing simulation. The contribution of the wind profile to miss distance for either condition was insignificant.

2. Selection of Inertial and Homing Sensors. Variations in several sensor anomalies were investigated for effect on miss distance. These were: inertial instrument errors (i.e., effect on dispersion at target acquisition), TV tracker bias errors and output noise level, and tracker blind range. Investigations of the various effects on proportional and pursuit guidance were conducted primarily with the analog simulation; the digital program was used to provide error information for optimal guidance and checks on the analog results.

a. Effects of Dispersion at Target Acquisition. There are two important considerations affecting allowable initial dispersions at the beginning of the terminal phase after target acquisition; the time required to correct the ASM heading errors with respect to the target, and the homing sensor target acquisition capability. Initial dispersion of up to twice the nominal values (nominals were approximately 1500 feet) had no effect on miss distance for optimal guidance for the minimal acquisition range of 15,000 feet. Examination of the analog simulation data indicated that the remaining range to the target, when the effects of initial errors were corrected by homing guidance, was 2000 feet. It is expected from these results that initial dispersion of the magnitude considered will have a minor effect unless the acquisition range is decreased significantly from 15,000 feet.

Initial dispersion may have a very significant effect on the acquisition of the target with the homing sensor. The effect of initial position and velocity vector errors must be considered within the limitations in homing sensor field of view, acquisition range, and allowable time for acquisition. The study of the target acquisition was not conducted in this program.

b. Effect of Tracker Bias Errors. Only pursuit and optimal guidance were investigated for bias effects. It was assumed that gimbaled tracker bias errors would be removed during acquisition with proportional guidance, because proportional guidance would be implemented using a line-of-sight rate signal. (The method of implementation was discussed in Section III.)

As indicated in Figure 9, other ASM errors were nominal. (The contribution of the nominal tracker noise of 1.0 milliradian to miss distance is less than 0.5 foot, so bias error effects are essentially isolated.)

The effect of angular bias errors in tracker look angle is shown in Figure 9. The bias error indicated was applied simultaneously to both the pitch angle and the yaw angle; results are shown in terms of analog average miss distance. Cross-range and down-range errors are comparable. Pursuit guidance errors are approximately proportional to bias error. The miss distances for pursuit guidance are larger than those that would be expected from a simple propagation of the bias error over the blind range. This larger error is caused by the inherent dynamic characteristic of pursuit guidance that causes it to lag a moving target, because a pointing error is required to generate a guidance command. The tracker bias error causes the target to have an apparent velocity. Results for pursuit guidance errors obtained from the digital linear analysis were comparable.

Bias errors of up to 3 degrees had no effect on optimal guidance miss distance.

c. Effect of Tracker Noise. Expected values for TV tracker noise (representing line-of-sight angle errors) are from 1 to 3 milliradians (rms). A range of up to 50 milliradians was examined. The effect of tracker noise on miss distance is shown in Figure 10 and Table IV. The analog data in Figure 10 is presented as average data plus the rms deviation from the average. The rms deviation is represented by the shaded areas. As discussed in Section III, the error data for each point was obtained from the reduction of miss distance from 15 to 20 analog runs. The linear analysis data presented in Table IV is the 1σ deviation from the target.

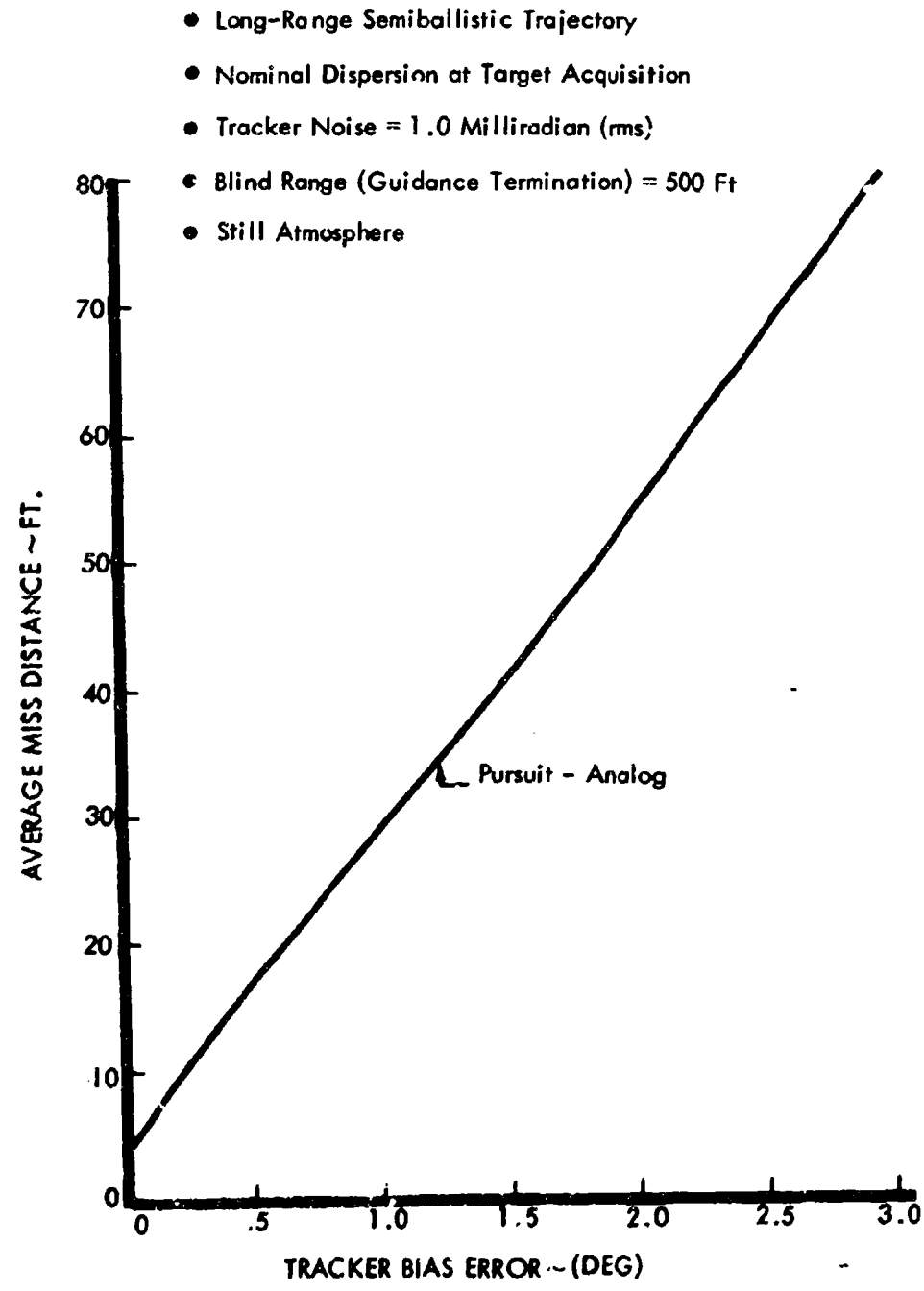

Figure 9: EFFECT OF TRACKER BIAS ERROR—PURSUIT GUIDANCE

- Long-Range Semiballistic Trajectory
- Nominal Dispersion at Target Acquisition
- Slant Range at Target Acquisition - 15,000 Ft.
- Tracker Bias - 0 Degree
- Blind Range (Guidance Termination) - 500 Ft.
- Still Atmosphere

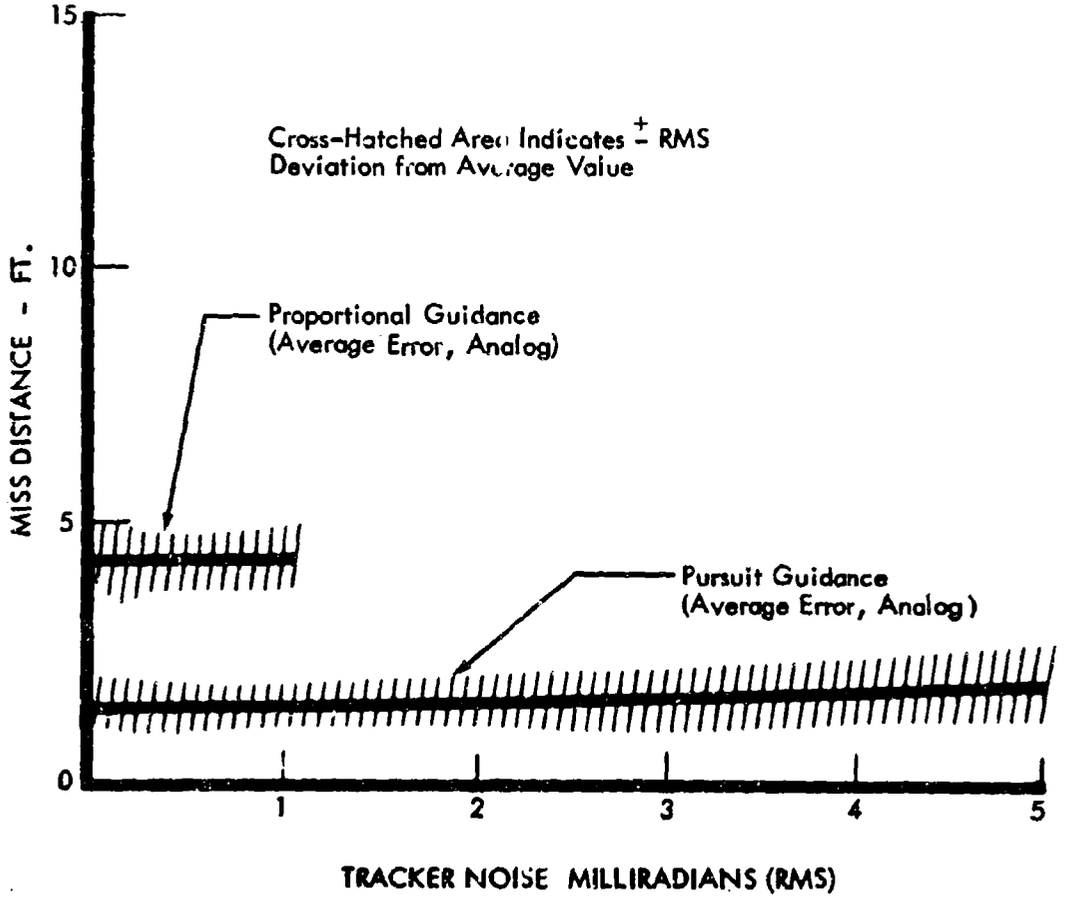

Figure 10: EFFECT OF TRACKER NOISE - LONG-RANGE TRAJECTORY

Tracker noise was represented in the analog simulation by a noise generator that supplies an approximate white noise output in the frequency range from 0 to 35 cps, while the statistical description of tracker noise used in the digital analysis included all frequencies. Other conditions were nominal as shown in Figure 10 and Table IV, and were introduced in the manner presented in Section III.

The effect of noise levels beyond the nominal value of 1 milliradian (rms) are not shown for proportional guidance in Figure 10 because higher levels of noise completely saturated the analog simulation. The pursuit guidance simulation provided slightly better inherent system filtering and levels to 5 milliradians were tried. This situation is comparable to what could be encountered in a real system. If sensor outputs with high noise levels are not filtered so they contain only the frequency spectrum required for control, the high frequency components can saturate the autopilot. For the values investigated on the analog, the noise does not have a large effect on miss distance.

Effects of tracker noise beyond 10 milliradians were evaluated with the digital linear analysis for proportional, pursuit, and optimal guidance. The digital results are shown in Table IV. An interesting result is that optimal guidance does not produce significantly better results. Apparently the inherent filtering of the ASM system dynamics is almost as good as the Kalman optimal filter with respect to resultant system error.

d. Effect of Tracker Blind Range. The effect of tracker blind range is shown in Figures 11 through 14. Data are shown for two autopilot command techniques following guidance termination: holding the last commanded normal accelerations during blind range traverse, and commanding zero normal acceleration ($\dot{z}_c = 0$) during blind range traverse.

As in the other analog studies, several runs were made for a given trajectory (i.e., long-range or skip) with the nominal set of initial position deviations. Because of the initial deviations, a maneuver is required to impact the target even in the absence of disturbances. Atmospheric turbulence of 10 fps rms was

TABLE IV

EFFECT OF TV TRACKER NOISE - 1σ MISS DISTANCE

RMS NOISE LEVEL MILLIRADIAN	* MISS DISTANCE (FEET)		
	PROPORTIONAL GUIDANCE	PURSUIT GUIDANCE	OPTIMAL GUIDANCE
1	3.1	3.3	2.2
10	15	13.3	14.3
50	72	64.8	59.4

CONDITIONS:

NOMINAL DISPERSION AT ACQUISITION
SLANT RANGE AT ACQUISITION — 15,000 FEET
TRACKER BIAS — 1.74 MILLIRADIANS
TRACKER BLIND RANGE -- 500 FEET

* ERROR MEASURED PERPENDICULAR TO TRAJECTORY .

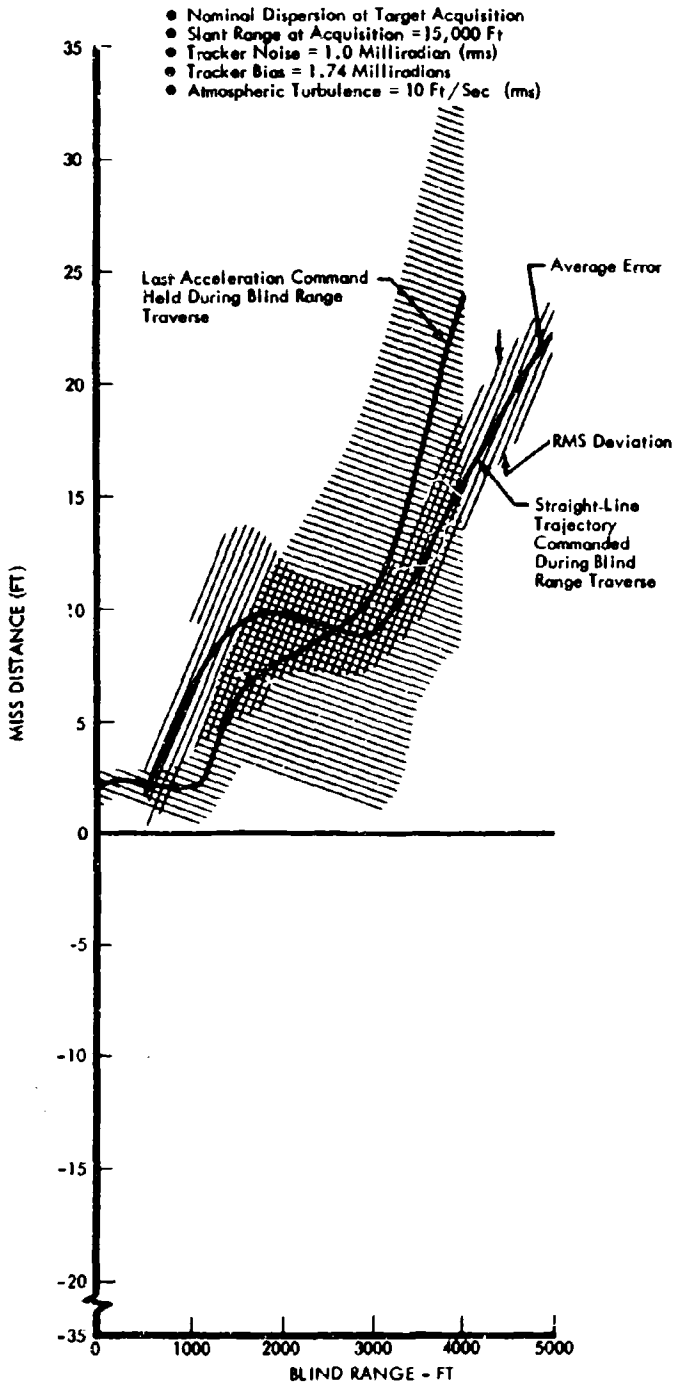

Figure 11: EFFECT OF BLIND RANGE FOR PURSUIT GUIDANCE; LONG-RANGE TRAJECTORY

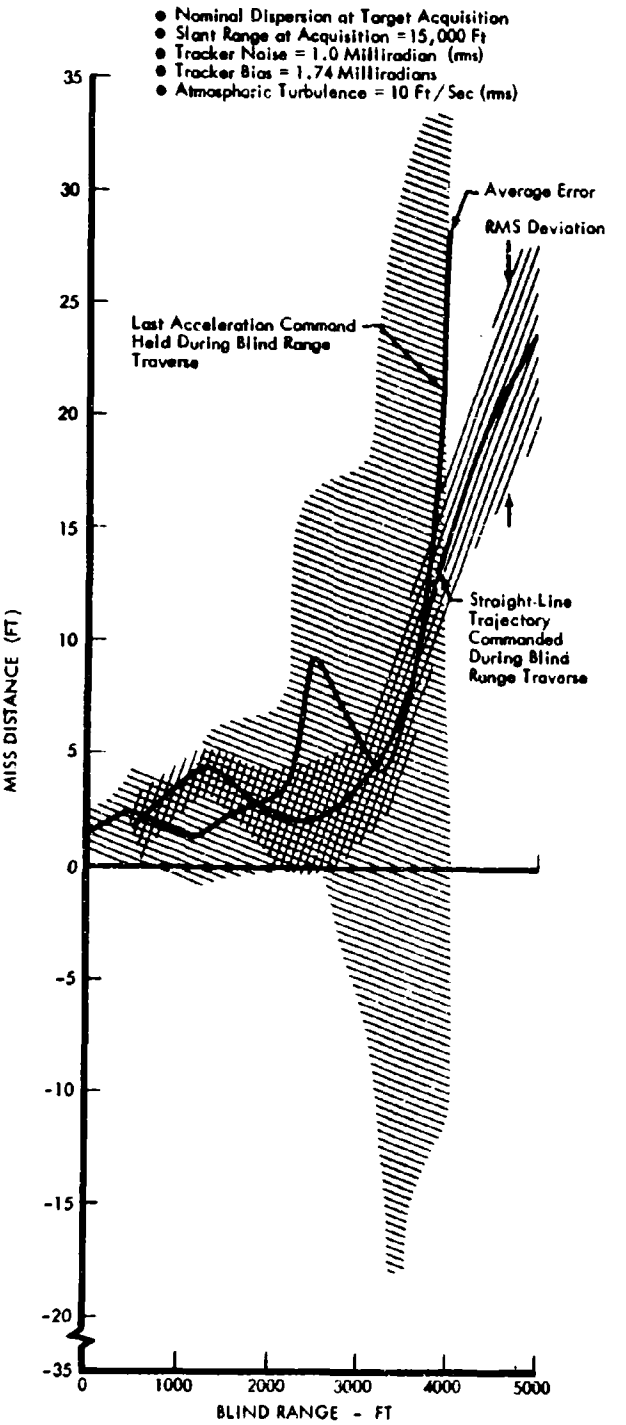

Figure 12: EFFECT OF BLIND RANGE FOR PURSUIT GUIDANCE-SKIP TRAJECTORY

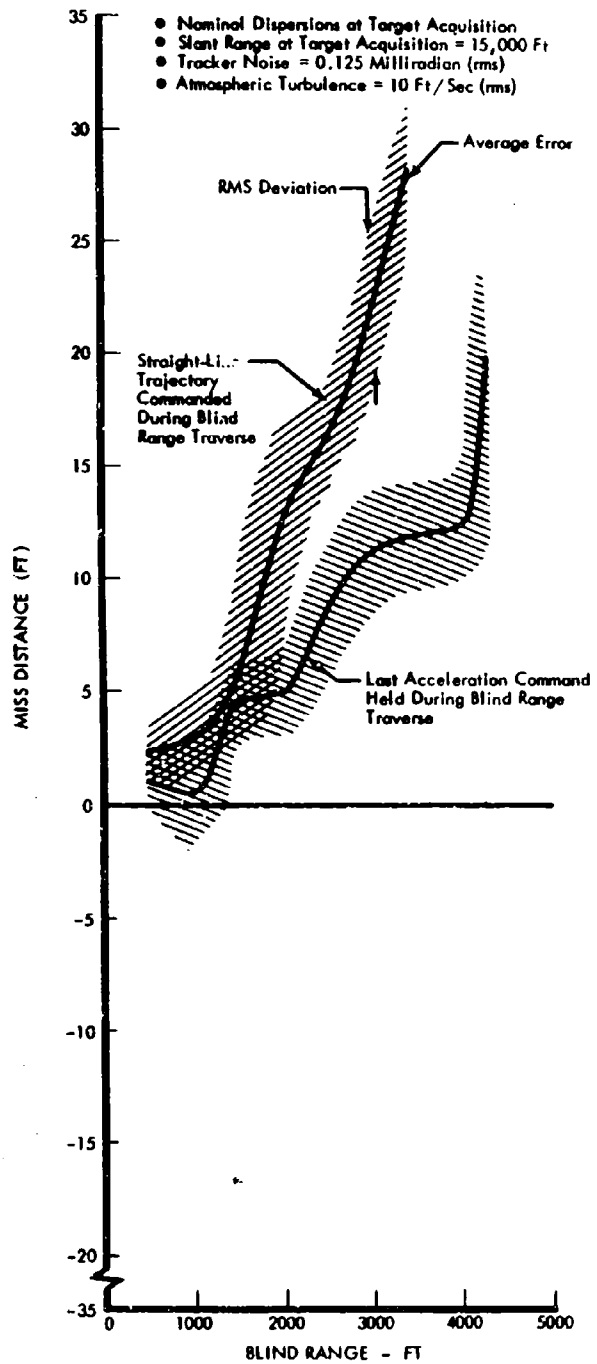

Figure 13: EFFECT OF BLIND RANGE FOR PROPORTIONAL GUIDANCE; LONG-RANGE TRAJECTORY

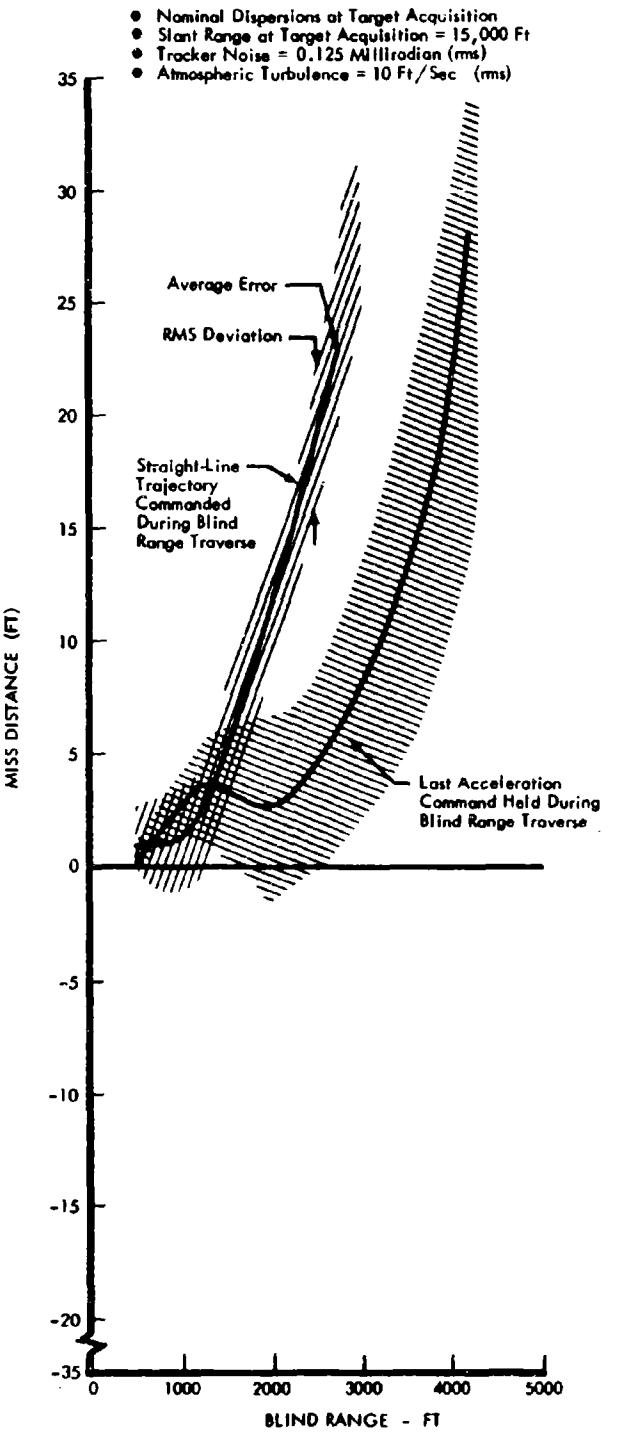

Figure 14: EFFECT OF BLIND RANGE FOR PROPORTIONAL GUIDANCE SKIP TRAJECTORY

included as a disturbance. Two effects are noted when blind range is increased. The average (or arithmetic mean) miss distance is increased. This effect appears to be primarily associated with the initial deviation. Some minimal time is required to reduce initial dispersion and to get the velocity vector directed at the target. This time varies between trajectories and guidance laws, but generally for the 15,000 feet of slant range at acquisition, is accomplished with a minimum of 2000 feet of slant range remaining. Figures 11 through 14 show that appreciable increases in average miss distance do not occur until the blind range is extended beyond 1500 feet. The second effect is the rms deviation about the average miss distance. (The rms deviation is indicated by the shaded areas.) This appears to be the result of dispersion in the acceleration command at the beginning of the blind range caused by turbulence and tracker noise. If the acceleration command is zeroed, rather than held at the value occurring at the beginning of the blind range, the rms deviation is reduced. The only exceptions to this rule occur at blind ranges of 2000 feet or less. At these blind ranges, the difference in rms deviation between holding the last command and setting the command to zero is very small (less than 1.5 feet), and the choice of one mode of command over the other is not critical.

3. Selection of Autopilot. This study was limited to the investigation of one type of autopilot. A normal acceleration autopilot was selected because it provides more direct flight path control than other types (such as an attitude autopilot). By limiting commands to the normal acceleration autopilot, a means of meeting structural load limit requirements is also obtained. The normal acceleration autopilot is compatible with a gimbaled homing sensor. A body fixed homing sensor may require a different type of autopilot if it has a small field of view.

The effect on miss distance of variations in the autopilot response frequency was investigated on a simplified 3-degree-of-freedom simulation and with the 6-degree-of-freedom analog simulation. The simplified studies used a third order autopilot with well damped quadratic poles at 20 radians/sec. With slant ranges and initial position offsets comparable to those used in the 6-degree-of-

freedom error studies, the first order pole could be reduced to 2 radians/sec with no effect on miss distance. A response of one radian/sec resulted in significantly larger miss distance so the autopilot response requirement was initially set at 2 radians/sec.

The effect of autopilot response, as obtained from the 6-degree-of-freedom analog simulation, is shown in Figure 15. The abrupt increase in miss distance below 6 radians/sec is caused by autopilot instability rather than "looseness" of control. In the final detailed autopilot design, the ASM rigid mode poles were significantly lower than the 20 radians/sec anticipated in the preliminary studies. Thus, with guidance loops closed, it was not possible to lower the response below 6 radians/sec without the ASM becoming unstable. Actually, in the nominal Type 1 normal acceleration autopilot simulated, the time response during the terminal phase of the nominal trajectories ranges from 0.1 to 0.17 second. These values were adequate for the range of initial dispersions and slant ranges investigated in this study. However, as mentioned in the discussion of blind range, ASM response (time to remove initial errors), slant range at acquisition, and blind range are very much interrelated. Shorter slant ranges, larger initial errors, and longer blind ranges may require faster autopilot response.

The effect of autopilot steady state error on accuracy was not investigated. Steady state autopilot errors tend to look like changes in guidance gain. Early in the study it was believed that it would be very difficult to obtain small impact errors, and that appreciable steady state autopilot errors could not be tolerated because of anticipated tight tolerances on autopilot gain. From the evaluation of guidance gain in paragraph 1.b. of this section it can be seen that not much tolerance is available for proportional guidance, while pursuit guidance is not quite as critical. A "Type O" autopilot (with constant gain) that was studied had steady state errors to step commands which varied from 2 to 16% during the homing phase. The missile configuration that was used in the study had near neutral aerodynamic stability. Therefore, it was relatively easy to add integral forward loop compensation to remove this steady state error, and at the same

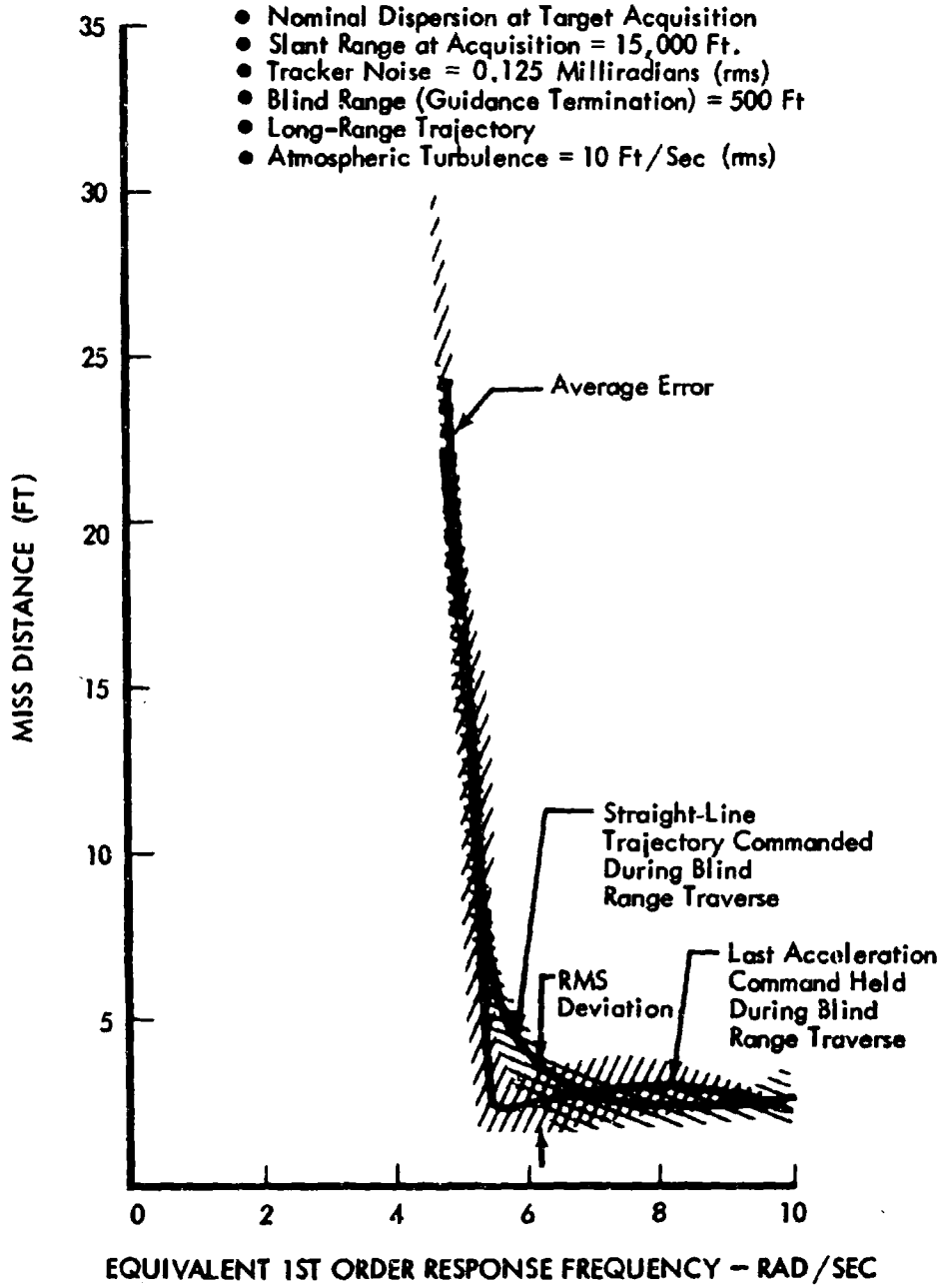

Figure 15: EFFECT OF FIRST ORDER RESPONSE FREQUENCY - PROPORTIONAL GUIDANCE; LONG-RANGE TRAJECTORY

time satisfy the requirements for adequate gain and phase margins. The resulting "Type 1" system had adequate response and damping as noted by the near 0.1 second response during the terminal phase. This relatively easy solution is not possible in all instances, and the effect of steady state autopilot error may be critical for other configurations.

SECTION V

ASM OPTIMAL GUIDANCE

An optimal guidance law for a given ASM is one that yields the minimum mean square miss distance. It gives the best possible performance attainable with the ASM and can serve as a standard of comparison for other guidance laws.

A well-developed theory exists for optimal control of linear systems with random errors. However, real missile systems are nonlinear, and an adequate theory of optimal control is not available for nonlinear systems with random errors. In this study, the realistic nonlinear ASM equations of motion are linearized about a nominal trajectory. Linear random control theory is used to compute the optimal control law for the linearized ASM equations of motion. Because these equations are an accurate approximation of actual nonlinear equations, this control law is a good approximation of the optimal nonlinear ASM control law. The ASM system and system errors considered are described in Section III.

The optimization theory on which the ASM optimal guidance was based states that the optimal guidance law consists of two parts. One is a Kalman optimal filter that supplies the best possible estimate of position and velocity coordinates in the presence of sensor and system noise. The other is an optimal linear feedback control law that converts these estimates into steering commands. This type of guidance system is represented in Figure 16. The Kalman optimal filter and the optimal feedback control law contain sets of time-varying coefficients that are dependent on the nominal trajectory. These coefficients are precomputed and stored in the onboard ASM computer. The performance criterion for the control law was the minimization of the sum of the mean square miss distance and the integral of a quadratic function of the control vector. The form of the guidance law depends on the type of sensors used in the ASM. Optimal guidance laws were considered for an ASM with both a TV tracker and an inertial platform (IMU) and with only a TV tracker.

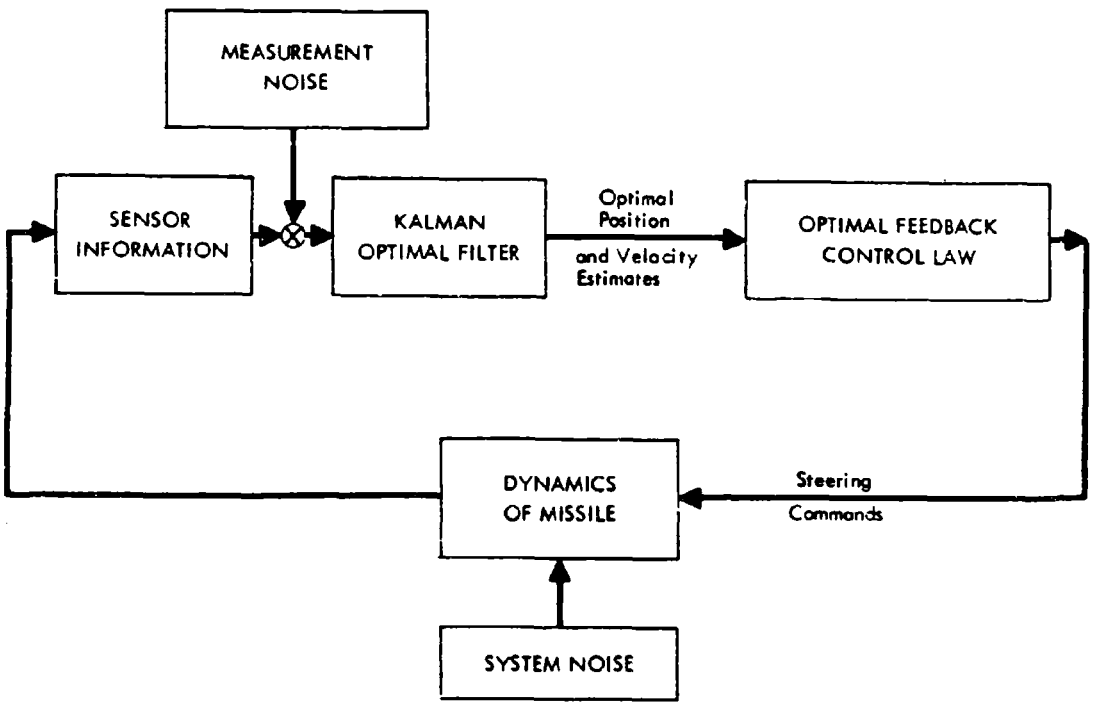

Figure 16: OPTIMAL TERMINAL GUIDANCE

The succeeding sections discuss in detail development of the optimal guidance law and sizing an airborne computer required to implement it, and draw some conclusions regarding the performance of the optimal guidance law.

1. ASM Description. The nominal ASM characteristics are described in Section III. The ASM equations of motion and sensor equations as used in the development of the optimal guidance law are presented in this section.

The ASM was represented as a point mass. The autopilot was considered ideal; i.e., normal acceleration commands are transcribed directly into acceleration of the ASM. Both body fixed and gimbaled TV trackers were considered in providing line-of-sight error information to the optimal guidance laws. ASM acceleration information was obtained with an inertial platform.

a. Equations of Motion. Because the terminal portion of the ASM trajectory is only a few miles, the equations of motion of the ASM are those of a vehicle with lift and drag moving in a constant gravitational field. The ASM coordinate variables are indicated in Figure 17. Expressed in flight path coordinates, the point mass equations of the ASM are:

$$\dot{x} = + V \cos \gamma \cos \chi \tag{10}$$

$$\dot{y} = + V \cos \gamma \sin \chi \tag{11}$$

$$\dot{z} = + V \sin \gamma \tag{12}$$

$$\dot{V} = - \frac{D (\alpha + \Delta\alpha_w, V + \Delta V_w, z)}{m} - g \sin \gamma \tag{13}$$

$$\dot{\chi} = - \frac{L (\alpha + \Delta\alpha_w, V + \Delta V_w, z)}{mV \cos \gamma} \sin (\beta + \Delta\beta_w) \tag{14}$$

$$\dot{\gamma} = + \frac{L (\alpha + \Delta\alpha_w, V + \Delta V_w, z)}{mV} \cos (\beta + \Delta\beta_w) - \frac{g}{V} \cos \gamma. \tag{15}$$

Note that the angle of attack, α, and bank angle, β, defined in Figure 17, are different variables than those usually used in aerodynamic studies. In this analysis, α is the missile body total angle of attack and β the bank angle relative to the

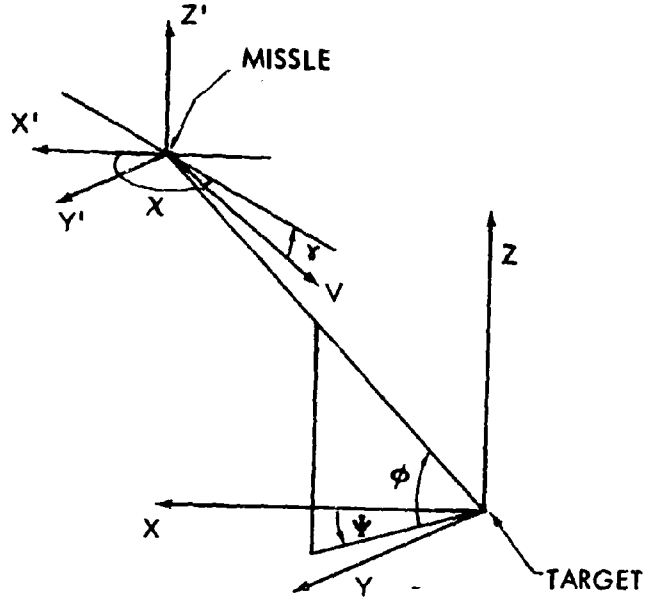

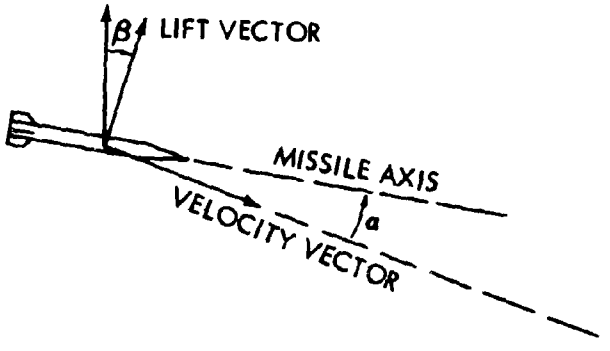

Figure 17: MISSILE TARGET COORDINATES

airstream. The aerodynamic drag (D) and lift (L) forces are expressed as functions of velocity, angle of attack, and Mach number with provisions for the inclusion of wind effects incorporated by the perturbed expressions $V + \Delta V_w$, $\alpha + \Delta\alpha_w$, and $\beta + \Delta\beta_w$.

The functional form of the expressions $L(\alpha, V, z)$ and $D(\alpha, V, z)$ is:

$$L(\alpha, V, z) = \frac{1}{2} \rho(z) V^2 C_L \left(\alpha, \frac{V}{V_s(z)}\right) \bar{S} \tag{16}$$

$$D(\alpha, V, z) = \frac{1}{2} \rho(z) V^2 C_D \left(\alpha, \frac{V}{V_s(z)}\right) \bar{S} \tag{17}$$

In these expressions the air density, ρ, is expressed as a function of altitude by standard ARDC tables; C_L and C_D are tabulated functions of angle of attack and Mach number obtained from wind tunnel data and the velocity of sound, V_s, is expressed as a tabulated function of altitude.

b. TV Tracker. TV trackers measure line-of-sight angles (LOS) to the target. Either body fixed or gimbaled TV trackers can be considered for instrumentation with the optimal guidance system.

A body fixed TV tracker measures the azimuth and elevation of the LOS for a coordinate system fixed in the missile, aligned with the missile axis. This can be combined with missile attitude information to provide measurements of LOS azimuth and elevation for an inertial coordinate system. There will be two types of error in this measurement: a bias error due to a misalignment of the sensor and a noise, which will be assumed to be a white Gaussian noise, due to the effects of target background and the measurement process. If ψ and Φ are the measured LOS azimuth and elevation, the equations for ψ and Φ may be written:

$$\psi = \tan^{-1} \frac{y}{x} + b_1 + N_1, \tag{18}$$

$$\Phi = \tan^{-1}\left(\frac{z}{\sqrt{x^2 + y^2}}\right) + b_2 + N_2 \tag{19}$$

in which b_1 and b_2 are the random biases and N_1 and N_2 are white noises.

In a basic implementation of a gimbaled tracker, the gimbals are inertially rate stabilized. This rate stabilized system is commanded to point at the target with an optical sensor loop that measures the tracker head deviation from the target line of sight. As described in Section III, this tracker was assumed to have a quadratic response. If the azimuth and elevation of the target are designated η_1 and η_2, the following equations represent the gimbaled tracker system:

$$\ddot{\eta}_1 + C_1 \dot{\eta}_1 = C_2\left(\tan^{-1}\frac{y}{x} + N_1 - \eta_1\right), \tag{20}$$

$$\ddot{\eta}_2 + C_3 \dot{\eta}_2 = C_4\left[\tan^{-1}\left(\frac{z}{\sqrt{x^2 + y^2}}\right) + N_2 - \eta_2\right]. \tag{21}$$

The arctangent functions represent, in target coordinates, the optical sensor measurements of tracker head deviation from the target, and C_1 and C_2 represent the traditional quadratic damping and natural frequency terms.

The quantities $y_1(t) = \dot{\eta}_1(t)$ and $y_2(t) = \dot{\eta}_2(t)$ are measured. It is possible to express the LOS angles ψ and Φ in terms of these measurements in the following way. From the definition of $y_1(t)$ and $y_2(t)$

$$\eta_1(t) = \eta_1(t_o) + \int_{t_o}^{t} y_1(s)\, ds \tag{22}$$

and

$$\eta_2(t) = \eta_2(t_o) + \int_{t_o}^{t} y_2(s)\, ds. \tag{23}$$

It follows that

$$\tan^{-1}\frac{y}{x} + N_1 = \frac{1}{C_2}\left(\dot{y}_1 + C_1 y_1\right) + \int_{t_o}^{t} y_1(s)\, ds + \eta_1(t_o) \tag{24}$$

and

$$\tan^{-1}\left(\frac{z}{\sqrt{x^2 + y^2}}\right) + N_2 = \frac{1}{C_4}\left(\dot{y}_2 + C_3 y_2\right) + \int_{t_o}^{t} y_2(s)\, ds + \eta_2(t_o). \tag{25}$$

The initial alignment, $\eta_1(t_o)$, $\eta_2(t_o)$, of the seeker axis is known except for the initial alignment bias errors b_1 and b_2; that is, the quantities $\eta_1(t_o) + b_1$, $\eta_2(t_o) + b_2$ can be measured. This implies that ϕ and Φ may be expressed in terms of the measurement quantities:

$$y_1,\ y_2,\ \dot{y}_1,\ \dot{y}_2,\ \int_{t_o}^{t} y_1(s)\,ds,\ \int_{t_o}^{t} y_2(s)\,ds,\ \eta_1(t_o) + b_1,\ \text{and } \eta_2(t_o) + b_2 \tag{26}$$

by the formulas;

$$\phi = \tan^{-1}\frac{y}{x} + b_1 + N_1$$

$$= \frac{1}{C_2}(\dot{y}_1 + C_1 y_1) + \int_{t_o}^{t} y_1(s)\,ds + \eta_1(t_o) + b_1 \tag{27}$$

and

$$\Phi = \tan^{-1}\left(\frac{z}{\sqrt{x^2 + y^2}}\right) + b_2 + N_2$$

$$= \frac{1}{C_4}(\dot{y}_2 + C_3 y_2) + \int_{t_o}^{t} y_2(s)\,ds + \eta_2(t_o) + b_2. \tag{28}$$

Thus, the optimal filter for a gimbaled TV seeker may also be designed, assuming that ϕ and Φ are measured.

Note that in the gimbaled tracker, the tracker input is assumed to be the difference between the line-of-sight angle plus white noise and the tracker axis angle. The only biases considered are those introduced by error in measurement of the initial alignment $\eta_1(t_o)$ and $\eta_2(t_o)$ of the tracker axis. If there are biases in the input to the tracker, this can be handled, using the same set of equations, by reinterpreting $\eta_1(t)$ and $\eta_2(t)$ as the tracker axis angles plus these biases. Because the derivatives of $\eta_1(t)$ and $\eta_2(t)$ are measured, Equations 27 and 28 hold without change in this situation.

c. Inertial Platform. A conventional inertial platform attempts to measure missile accelerations in a coordinate system fixed in space. If $a_1(t)$, $a_2(t)$, $a_3(t)$ are the measured accelerations, missile position and velocity are obtained

by integrating the equations

$$\begin{pmatrix} \ddot{x} \\ \ddot{y} \\ \ddot{z} \end{pmatrix} = \begin{pmatrix} a_1(t) \\ a_2(t) \\ a_3(t) - g \end{pmatrix} \tag{29}$$

with initial conditions given by initial estimates of position and velocity. The "g" in the equation represents the bias needed to represent the effect of the gravitational acceleration on the vehicle.

The two sources of error in the computation of position and velocity are in the initial estimates of position and velocity, and in the acceleration measurements. The major source of error in the computation of missile positions and velocities from integrating Equation 29 is in the knowledge of the missile's initial position and velocity. The errors in measurement caused by the rotation of the platform, scale factor, and bias are of a lower order of magnitude. This conclusion is substantiated by the inertial platform error analysis studies discussed in Appendix I. For this reason, the acceleration measurements $a_1(t)$, $a_2(t)$, $a_3(t)$ will be treated as exact. This assumption considerably reduces the complexity of the optimal filter implementation.

If measurement bias, scale factor, and platform tilt errors must be taken into account, the true missile accelerations and measured missile accelerations are related by the formula:

$$\begin{pmatrix} \ddot{x} \\ \ddot{y} \\ \ddot{z} \end{pmatrix} = C \begin{pmatrix} a_1(t) - b_1 \\ a_2(t) - b_2 \\ a_3(t) - b_3 \end{pmatrix} - \begin{pmatrix} 0 \\ 0 \\ g \end{pmatrix} \tag{30}$$

In this formula, b_1, b_2, and b_3 are measurement bias errors and C is a matrix that expresses the scale factor errors in measurements and the amount the inertial platform has rotated out of alignment with its desired inertial coordinate system. To take into account the random effects of scale factor and bias errors in the optimal filter, the elements of the matrix C and b_1, b_2, b_3 would have to be introduced as new state variables. This greatly increases the order of the optimal filter equations.

2. Optimal Control of Linear Systems with Gaussian Noises. The techniques used to compute the optimal guidance law will be based on the theory given in Reference 3. These results are summarized in this section.

Let a linear system be defined by:

$$\dot{x} = F(t)x + G(t)u + \zeta(t) , \tag{31}$$

where x(t) is an n-vector of state variables, and u(t) an m-vector of control variables; F(t) and G(t) are known n x n and n x m matrices; $\zeta(t)$ is an n-vector of Gaussian white noises with zero means. The covariance matrix of $\zeta(t)$ is assumed known and given by:

$$E\left\{\zeta(t)\,\zeta(\tau)^T\right\} = Q(t)\,\delta(t-\tau) . \tag{32}$$

The symbol $E\{\ \}$ denotes the expected value of the quantity in the brackets. The quantity $\delta(t-\tau)$ is the Dirac δ-function. Suppose the p-vector

$$y(t) = H(t)\,x(t) + \eta(t) \tag{33}$$

is observed. H(t) is a known p x n matrix and $\eta(t)$ a p-vector of Gaussian white noises with zero means and known covariance matrix

$$E\left\{\eta(t)\,\eta(\tau)^T\right\} = R(t)\,\delta(t-\tau). \tag{34}$$

In addition, the cross correlations of $\zeta(t)$ and $\eta(t)$ are assumed to be given by:

$$E\left\{\zeta(t)\,\eta(\tau)^T\right\} = S(t)\,\delta(t-\tau). \tag{35}$$

Let t_o be the initial and t_1 the final times. Let the performance index be:

$$E\left[\sum_{i,j=1}^{n} a_{i,j}\,x_i(t_1)\,x_j(t_1) + \int_{t_o}^{t_1}\sum_{i,j=1}^{m} b_{i,j}\,u_i(s)\,u_j(s)\,ds\right] \tag{36}$$

The first term in the performance index is a quadratic function of the state vector at the final time, while the second term in the time integral of a quadratic function of the control vector. This performance index penalizes final error and control effort used to achieve the final state.

Consider the problem of choosing u(t) as a function of the past observations:

$$u(t) = U\left[y(s), u(s), t_o \leq s < t \leq t_1\right] \tag{37}$$

so that the performance index is minimized.

THEOREM: Let the matrices R and $M = (b_{ij})$ be positive definite. Then the optimal control law is given by:

$$u(t) = -M^{-1} G^T U\hat{x} \tag{38}$$

in which $\hat{x}$, an estimate of x, is the n-vector output of the filter whose input is the observation vector, y(t), and whose equations are given by:

$$\dot{\hat{x}} = (F - SR^{-1} H - \Sigma H^T R^{-1} H)\,\hat{x} - GM^{-1} G^T U\hat{x} + (SR^{-1} + \Sigma H^T R^{-1})y \tag{39}$$

The quantity U is an n x n matrix which satisfies the differential equations

$$\dot{U} = UGM^{-1} G^T U - UF - F^T U \tag{40}$$

with the terminal condition

$$U(t_1) = (a_{i,j}) \tag{41}$$

The quantity Σ is an n x n matrix which satisfies the differential equation

$$\dot{\Sigma} = -\Sigma H^T R^{-1} H\Sigma + (F - SR^{-1} H)\,\Sigma + \Sigma(F^T - H^T R^{-1} S^T) + Q - SR^{-1} S^T \tag{42}$$

The matrix Σ must satisfy the initial condition

$$\Sigma(t_o) = E\left\{x(t_o)\, x(t_o)^T\right\} \tag{43}$$

Remarks

The optimal feedback control law for the deterministic system with equation

$$\dot{x} = F(t)\, x + G(t)\, u \tag{44}$$

and performance criteria given by

$$\sum_{i,j=1}^{n} a_{i,j}\, x_i(t_1)\, x_j(t_1) + \int_{t_o}^{t_1} \sum_{i,j=1}^{m} b_{i,j}\, u_i(s)\, u_j(s)\, ds \tag{45}$$

is given by

$$u(t) = - M^{-1} G^T U x \tag{46}$$

in which U is a solution of Equation 40. The optimal least squares estimate of the state variables, that is the Kalman-Wiener estimate, for the system

$$\dot{x} = F(t)\, x - G(t)\, M^{-1}\, G(t)^T\, U(t)\, x + \zeta(t) \tag{47}$$

with measurements

$$y(t) = H(t)\, x(t) + \eta(t) \tag{48}$$

is given by $\hat{x}(t)$ which is the solution of Equations 39 and 42.

These two remarks show that the results of the theorem can be stated intuitively by saying: The optimal filter may be computed by ignoring the noises and computing the optimal feedback control law, Equation 46, for the deterministic system. Substitute this control law for the control law of the system and compute the Kalman-Wiener optimal estimates of the state variables, Equation 39. The optimal control law is then obtained by substituting these estimates for the state variables in the deterministic optimal feedback control law.

The matrix $\Sigma(t)$, which is the solution of Equation 42, and is used in defining the filter Equation 39, has another important property. The matrix $\Sigma(t)$ is the covariance matrix of the difference between the state vector, $x(t)$, and the state vector estimate, $\hat{x}(t)$.

3. Application of Optimal Control Theory to ASM Guidance — In this subsection the theory of the previous subsection is applied to determine the equations for the ASM optimal guidance law. The approximations of the system model that are necessary to apply the theory to this problem are carried out. The theory of Section V, 2. implies the optimal guidance law consists of two parts: a Kalman optimal filter, and an optimal feedback control law. The equations that determine each of these are specified. The equations for the optimal filter are obtained for an ASM that uses both a TV tracker and an inertial platform, and an ASM that uses only a TV tracker. Some of the relative advantages of these types of filters are discussed. In one of these filters the equations call for the

derivative of a measurement whose derivative contains white noise. Because it is not practical to instrument a system to compute such a derivative, a procedure is given that avoids the problem.

a. Linearization of the Equations of the ASM. The theory of the preceding section applies to linear systems. In order to apply this theory to the ASM, nominal trajectories were selected and the equations of motion linearized about them. The two different nominal trajectories that were used are discussed in Section III.

Equations 10 through 15 were linearized about the nominal trajectories by approximating the ASM trajectory by the nominal trajectory plus variations from the nominal trajectory. The variations are solutions of the equations:

$$\begin{pmatrix} \delta x \\ \delta y \\ \delta z \\ \delta V \\ \delta \chi \\ \delta \gamma \end{pmatrix} = F(t) \begin{pmatrix} \delta x \\ \delta y \\ \delta z \\ \delta V \\ \delta \chi \\ \delta \gamma \end{pmatrix} + G(t) \begin{pmatrix} \delta \alpha \\ \delta \beta \end{pmatrix} + D(t) \begin{pmatrix} \Delta V_w \\ \Delta \alpha_w \\ \Delta \beta_w \end{pmatrix} \tag{49}$$

in which the matrices $F(t)$, $G(t)$ and $D(t)$ are respectively matrices of partial derivatives of the right sides of Equations 10 through 15 with respect to the state variables, the control variables, and the variations ΔV_w, $\Delta \alpha_w$, $\Delta \beta_w$ due to wind. In the matrices, the partial derivatives are expressed as functions of time by substituting values of the state and control variables of the nominal trajectory at the corresponding time in these expressions. These three matrices of partial derivatives are given in Figures 18, 19, and 20. The approximation of the trajectory by a nominal plus variations from the nominal is a standard technique for approximating a nonlinear system by a linear system. A good approximation is obtained if the actual trajectory is close to the nominal trajectory.

To illustrate the variational equations more concretely, the equation for δx could be obtained as follows: Let $\bar{x}(t)$, $\bar{y}(t)$, $\bar{z}(t)$, $\bar{v}(t)$, $\bar{\chi}(t)$, $\bar{\gamma}(t)$, $\bar{\alpha}(t)$, $\bar{\beta}(t)$ denote the

$$
F(t) = \begin{pmatrix}
0 & 0 & 0 & \cos\gamma\cos\chi & -V\cos\gamma\sin\chi & -V\sin\gamma\cos\chi \\
0 & 0 & 0 & \cos\gamma\sin\chi & V\cos\gamma\cos\chi & -V\sin\gamma\sin\chi \\
0 & 0 & 0 & \sin\gamma & 0 & V\cos\gamma \\
0 & 0 & -\frac{1}{m}\frac{\partial D}{\partial z} & -\frac{1}{m}\frac{\partial D}{\partial V} & 0 & -g\cos\gamma \\
0 & 0 & \frac{-\sin\beta}{mV\cos\gamma}\frac{\partial L}{\partial z} & \left(\frac{-\sin\beta}{mV\cos\gamma}\frac{\partial L}{\partial V}+\frac{L\sin\beta}{mV^2\cos\gamma}\right) & 0 & \frac{L\sin\beta\sin\gamma}{mV\cos^2\gamma} \\
0 & 0 & \frac{\cos\beta}{mV}\frac{\partial L}{\partial z} & \left(\frac{\cos\beta}{mV}\frac{\partial L}{\partial V}-\frac{L\cos\beta}{mV^2}+\frac{g\cos\gamma}{V^2}\right) & 0 & \frac{g}{V}\sin\gamma
\end{pmatrix}
$$

Figure 18: MATRIX F (t) OF INFLUENCE COEFFICIENTS OF THE STATE VARIABLES IN THE LINEARIZED EQUATIONS

$$G(t) = \begin{pmatrix} 0 & 0 \\ 0 & 0 \\ 0 & 0 \\ -\frac{1}{m}\frac{\partial D}{\partial \alpha} & 0 \\ \frac{-\sin\beta}{mV\cos\gamma}\frac{\partial L}{\partial \alpha} & \frac{-L\cos\beta}{mV\cos\gamma} \\ \frac{\cos\beta}{mV}\frac{\partial L}{\partial \alpha} & \frac{-L\sin\beta}{mV\cos\gamma} \end{pmatrix}$$

Figure 19: MATRIX G(t) OF INFLUENCE COEFFICIENTS OF THE CONTROL VARIABLES IN THE LINEARIZED EQUATIONS

$$D(t) = \begin{pmatrix} 0 & 0 & 0 \\ 0 & 0 & 0 \\ 0 & 0 & 0 \\ -\frac{1}{m}\frac{\partial D}{\partial V} & -\frac{1}{m}\frac{\partial D}{\partial \alpha} & 0 \\ \frac{-\sin\beta}{mV\cos\gamma}\frac{\partial L}{\partial V} & \frac{-\sin\beta}{mV\cos\gamma}\frac{\partial L}{\partial \alpha} & \frac{-L}{mV\cos\gamma}\cos\beta \\ \frac{\cos\beta}{mV}\frac{\partial L}{\partial V} & \frac{\cos\beta}{mV}\frac{\partial L}{\partial \alpha} & -\frac{L}{mV}\sin\beta \end{pmatrix}$$

Figure 20: MATRIX D(t) OF INFLUENCE COEFFICIENTS OF WIND VARIATIONS IN THE LINEARIZED EQUATIONS

state and control variables of the nominal trajectory. The first rows of F(t), G(t), and D(t) are the vectors

$$\left[0,\ 0,\ 0,\ \cos\bar{\gamma}(t)\cos\bar{\chi}(t),\ -\bar{V}(t)\cos\bar{\gamma}(t)\sin\bar{\chi}(t),\ -\bar{V}(t)\sin\bar{\gamma}(t)\cos\bar{\chi}(t)\right], \quad (50)$$

$$\left[0,\ 0\right] \text{ and } \left[0,\ 0,\ 0\right]$$

Hence the equation for $\dot{\delta x}$ is given by:

$$\dot{\delta x} = \cos\bar{\gamma}(t)\cos\bar{\chi}(t)\,\delta V(t) - \bar{V}(t)\cos\bar{\gamma}(t)\sin\bar{\chi}(t)\,\delta\chi(t) \quad (51)$$

$$- \bar{V}(t)\sin\bar{\gamma}(t)\cos\bar{\chi}(t)\,\delta\gamma(t)$$

b. Performance Index. To use the theory of Section V.2, the performance index must be a quadratic function of the state variables at the final time plus the integral of a positive definite quadratic form in the control variables. The true miss distance of the ASM is the distance along the ground from the impact point to the target. The final time is considered to be the time when the nominal trajectory hits the target. The magnitude of the position deviation of the actual trajectory from the nominal trajectory at this time does not give the true miss distance. Suppose the position deviation at this time is resolved into a vector parallel to the nominal trajectory and a vector perpendicular to the nominal trajectory. The true miss distance may be approximated by the magnitude of the deviation perpendicular to the nominal trajectory times the cosine of the angle the nominal trajectory makes with the ground.

A trajectory with a nonzero component of deviation parallel to the nominal trajectory will have approximately the same miss distance as one with a zero component. Because the ASM velocity vector will be nearly aligned with the nominal trajectory near the target, this component of position deviation will not contribute significantly to the miss distance.

Based on this reasoning, the performance criterion will be taken to be the expected value of the square of the component of deviation perpendicular to nominal trajectory at the final time plus the integral of a constant multiple of the sum of squares of angle of attack and bank angle. (The reciprocal of the cosine of the angle the nominal trajectory makes with the ground has been incorporated

into the constant multiple.) It is necessary to have the integral term in the control variables in the performance criterion in order to ensure that a solution exists. The constant multiple of this factor was chosen to make this factor small compared to the perpendicular component of deviation. This implies that the dominant term in the performance criterion is the square of the perpendicular component of deviation. This performance criterion is given by the expected value of the expression:

$$\left(\delta x(t_1) \sin \bar{\gamma}(t_1) - \delta z(t_1) \cos \bar{\gamma}(t_1)\right)^2 + \delta y(t_1)^2 + a \int_{t_o}^{t_1} \left(\delta\alpha(s)^2 + \delta\beta(s)^2\right) ds \tag{52}$$

c. Computation of the Optimal Feedback Control Law. The theorem of Reference 3 that is stated in Section V.2 asserts that the optimal feedback control law for system (31) with performance criteria, Equation 52, is given by:

$$\begin{pmatrix} \delta\alpha \\ \delta\beta \end{pmatrix} = - M^{-1} G^T U \begin{pmatrix} \delta x \\ \delta y \\ \delta z \\ \delta V \\ \delta\chi \\ \delta\gamma \end{pmatrix} \tag{53}$$

in which U is the solution of the matrix differential equation

$$\dot{U} = UGM^{-1} G^T U - UF - F^T U \tag{54}$$

with terminal condition

$$U(t_1) = \begin{pmatrix} \sin^2 \bar{\gamma}(t_1) & 0 & - \sin \bar{\gamma}(t_1) \cos \bar{\gamma}(t_1) & 0 & 0 & 0 \\ 0 & 1 & 0 & 0 & 0 & 0 \\ - \sin \bar{\gamma}(t_1) \cos \bar{\gamma}(t_1) & 0 & \cos^2 \bar{\gamma}(t_1) & 0 & 0 & 0 \\ 0 & 0 & 0 & 0 & 0 & 0 \\ 0 & 0 & 0 & 0 & 0 & 0 \\ 0 & 0 & 0 & 0 & 0 & 0 \end{pmatrix} \tag{55}$$

The matrix, M, of Equations 53 and 54 is a 2 x 2 diagonal matrix with the constant "a" of the performance criteria in each diagonal position. The only unknown quantity in Equation 53 is the matrix U(t), which must be computed by numerically integrating Equation 54.

In Figures 21, 22, and 23, typical nonzero coefficients of the optimum control law are given. The variation in angle of attack is a linear sum of these coefficients times the variations in the state variables.

The coefficients illustrated are the elements of the first row of the matrix $-M^{-1}G^{T}U$ given in Equation 53. Because there is a wide variation in the values of these coefficients, they have been plotted with a scale change.

The coefficients are relatively small until near the time the nominal trajectory reaches the target. Part of this behavior may be accounted for by noting that if there is still a position deviation just prior to the terminal time, a large control force is needed to correct it. As the terminal time is approached, the coefficients approach zero. This may be explained by noting that very close to the terminal time there is not sufficient time left to make an appreciable position correction. Hence, the controller merely minimizes the integral term in performance criterion, Equation 36, by letting the control approach zero.

d. Optimal Guidance Filter. The optimal filter depends on the type of sensors used on the missile. In the following discussion, the application of the theory of Reference 3 to two combinations of sensors will be discussed. An optimal filter based on measurements from both a TV tracker and an inertial platform will give better estimates of position than one based only on a TV tracker. Because an optimal filter based on a TV tracker alone would be less expensive to implement, and could be designed in a simple way from the theory in Section V.2, both types of filters are discussed in the following sections.

(1) Optimal Filter Based on a TV Tracker. In Section V.1.b., it was shown that either a body fixed wide angle field of view or a gimbaled narrow field of

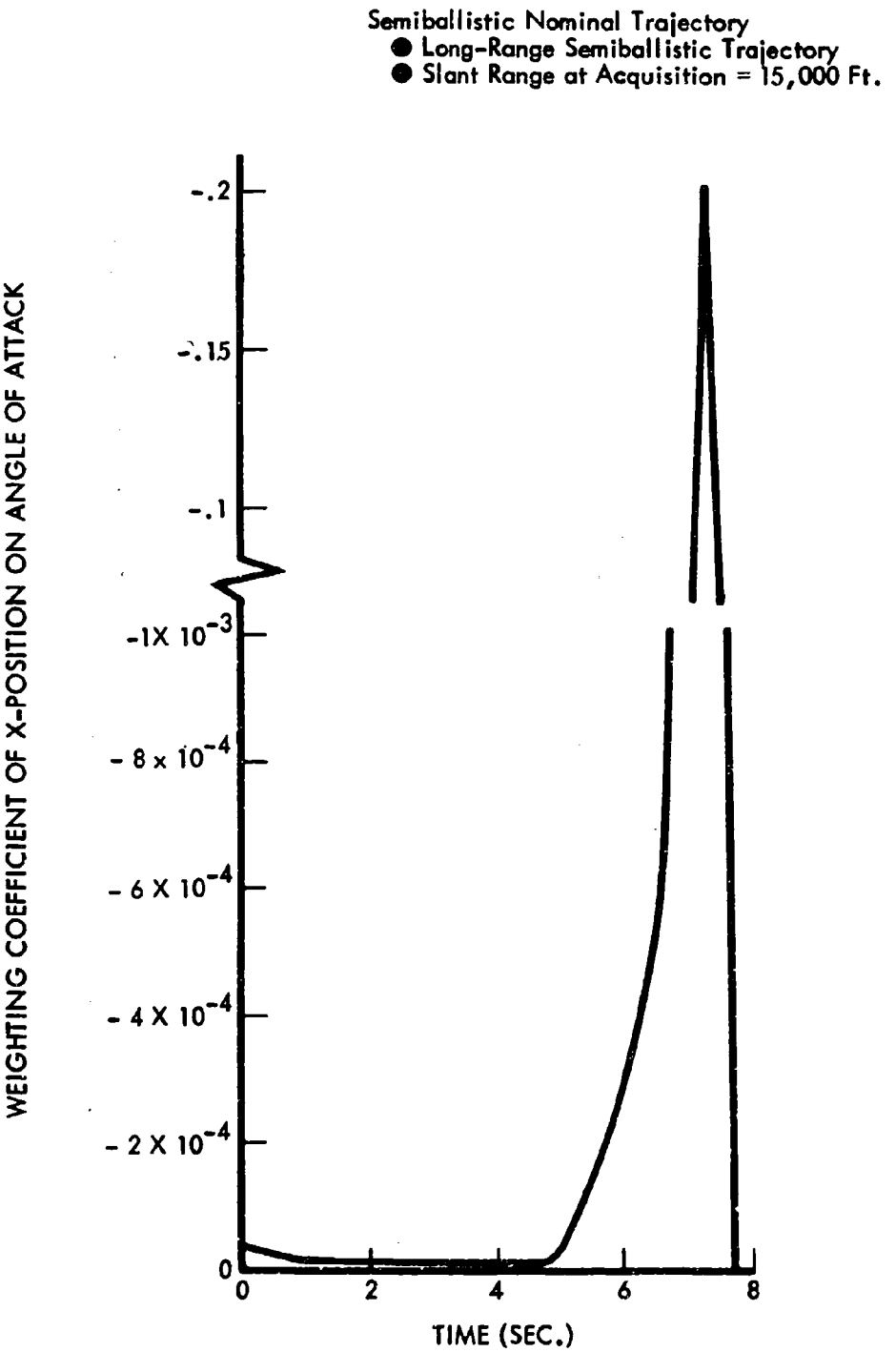

Figure 21: OPTIMAL CONTROL LAW WEIGHTING COEFFICIENT

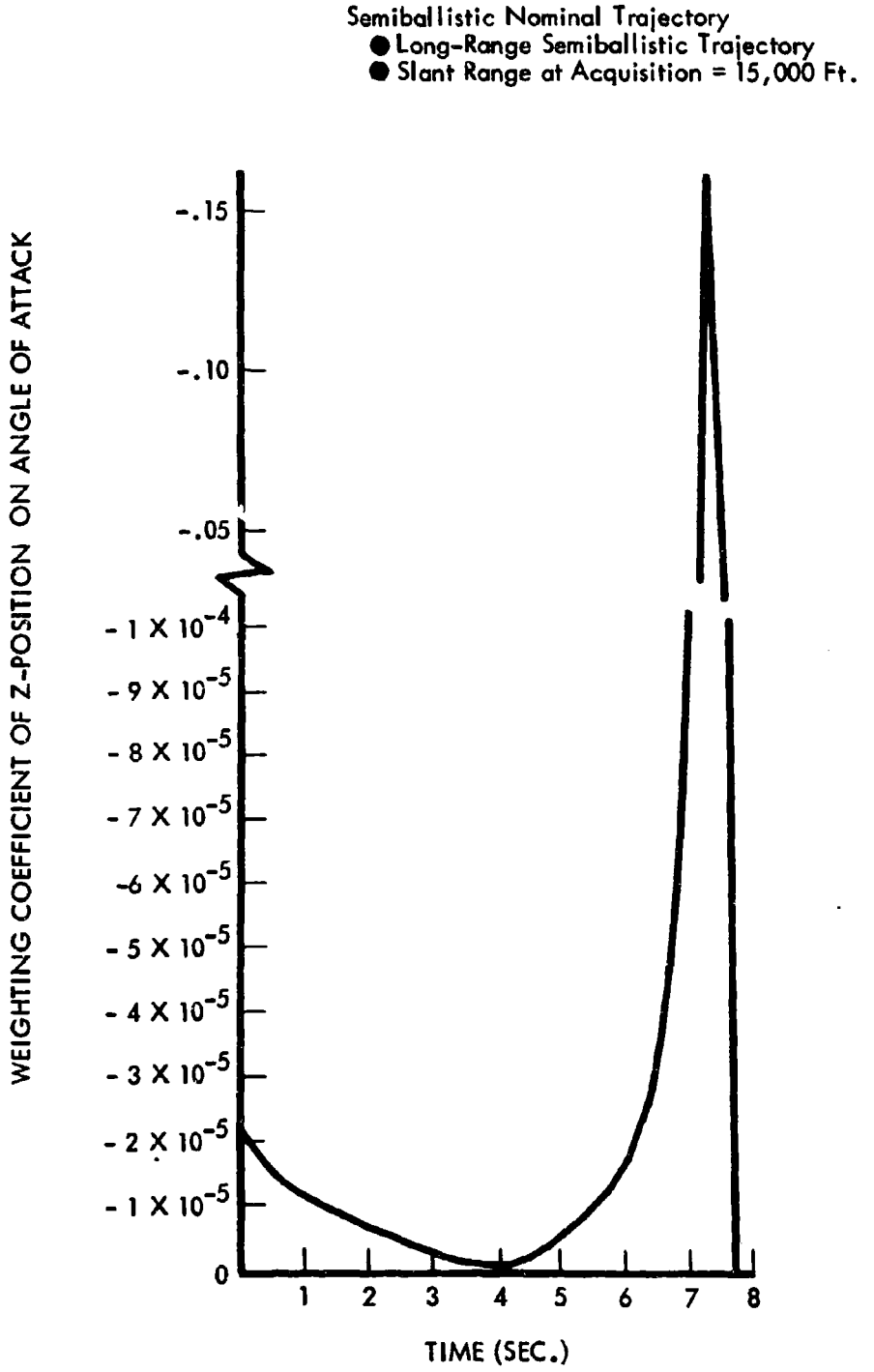

Figure 22: OPTIMAL CONTROL LAW WEIGHTING COEFFICIENT

Semiballistic Nominal Trajectory
- Long-Range Semiballistic Trajectory
- Slant Range at Acquisition = 15,000 Ft.

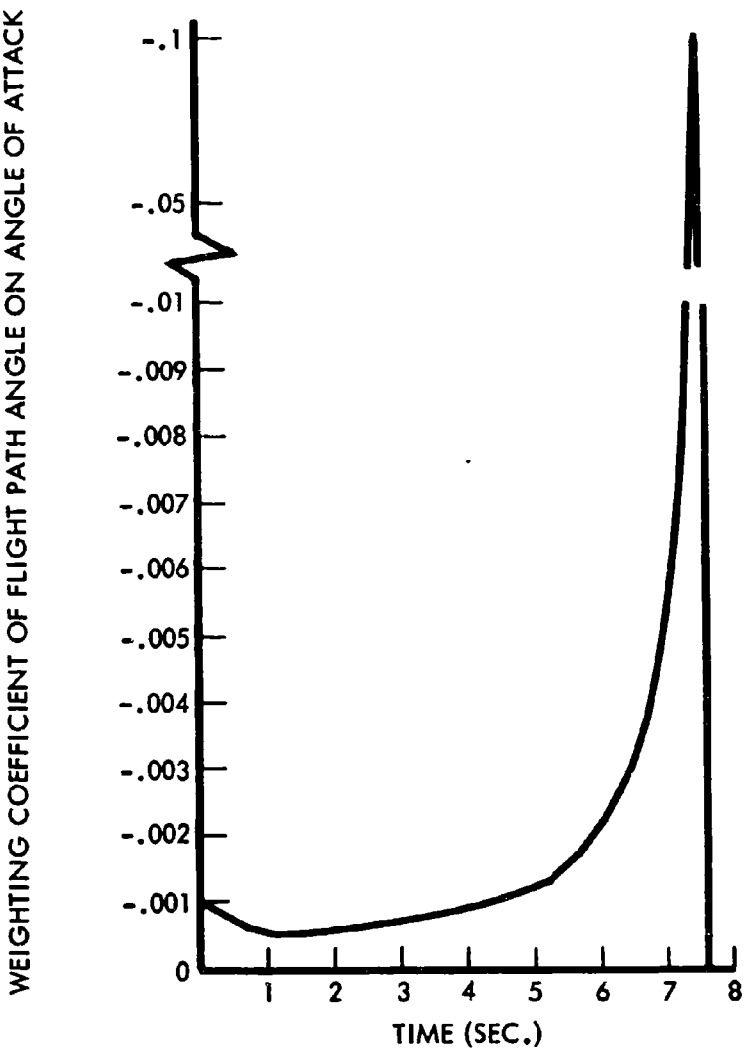

Figure 23: OPTIMAL CONTROL LAW WEIGHTING COEFFICIENT

view TV tracker may be used to produce measurements of line-of-sight azimuth and elevation angles with additive biases and Gaussian white noises. The equations of these measurements:

$$\psi = \tan^{-1} \frac{y}{x} + b_1 + N_1$$

$$\Phi = \tan^{-1} \frac{z}{\sqrt{(x^2 + y^2)}} + b_2 + N_2 \tag{56}$$

in which b_1 and b_2 are random biases with;

$$\dot{b}_1 = \dot{b}_2 = 0 \tag{57}$$

and N_1 and N_2 are Gaussian white noises with mean zero and covariance matrix;

$$R(t) = \begin{pmatrix} E\left\{ N_1(t)^2 \right\} & E\left\{ N_1(t)\, N_2(t) \right\} \\ E\left\{ N_2(t)\, N_1(t) \right\} & E\left\{ N_2(t)^2 \right\} \end{pmatrix}. \tag{58}$$

These line-of-sight measurement equations were linearized about the nominal trajectory to obtain measurements that are linear in the variations from the nominal trajectory. When this is done the equations,

$$\begin{aligned} \delta\psi &= A_1(t)\, \delta x + A_2(t)\, \delta y + b_1 + N_1 \\ \delta\Phi &= B_1(t)\, \delta x + B_2(t)\, \delta y + B_3(t)\, \delta z + b_2 + N_2 \end{aligned} \tag{59}$$

are obtained. $A_i(t)$ and $B_i(t)$ are the partial derivatives of the appropriate arctangent expressions evaluated on the nominal trajectory. In order to apply the theory of Section V.2, the biases b_1 and b_2 are considered as extra state variables and the equations $\dot{b}_1 = 0$ and $\dot{b}_2 = 0$ are added to the equations of motion. Let $H(t)$ denote the matrix

$$H(t) = \begin{pmatrix} A_1(t) & A_2(t) & 0 & 0 & 0 & 0 & 1 & 0 \\ B_1(t) & B_2(t) & B_3(t) & 0 & 0 & 0 & 0 & 1 \end{pmatrix}. \tag{60}$$

Let ΔV_w, $\Delta\alpha_w$, $\Delta\beta_w$ be the vector of white noises which represents the three components of force on the missile caused by winds. Let the 3 x 3 covariance matrix of these white noises be denoted by $Q(t)$.

From Theorem 1, Section V.2, Equations 39 and 42, it is seen that the optimal filter satisfies the equations:

$$\begin{pmatrix} \dot{\hat{\delta x}} \\ \dot{\hat{\delta y}} \\ \dot{\hat{\delta z}} \\ \dot{\hat{\delta V}} \\ \dot{\hat{\delta \gamma}} \\ \dot{\hat{\delta \chi}} \\ \dot{\hat{b}}_1 \\ \dot{\hat{b}}_2 \end{pmatrix} = \left(\begin{array}{c|c} F-GM^{-1}G^T U & 0 \\ \hline 0 & 0 \end{array}\right) \begin{pmatrix} \hat{\delta x} \\ \hat{\delta y} \\ \hat{\delta z} \\ \hat{\delta V} \\ \hat{\delta \gamma} \\ \hat{\delta \chi} \\ \hat{b}_1 \\ \hat{b}_2 \end{pmatrix} \tag{61}$$

$$+ K(t) \begin{pmatrix} \delta\psi - A_1(t)\,\hat{\delta x} - A_2(t)\,\hat{\delta y} - \hat{b}_1 \\ \delta\Phi - B_1(t)\,\hat{\delta x} - B_2(t)\,\hat{\delta y} - B_3(t)\,\hat{\delta z} - \hat{b}_2 \end{pmatrix}$$

The matrix right of the equal sign is indicated in terms of submatricies. This notation is used frequently in succeeding sections.
The hat symbols are used to denote estimated values. The expression K (t) is given by:

$$K(t) = \Sigma(t)\, H(t)^T\, R(t)^{-1} \tag{62}$$

The matrix Σ is the solution of the equation:

$$\dot{\Sigma} = -\Sigma H^T R^{-1} H\Sigma + F\Sigma + \Sigma F^T + DQD^T\ . \tag{63}$$

Note that if the vehicle was at the position

$$\begin{pmatrix} x(t) + \delta x \\ y(t) + \delta y \\ z(t) + \delta z \\ V(t) + \delta V \\ \gamma(t) + \delta\gamma \\ \chi(t) + \delta\chi \\ b_1 \\ b_2 \end{pmatrix} \tag{64}$$

using the control law:

$$\begin{pmatrix} \alpha\ (t) \\ \beta\ (t) \end{pmatrix} = \begin{pmatrix} \bar{\alpha}\ (t) \\ \bar{\beta}\ (t) \end{pmatrix} + M^{-1}\ G^T\ U \begin{pmatrix} \delta x \\ \delta y \\ \delta z \\ \delta V \\ \delta \gamma \\ \delta \chi \end{pmatrix} \tag{65}$$

and the wind variations ΔV_w, $\Delta \alpha_w$, and $\Delta \beta_w$ were zero, the linearized equations of motion, Equation 49, imply that the derivatives of the variations, δx, δy, etc., are given by:

$$\begin{pmatrix} \dot{\delta x} \\ \dot{\delta y} \\ \dot{\delta z} \\ \dot{\delta V} \\ \dot{\delta \gamma} \\ \dot{\delta \chi} \\ \dot{b}_1 \\ \dot{b}_2 \end{pmatrix} = \left(\begin{array}{c|c} F(t) - G(t) M^{-1}(t) G^T(t) U(t) & 0 \\ \hline 0 & 0 \end{array}\right) \begin{pmatrix} \delta x \\ \delta y \\ \delta z \\ \delta V \\ \delta \gamma \\ \delta \chi \\ b_1 \\ b_2 \end{pmatrix} \tag{66}$$

Hence, Equation 66, with the variation δx, δy, etc. replaced by these estimated values $\hat{\delta x}$, $\hat{\delta y}$, etc., is the estimated value of this derivative based on past observations.

The expression

$$K\ (t) \begin{pmatrix} \delta \psi - A_1\ (t) \hat{\delta x} - A_2\ (t) \hat{\delta y} - \hat{b}_1 \\ \delta \Phi - B_1\ (t) \hat{\delta x} - B_2\ (t) \hat{\delta y} - B_3\ (t) \hat{\delta z} - \hat{b}_2 \end{pmatrix} \tag{67}$$

is a weighting by the matrix K (t) of the difference between the actual measured variations in line-of-sight angles and estimates for these quantities based on past observations. These two quantities are added together in Equation 61 to produce the derivative of the estimates of the deviations.

(2) Optimal Filter Based TV Tracker and Inertial Platform. In Section V.1.c, a discussion of inertial platform measurements is given. The conclusion of this discussion is that the platform accelerations should be treated as exactly measured quantities. The equations for the missile accelerations may be written:

$$\ddot{x} = a_1(t) \quad \ddot{y} = a_2(t) \quad \ddot{z} = a_3(t) \tag{68}$$

in which $a_1(t)$, $a_2(t)$, and $a_3(t)$ are the three measured missile accelerations in an inertial coordinate system. Because these measurements are exact, no additive white noises are involved in them. Thus, they do not exactly fit the theory given in Section V.2. To handle this situation, the Kalman optimal estimate of the positions and velocities will be computed in a different manner using techniques from Reference 4. A similar situation in a simpler case is discussed in Reference 4, Pages 78 to 82.

Because exact measurements of the missile accelerations are being made, the expressions for the accelerations given by the equations of motion are redundant. Thus, measured accelerations of the platform will be used to replace the equations of motion. The equations for the missile accelerations and line-of-sight measurements are given by:

$$\ddot{x} = a_1(t) \tag{69}$$

$$\ddot{y} = a_2(t) \tag{70}$$

$$\ddot{z} = a_3(t) - g \tag{71}$$

$$\psi = \tan^{-1}\frac{y}{x} + b_1 + N_1 \tag{72}$$

$$\Phi = \tan^{-1}\frac{z}{\sqrt{(x^2 + y^2)}} + b_2 + N_2 \tag{73}$$

The Kalman optimal filter for this system will be computed considering Equations 69, 70, and 71 as equations of motion and Equations 72 and 73 as measurements.

To apply the theory of Reference 4, Pages 54 - 55, formulas 11c and 111c, the equations must be linear, first order, homogeneous equations. Let $\tilde{x}(t)$, $\tilde{y}(t)$,

$\tilde{z}$ (t), $\tilde{u}$ (t), $\tilde{v}$ (t), and $\tilde{w}$ (t) denote the positions and velocities in a rectangular coordinate system of an object whose initial position and velocity are the same as the initial estimates of the missile's position and velocity and is acted on by accelerations a_1 (t), a_2 (t), a_3 (t) - g. Let x (t), y (t), z (t), u (t), v (t), and w (t) denote the actual positions and velocities of the missile. Denote x (t) - $\tilde{x}$ (t), y (t) - $\tilde{y}$ (t), etc., by $\tilde{\delta}x$, $\tilde{\delta}y$, etc. Then the equations

$$\begin{aligned} \dot{\tilde{\delta}}x &= \tilde{\delta}u \quad \dot{\tilde{\delta}}u = 0 \quad \dot{b}_1 = 0 \\ \dot{\tilde{\delta}}y &= \tilde{\delta}v \quad \dot{\tilde{\delta}}v = 0 \quad \dot{b}_2 = 0 \\ \dot{\tilde{\delta}}z &= \tilde{\delta}w \quad \dot{\tilde{\delta}}w = 0 \end{aligned} \tag{74}$$

are satisfied. Equations 59 are approximately valid with δx, δy, δz, replaced by $\tilde{\delta}x$, $\tilde{\delta}y$, $\tilde{\delta}z$.

From Equations 11c and 111c of Reference 4, Page 54, the optimal estimates of $\tilde{\delta}x$, $\tilde{\delta}y$, etc., satisfy the equations

$$\begin{pmatrix} \dot{\hat{\delta}}x \\ \dot{\hat{\delta}}y \\ \dot{\hat{\delta}}z \\ \dot{\hat{\delta}}u \\ \dot{\hat{\delta}}v \\ \dot{\hat{\delta}}w \\ \dot{\hat{b}}_1 \\ \dot{\hat{b}}_2 \end{pmatrix} = \begin{pmatrix} \hat{\delta}u \\ \hat{\delta}v \\ \hat{\delta}w \\ 0 \\ 0 \\ 0 \\ 0 \\ 0 \end{pmatrix} + K(t) \begin{pmatrix} \delta\psi - A_1(t)\,\hat{\delta}x - A_2(t)\,\hat{\delta}y - \hat{b}_1 \\ \delta\Phi - B_1(t)\,\hat{\delta}x - B_2(t)\,\hat{\delta}y - B_3(t)\,\hat{\delta}z - \hat{b}_2 \end{pmatrix}. \tag{75}$$

The weighting matrix K (t) is given by:

$$K(t) = \Sigma(t)\, H^T(t)\, R^{-1}(t)\ . \tag{76}$$

The 8 x 8 matrix Σ (t) satisfies the differential equation

$$\dot{\Sigma} = F\Sigma + \Sigma F^T - \Sigma H^T R^{-1} H\Sigma \tag{77}$$

in which,

$$F = \begin{pmatrix} 0 & 0 & 0 & 1 & 0 & 0 & 0 & 0 \\ 0 & 0 & 0 & 0 & 1 & 0 & 0 & 0 \\ 0 & 0 & 0 & 0 & 0 & 1 & 0 & 0 \\ 0 & 0 & 0 & 0 & 0 & 0 & 0 & 0 \\ 0 & 0 & 0 & 0 & 0 & 0 & 0 & 0 \\ 0 & 0 & 0 & 0 & 0 & 0 & 0 & 0 \\ 0 & 0 & 0 & 0 & 0 & 0 & 0 & 0 \\ 0 & 0 & 0 & 0 & 0 & 0 & 0 & 0 \end{pmatrix} \tag{78}$$

Letting $\hat{x}(t) = \tilde{x}(t) + \hat{\delta x}(t)$, $\hat{y}(t) = \tilde{x}(t) + \hat{\delta x}(t)$, the equation of the filter may be expressed in terms of $\hat{x}$, $\hat{y}$, ... by:

$$\begin{pmatrix} \dot{\hat{x}} \\ \dot{\hat{y}} \\ \dot{\hat{z}} \\ \dot{\hat{u}} \\ \dot{\hat{v}} \\ \dot{\hat{w}} \\ \dot{\hat{b}}_1 \\ \dot{\hat{b}}_2 \end{pmatrix} = \begin{pmatrix} \hat{u} \\ \hat{v} \\ \hat{w} \\ a_1(t) \\ a_2(t) \\ a_3(t) - g \\ 0 \\ 0 \end{pmatrix} + K(t) \begin{pmatrix} \phi - \hat{b}_1 - \tan^{-1}\dfrac{\hat{y}}{\hat{x}} \\ \Phi - \hat{b}_2 - \tan^{-1}\dfrac{\hat{z}}{\sqrt{\left(\hat{x}^2 + \hat{y}^2\right)}} \end{pmatrix} \tag{79}$$

(3) Discussion of Optimal Filters. In the filter based on the tracker and IMU, exact measurements are used for the derivatives of the estimated velocities. In the filter based on the tracker, these accelerations were estimated using past estimates of the missile's position and velocity and the equations of motion. The filter for the tracker and IMU should give better estimates in that there will not be an accumulation of error from the estimation of accelerations as in the filter for the tracker only. In the filter for the tracker and IMU, the effects of winds are taken directly into account by the measured missile accelerations.

Note that in the filter for the tracker and IMU, Equation 77 for the matrix Σ does not involve the covariance matrix, Q, of the winds, while in Equation 63,

concerning the filter for the ASM with tracker only, the matrix DQD^T appears as an additive term. The matrix Σ is the covariance matrix of the difference between the true and estimated position deviations. An extra nonnegative term, DQD^T, in the derivative of this quantity will make the covariances larger. Notice, though, that a precise comparison of the two covariance matrices, Σ, cannot be made on this basis because the F matrices in Equations 77 and 63 are different.

In each of these filters discussed, the biases b_1 and b_2 in the line-of-sight angle measurements are estimated. These quantities are called boresight errors. In a conventional tracking seeker the angular rate of turning of the seeker axis is used as an estimate of the angular rate of change of the line of sight. This quantity is used primarily to eliminate the boresight error problem.

Both the estimate of line-of-sight angle rate from tracker axis rate and the estimate of bias error in the optimal filter will have a transient response. The transient response of the axis rate estimate will be due to the tracker dynamics. The transient responses in the estimates of the biases are governed by the filter equations. Estimating the biases with the filter equations has the advantage that the errors due to the response of the tracker to missile motions are eliminated.

In instrumenting the filter when a gimbaled TV tracker is used, a difficulty is encountered in that to compute ψ and Φ, the measurements y_1 and y_2 of Section V.1.b must be differentiated. The derivatives of y_1 and y_2 contain white noise. It is not practical to instrument a device to obtain such derivatives. This difficulty may be avoided by using a technique suggested in Reference 5. This technique, as applied to the present situation, follows. The equations of the optimal filter are given by Equation 79.

Define new variables by the formula:

$$\begin{pmatrix} x^* \\ y^* \\ z^* \\ u^* \\ v^* \\ w^* \\ b_1^* \\ b_2^* \end{pmatrix} = \begin{pmatrix} \hat{x} \\ \hat{y} \\ \hat{z} \\ \hat{u} \\ \hat{v} \\ \hat{w} \\ \hat{b}_1 \\ \hat{b}_2 \end{pmatrix} - K(t) \begin{pmatrix} y_1/c_2 \\ y_2/c_4 \end{pmatrix} \tag{80}$$

in which y_1 and y_2 are the measured tracker angle rates that are defined in Section V.1.b and K (t) is the matrix given by Equation 76.

Then, using Equations 79 and 80 and eliminating $\psi - \dot{y}_1/c_2$ and $\Phi - \dot{y}_2/c_4$ by use of Equations 27 and 28:

$$\begin{pmatrix} \dot{x}^* \\ y^* \\ z^* \\ u^* \\ v^* \\ w^* \\ b_1^* \\ b_2^* \end{pmatrix} = \begin{pmatrix} \hat{u} \\ \hat{v} \\ \hat{w} \\ a_1(t) \\ a_2(t) \\ a_3(t) - g \\ 0 \\ 0 \end{pmatrix} + K(t) \begin{pmatrix} \frac{c_1}{c_2} y_1 + \int_{t_o}^{t} y_1(s)\, ds + \eta_1(t_o) + b_1 \\ \frac{c_3}{c_4} y_2 + \int_{t_o}^{t} y_2(s)\, ds + \eta_2(t_o) + b_2 \end{pmatrix}$$

$$- \dot{K}(t) \begin{pmatrix} y_1/c_2 \\ y_2/c_4 \end{pmatrix} - K(t) \begin{pmatrix} \tan^{-1} \frac{\hat{y}}{\hat{x}} + \hat{b}_1 \\ \tan^{-1} \left(\frac{\hat{z}}{\sqrt{\hat{x}^2 + \hat{y}^2}} \right) + \hat{b}_2 \end{pmatrix} \tag{81}$$

The hatted quantities may be eliminated from the right side of Equation 81 by using Equation 80. Thus, a filter for the starred variables is obtained whose inputs are y_1, y_2, $\int_{t_o}^{t} y_1(s)\,ds$, $\int_{t_o}^{t} y_2(s)\,ds$, $\eta_1(t_o) + b_1$, and $\eta_2(t_o) + b_2$. Thus, derivatives of y_1 and y_2 are not involved as inputs to this filter. Equation 80 implies that the desired estimates are obtained by adding $K(t)\begin{pmatrix} y_1/c_2 \\ y_2/c_4 \end{pmatrix}$ to the output of this filter.

A set of typical weighting factors for the optimal filter are plotted in Figures 24 and 25. These weighting factors are the elements of the matrix K (t) defined by Equation 76, and used in the optimal filter, Equation 79. Examination of the right side of Equation 79 shows that the matrix K (t) gives the relative weighting of the two bracketed vector quantities on the right side of this equation in the derivative of the position and velocity estimates. The nonzero elements of the first vector in the right-hand side of Equation 79 are the estimated ASM velocity components and the measured ASM acceleration components. The second vector is the difference between the estimated and measured line-of-sight angles. The matrix K (t) is the "assignment of relative importance of these quantities" in the derivative of estimated position and velocity.

In Figure 26 the weighting coefficient of line-of-sight azimuth on y velocity is plotted for each of the three nominal trajectories used to illustrate the dependence of a typical weighting coefficient on the nominal trajectory.

4. Optimal Navigation Implementation. To discuss the implementation of the optimal navigation system, consider the case in which both an inertial platform and a gimbaled TV tracker are used as sensors by the ASM. In the cases in which the gimbaled tracker is replaced by a body fixed tracker or the inertial platform omitted, the equations of the optimal navigation system are much simpler.

Equations 80 and 81 give the optimal filter and Equation 53 the optimal control law. These make up the optimal navigation system. In implementing this system, the inertial platform acceleration measurements $a_1(t)$, $a_2(t)$, $a_3(t)$, the TV tracker line-of-sight angle rates $y_1(t)$, $y_2(t)$, and the measurement of initial tracker angles $\eta_1(t_o) + b_1$, $\eta_2(t_o) + b_2$, are inputs to the differential Equations 81. Initial

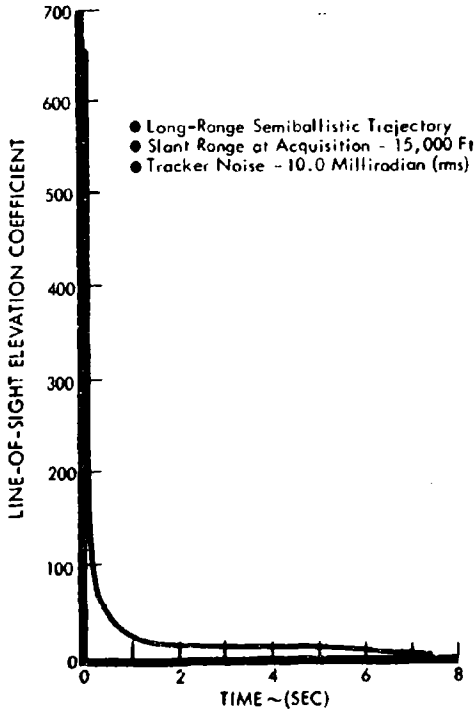

(A) WEIGHTING COEFFICIENT — X-POSITION ESTIMATE

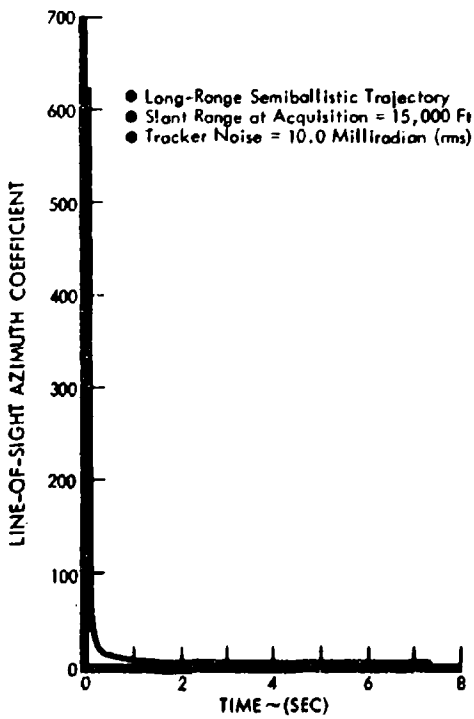

(B) WEIGHTING COEFFICIENT — Y - POSITION ESTIMATE

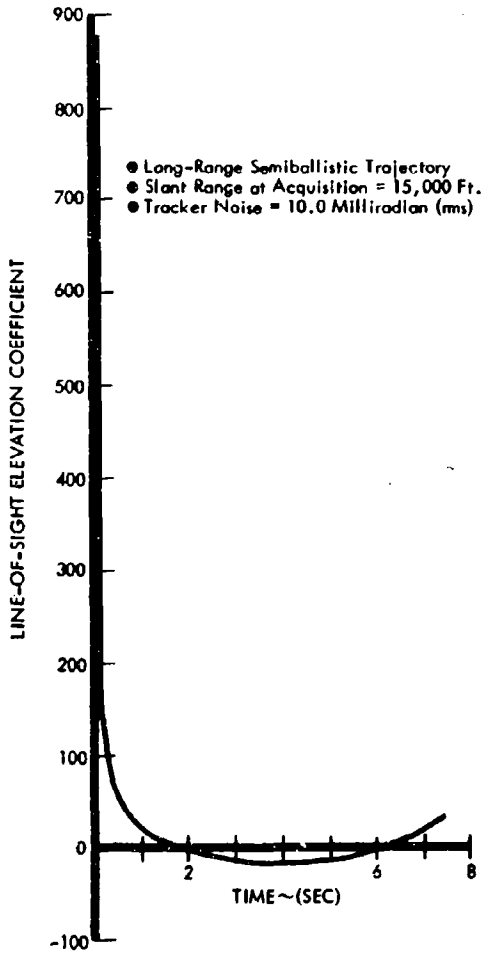

(C) WEIGHTING COEFFICIENT — Z- POSITION ESTIMATE

Figure 24: OPTIMAL FILTER COEFFICIENTS FOR POSITION ESTIMATE

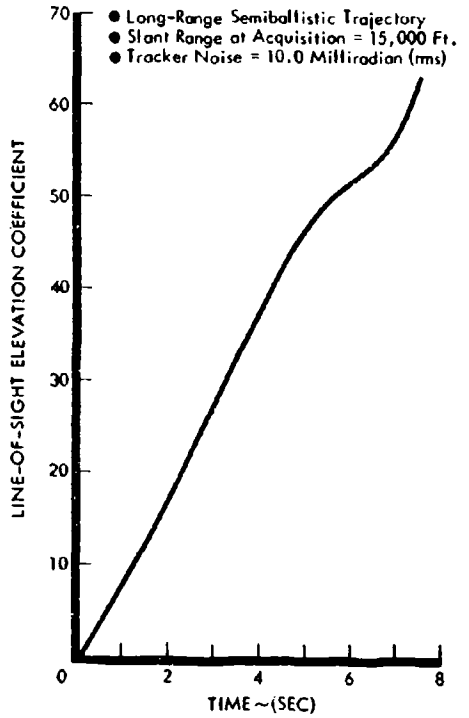

(A) WEIGHTING COEFFICIENT — X - VELOCITY ESTIMATE

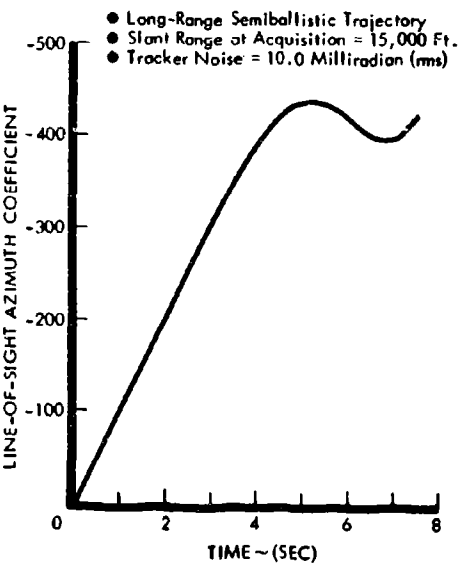

(B) WEIGHTING COEFFICIENT — Y - VELOCITY ESTIMATE

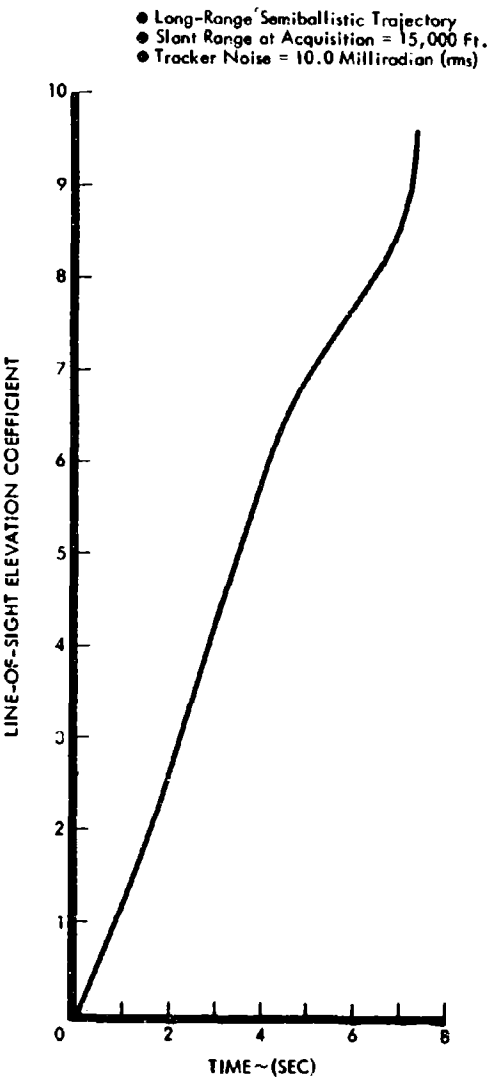

(C) WEIGHTING COEFFICIENT — Z - VELOCITY ESTIMATE

Figure 25: OPTIMAL FILTER COEFFICIENTS FOR VELOCITY ESTIMATES

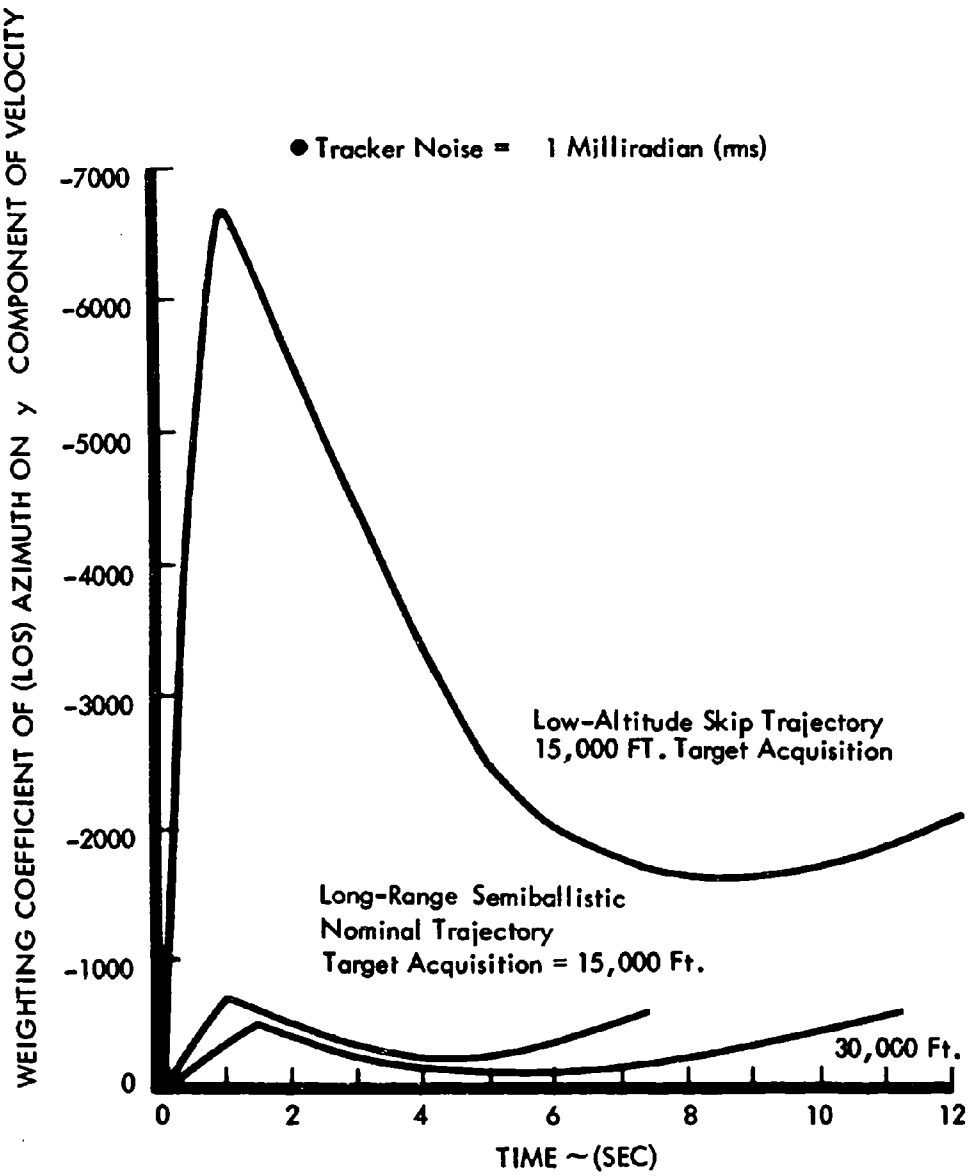

Figure 26: EFFECT OF NOMINAL TRAJECTORY ON OPTIMAL FILTER COEFFICIENTS

conditions for this differential equation are the estimates of position and velocity of the ASM at target acquisition supplied by the inertial platform. The matrices K (t) and $\dot{K}$ (t), which are coefficients of Equations 81 and 80, may be precomputed from Equations 76 and 77 and stored in the onboard ASM computer. Typical examples of these filter coefficients are shown in Figures 24, 25, and 26. Equations 80 and 81 would be solved by the computer to obtain estimates of the missile's position and velocity in rectangular coordinates. These position and velocity estimates would be subtracted from values of the same variables of the nominal trajectory to obtain estimated deviations from the nominal trajectory. The nominal trajectory in rectangular coordinates would be stored in the ASM on board computer.

The estimated deviations from the nominal trajectory, in rectangular coordinates, would be multiplied by the linearized transformation matrix between rectangular and flight path coordinates to express these estimated deviations in flight path coordinates. The transformation is given by the matrix Ξ that is used in Appendix II, Equation 107.

These variations are then multiplied by the matrix $-M^{-1}G^{T}U$ of Equation 53 to obtain the optimal control variations in angle of attack and bank angle. These variations are then added to the nominal values of these variables stored on the ASM.

In this computation the variations in position and velocity are multiplied by the two by six product matrix $-M^{-1}G^{T}U\,\Xi$ and the result added to the nominal bank angle and angle of attack. Typical control law coefficients for this matrix are shown in Figures 21 through 23. The matrix U is precomputed from Equation 54 with boundary condition from Equation 55. The matrices M^{-1}, G^{T}, and Ξ are known. Hence, this product matrix may be precomputed and stored onboard the ASM. The angle of attack and bank angle are then fed as command variables to the autopilot.

The missile-borne digital computer requirements for implementation of the ASM optimal navigation were obtained by coding Equations 53, 80, and 81 in a whole num-

ber digital computer language. The results of the analysis performed on the navigation loop were combined with estimates of the remaining computational load to size the missile-borne computer.

A timing summary and an airborne computer storage requirement for the various quantities of the computation are presented in Tables V and VI.

In obtaining this table, the functions $K(t)$, $\dot{K}(t)$, and $-M^{-1} G^T U \Xi$ were represented by tabular functions of time with fifty points for each variable. The nominal trajectory was expressed as a tabular function of time with twenty five data points. The estimated 2650 word storage capability is about 1500 words greater than similar estimates for conventional proportional, and pursuit guidance data. Any improvement is not expected to be so great as to change the class of the airborne digital computer required.

Due to the large quantities of numerical data, a whole number general purpose (or hard wired special purpose) computer is dictated for the optimal control application.

Table V: STORAGE SUMMARY

Navigation	Words
K (t) table	400
$\dot{K}$ (t) table	400
$-M^{-1} G^T U \Xi$ table	250
Nominal State and Control Variables	150
Constants	38
Variables	30
Incremental Inputs	5
Instructions	581
SUB TOTAL	1854
Nonnavigation Estimates	
Resolver Inputs	5
Gyro Torquing	100
Flight Control Functions	50
Check and Calibration	150
Initial Alignment	40
Discrete Functions	30
Monitor	25
Status	50
SUB TOTAL	450
TOTAL	2304
15% uncertainty	346
RESULTANT TOTAL	2650

Table VI: TIMING SUMMARY

Navigation Instructions per major cycle	3397
Other instructions per major cycle	250
TOTAL	3647

For a 0.2 second major cycle, which is quite fast, the average instruction execution time must be less than 54.8 microseconds.

In the weight category of 10 to 30 pounds, the following is a brief survey of some available computers that satisfy the requirements of the missile-borne digital computer.

Manufacturer	Model
A. C. Sparkplug	Magic series
Arma	M169
Autonetics	D-26 series
Control Data Corp.	5300 series
Honeywell	ALERT
Hughes	HCM 205 and 206
Lear Siegler	DIVIE
Litton	C-221
Nortronics	NDC-1051

The following numerical approximations were made in coding the optimal navigation problem.

1. $\mathrm{Tan}^{-1} V = V - \left(\frac{V^3}{3}\right)$

2. Given y_o as an estimate of $y = \sqrt{z}$, the second order recursion formula

$$y_i + 1 = y_i - \frac{2y_i\ (y_i^2 - z)}{3y_i^2 + z}$$

is assumed to be adequate after two iterations. Y_o is given for the first Δt and thereafter the starting y_o is obtained by using the result of the previous guidance cycle.

3. Second order interpolation is required to extract values of the tabular functions from their tables.

Second order interpolation was used for the table look-up functions. Improvements in computer requirements could result if data was supplied as segments of polynomials pieced together to provide an adequate fit to the numerical data.

a. Conclusions from the Optimization Computation. Tables III and IV of Section IV compare the standard deviation of miss distance for the optimal system to the standard deviation of miss distance for pursuit and proportional guidance for several nominal trajectories and sensor noise levels. Appendix II contains the method used to make the calculations for these tables.

In Appendix II, it is shown that the miss distance can be resolved into a term that is due to the error in estimating the ASM position deviation and a term that depends on the controller. These are called filter error and controller error, respectively. Examples of the time history of these errors are given in Figure 27. The square root of the sum of the squares of these quantities at the final time gives the miss distance. In all of the calculations carried out, the contribution of the controller error to miss distance was negligible. This shows that almost all the miss distance is due to error in estimating the ASM position deviation.

The comparison with proportional and pursuit guidance, given in Table IV, shows that these guidance laws have almost the same miss distances as the optimal system for a variety of sensor noise levels. This shows that these simple systems are using the sensor information and controlling in a nearly optimal manner.

In Appendix II, it is shown that the filter error is completely independent of the controller, and that, if a linear feedback controller of the form

$$\begin{pmatrix} \delta\alpha \\ \delta\beta \end{pmatrix} = \Lambda(t) \begin{pmatrix} \delta x \\ \delta y \\ \delta z \\ \delta V \\ \delta \chi \\ \delta \gamma \end{pmatrix} \tag{82}$$

Long-Range Semiballistic Trajectory
Slant Range at Acquisition = 15,000 Ft.
Tracker Noise = 50 Milliradians

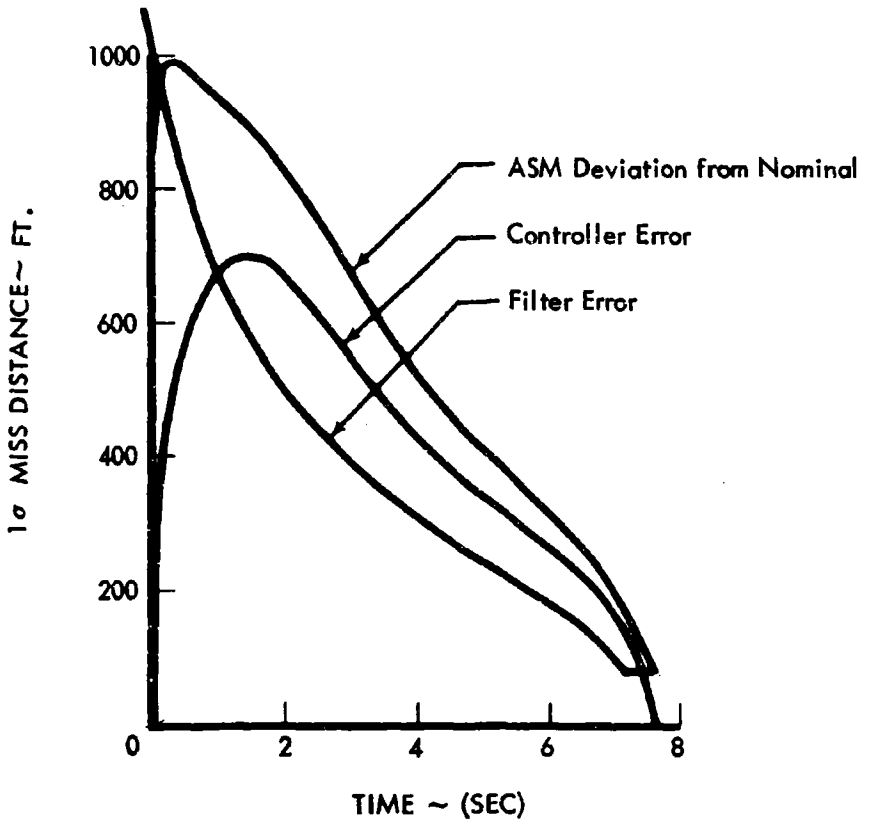

Figure 27: COMPARISON OF CONTROL AND FILTER ERROR

was used with the optimal filter, a modification of Equation 110 governing controller error still holds. It can be shown that, if the controller $\Lambda(t)$ is chosen, so that the system

$$\begin{pmatrix} \dot{\delta x} \\ \delta y \\ \delta z \\ \delta V \\ \delta \chi \\ \delta \gamma \end{pmatrix} = \left(F(t) - G(t)\Lambda(t)\right) \begin{pmatrix} \delta x \\ \delta y \\ \delta z \\ \delta V \\ \delta \chi \\ \delta \gamma \end{pmatrix} \tag{83}$$

drives the component of position deviation normal to the nominal trajectory to zero, that controller error will be driven to zero. There are many choices of $\Lambda(t)$ that will fulfill this requirement. Therefore, there are many linear feedback controllers that will behave in a nearly optimal fashion.

In the computation of the optimum filter coefficients, the matrix differential Equation 63 for the matrix Σ must be solved. This matrix is the covariance matrix of the difference of the actual state vector of the ASM and the value estimated for this vector by the filter. Examination of the elements of this matrix at various times will show how rapidly the optimal filter is estimating corresponding components of the state vector. This is illustrated in Figures 28 and 29.

In Figure 28 the standard deviations of the differences between the true values and the estimated values of the variations in x and z are plotted. Note that these standard deviations do not substantially decrease with time. In Figure 29 these same values are expressed in a different coordinate system. In this figure the standard deviations of the same differences resolved into components parallel to and perpendicular to the nominal trajectory are plotted. Note that the component perpendicular to the nominal trajectory decreases very rapidly to zero, while the component parallel to the nominal trajectory decreases very slowly.

This may be explained by noting that only line-of-sight angles and ASM accelerations are being measured. Therefore, very little information about the missile's position along the nominal trajectory is being supplied. These measurements do supply information about the missile's position normal to the nominal trajectory. Fortunately, as was pointed out in Section V.3.b, the deviation in position normal to the nominal trajectory is the important component in computing miss distance. This question is explored in further detail in Appendix III.

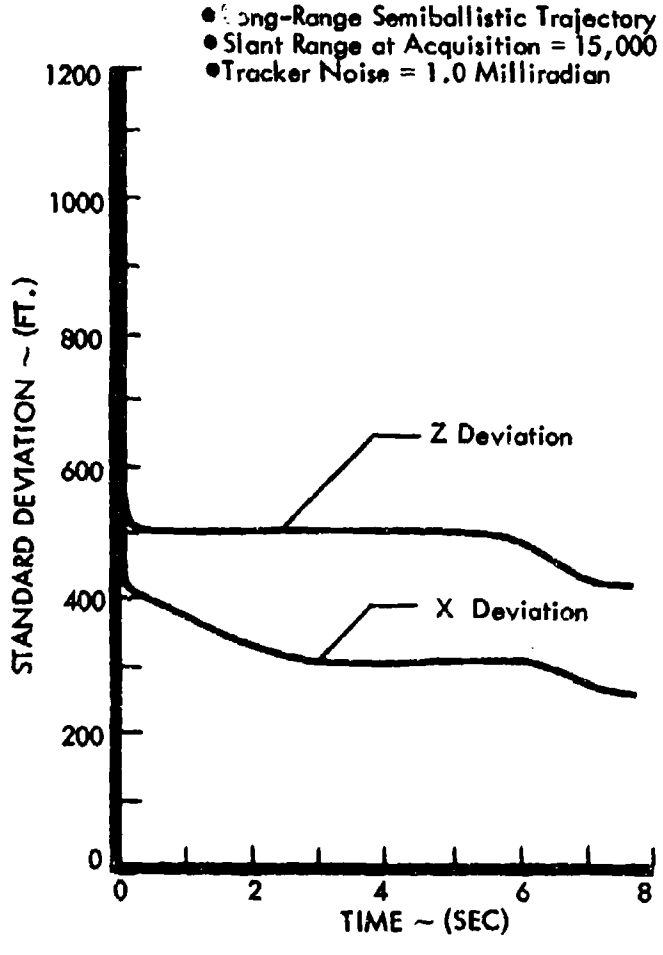

Figure 28: STANDARD DEVIATIONS OF X AND Z POSITION ESTIMATES

- Long-Range Semiballistic Trajector,
- Slant Range at Acquisition = 15000 Ft.
- Tracker Noise = 1.0 Milliradian(rms)

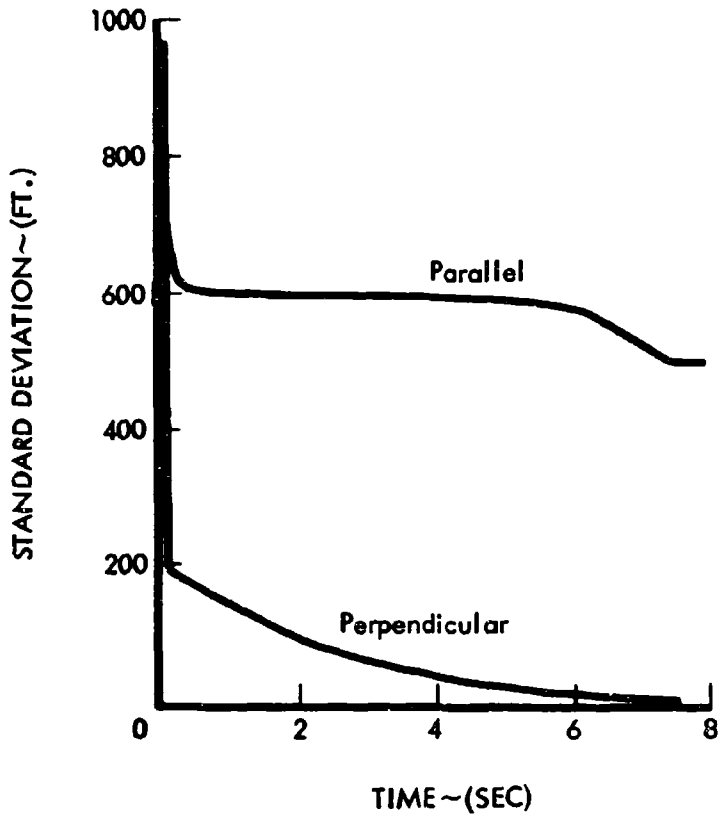

Figure 29: COMPARISON OF THE ACCURACY OF ESTIMATION OF POSITION DEVIATION, PARALLEL TO AND PERPENDICULAR TO THE NOMINAL TRAJECTORY

SECTION VI

NORMAL-ACCELERATION AUTOPILOT STUDIES

A normal-acceleration commanded autopilot was selected for the ASM because normal acceleration is a direct command parameter for flight-path corrections. Because of this feature, it leads to simpler guidance laws for the near-impact phase than attitude control. Thus, the practicality of instituting optimal control techniques in the near-impact phase is increased through simplification of guidance law expressions using this control parameter. Normal acceleration control also provides a parameter for limiting commanded maneuvers to stay within the structural limitations of the missile.

The normal-acceleration autopilot was investigated for launch, midcourse, and near-impact (flight from target acquisition to impact) phases of three nominal trajectories — long-range semiballistic, short-range semiballistic, and low-altitude skip. Dynamic pressures from 10 to 5500 lb/ft^2 were considered. The Mach number range was 0.59 to 4.2. Seven representative flight conditions (Figure 30) were investigated in fixed point studies. Because the major interest of the program was in the homing phase of the ASM, emphasis was placed upon selecting autopilot gains and compensation to obtain satisfactory control system response during the terminal phases of nominal trajectories (approximated by Flight Conditions 1, 2, and 3).

Stability and time response criteria for the autopilot were:

(1) The rigid mode must exhibit, as minimal stability characteristics, a 6-db gain margin and a 30-degree phase margin;

(2) All body-bending modes must be at least 6-db gain stable (to account for uncertainty in the phase of the servo response at the body-bending frequencies);

(3) The controlled missile must have a time response as fast as a first-order system with a time constant of 0.5 second.

The time response criteria were based on the results of the preliminary near-impact phase digital simulations that indicated that a 0.5 second constant made a negligible contribution to impact error. This preliminary simulation included position offset

errors and wind shear effects. As was indicated in the discussion of autopilot response in Section IV, this criterion was not adequate when the more complete simulation was used. No criterion was set for acceptable steady-state errors in response to commands. The nominal autopilot design was a Type 1 controller, and therefore exhibited zero steady-state error for step inputs.

The autopilot study was conducted in two phases. The first phase consisted of the development, through analytical methods (root locus and frequency response analyses), of a programmed gain nominal autopilot that could be used in the guidance evaluation studies. This phase resulted in the Type 1 autopilot with compensation selected to give adequate response during the near-impact phase of flight. Gains were developed to meet the stability criteria for all flight conditions (except Condition 7, a condition of very low dynamic pressure, which was unstable). The synthesis of a normal acceleration autopilot presented no unusual difficulties for the configuration studied. However, care was required in selecting autopilot gains that provided acceptable time response and steady error performance and did not violate the stability requirements when body-bending and tail-wags-dog effects were considered.

A somewhat unconventional root locus technique was used and aided in arriving at a satisfactory compromise. This approach is presented in the discussion that follows.

The second phase consisted of analog computer verification of the analytical studies of the nominal Type 1 autopilot design, and the investigation of three nonlinear effects on the controlled missile performance. The nonlinear quantities studied were: (1) control servomechanism rate limiting; (2) pure transport lag in the servomechanism; and (3) variations in control fin effectiveness due to "masking" effects at angle of attack.

Additional analytical and computer investigations were made of an advanced controller (a quasiadaptive concept) that eliminates the need for gain changing or programming during the flight. This controller concept was based on inhouse extensions of optimal bistable controller investigations initiated by Gieseking

(Reference 7) and others. This study resulted in an autopilot which combined a bistable controller and a Type 0 (no integral compensation) autopilot. The need for gain and bistable controller coefficient changes was eliminated, and satisfactory response and steady-state error performance was obtained for all six of the major flight conditions. A discussion is also presented on other advanced control concepts that appear applicable to the ASM autopilot.

1. Nominal Autopilot Design. For all autopilot studies, the ASM configuration representation included two flexible body-bending modes, a first order fin servo, the tail-wags-dog effect of fin inertia, and a linearized representation of the rigid body dynamics for Flight Conditions 1 through 6, which were shown in Figure 30.

The resulting autopilot design is shown in Figure 31. Feedback signals for the functional autopilot were taken to be linear body normal acceleration and body angular rate. The location of the normal accelerometer, dictated by the constraint of available space in the missile's internal arrangement, was about 5.3 feet ahead of the vehicle's center of gravity. This instrument location yielded a feedback signal having more than a desired content of vehicle angular acceleration and body-bending signal amplitude. However, accelerometer placement was near the second body-bending node, so it did not sense second body bending motion. The attitude rate sensor was located in the autopilot electronics section, near the antinode of the first body bending mode, and hence sensed the flexible body modal motions of only the second and higher modes. A hydraulic fin actuator was assumed, having a first order response with a 60 rad/sec characteristic frequency and (for the final analog computer studies) a deflection rate limit of 150 degrees/second.

The compensation used for body bending stabilization consists of two sets of second-order filters employing complex zeros in conjunction with real-axis poles. This form of body bending compensation has a less adverse effect on rigid mode response than simple lag compensation, and can be implemented using RC networks and a single operational amplifier for each of the quadratic filters. The zeros of this quadratic compensation are placed at the middle of the range of variation

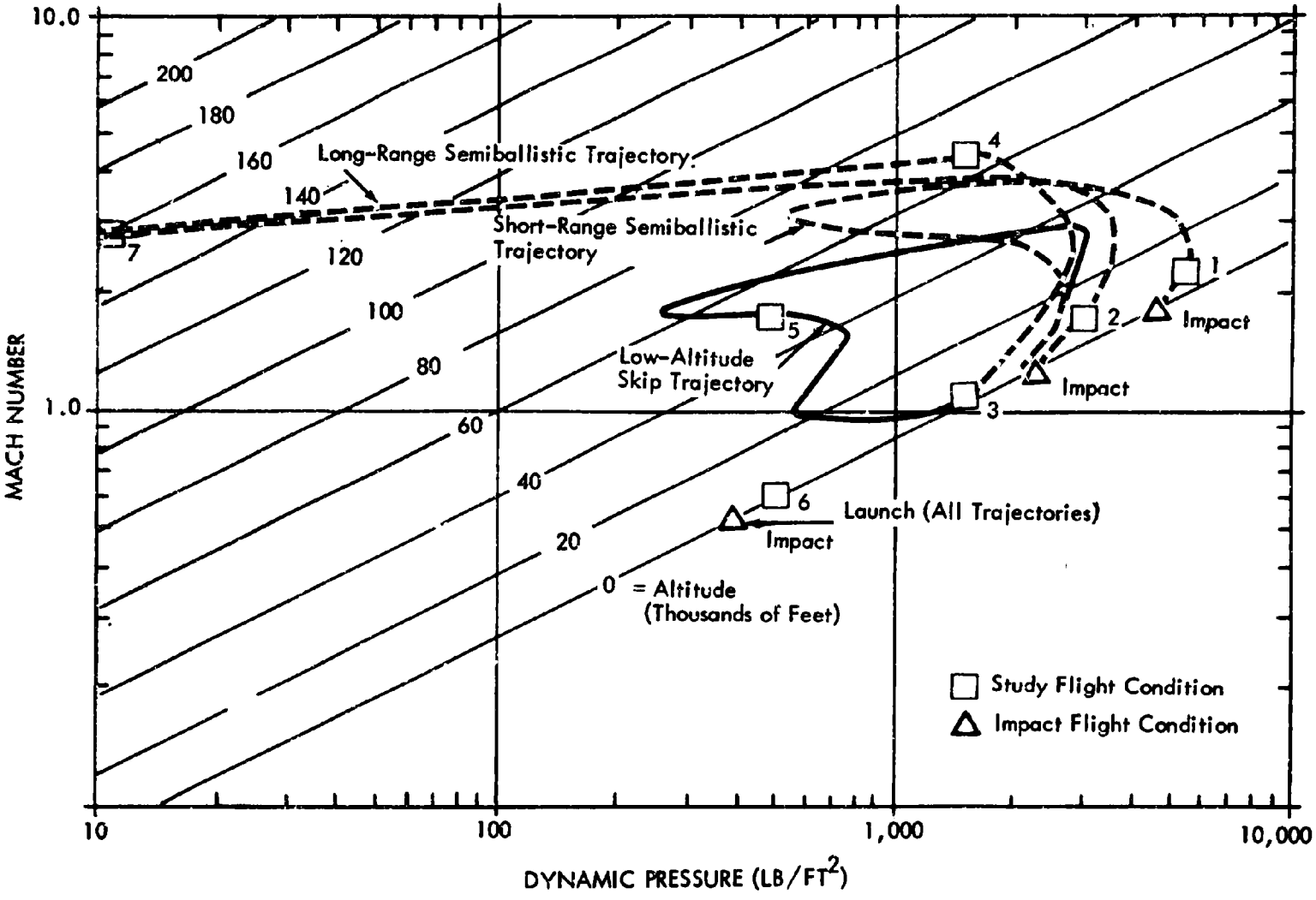

Figure 30: ASM FLIGHT CONDITIONS

of first body bending frequency from launch to burnout, so that the compensation will ensure first body bending stability throughout the flight. The compensation network parameters are fixed at values that permit satisfactory controlled system response for all flight conditions in the terminal homing phases of the three reference trajectories. The required values for $K_I/K_{\dot{z}}$, $K_{\dot{\theta}}$, and $K_{\dot{z}}$ are shown in Table VII for Flight Conditions 1 through 6.

Table VII: REQUIRED AUTOPILOT GAINS

Flight Condition	$K_I/K_{\dot{z}}$	$K_{\dot{z}}$	$K_{\dot{\theta}}$
1	3	-0.0274	-0.042
2	3	-0.0371	-0.050
3	3	-0.0525	-0.056
4	3	-0.0525	[illegible]
5	3	-0.0909	-0.08
6	3	-0.0909	-0.08

A somewhat unconventional procedure was used for selecting satisfactory autopilot gains (K_I, $K_{\dot{z}}$, and $K_{\dot{\theta}}$). The procedure used was to select values of K_I and $K_{\dot{z}}$ based on the roots of the numerator of the $\dot{\theta}_\epsilon/\delta$ transfer function. It can be shown that the roots of the numerator become zeros in the final loop closure for $\ddot{z}/\ddot{z}_c$ using the $K_{\dot{\theta}}$ gain. Placing these zeros in a well damped position assists in meeting the overall system stability and response requirements with the final loop closure.

The intermediate missile dynamics transfer functions, $\dot{\theta}/\delta$ and $\ddot{z}/\delta$, and the appropriate pole and zero values as a function of flight condition are shown in Table VIII. Note that, because of sensor location, $Z_{6,7}$ and $P_{5,6}$ cancel in $\dot{\theta}/\delta$ and, similarly in $\ddot{z}/\delta$, $Z_{18,19}$, and $P_{5,6}$ cancel. The inclusion of tail-wags-dog (fin inertia) effects in the vehicle dynamics transfer functions results in higher order numerators than denominators. When the remainder of the servo and sensor dynamics and loop closures, as shown in Figure 31, are completed, final transfer functions have the expected lower order numerators. Root loci with $K_{\dot{z}}$ as the gain parameter were first obtained for the numerator of the $\dot{\theta}_\epsilon/\delta$ transfer function for a wide range

Table VIII: MISSILE DYNAMICS TRANSFER FUNCTIONS

$$\frac{\phi(s)}{\delta(s)} = \frac{9.2\times10^{-6}\, s^3 \overbrace{(s+z_1)}^{\text{Rigid Mode Zeros}} \overbrace{(s+z_2)(s+z_3)}^{\text{2nd Body-Bending Mode Zeros}} \overbrace{(s+z_4)(s+z_5)}^{\text{Tail-Wags-Dog Zeros}} \overbrace{(s+z_6)(s+z_7)}^{\text{1st Body-Bending Mode Zeros}}}{s^2 \underbrace{(s+p_1)(s+p_2)}_{\text{Rigid Mode Poles}} \underbrace{(s+p_3)(s+p_4)}_{\text{2nd Body-Bending Mode Poles}} \underbrace{(s+p_5)(s+p_6)}_{\text{1st Body-Bending Mode Poles}}}$$

NOTE: Rate sensor located at first body-bending antinode

$$\frac{A(s)}{\delta(s)} = \frac{-1.196\times10^{-4}\, s \overbrace{(s-z_{11})}^{\text{Rigid Mode Zeros}} \overbrace{(s+z_{12})(s+z_{13})}^{\text{1st Body-Bending Mode Zeros}} \overbrace{(s+z_{14})(s+z_{15})}^{\text{Accelerometer Zeros}} \overbrace{(s+z_{16})(s+z_{17})}^{\text{Tail-Wags-Dog Zeros}} \overbrace{(s+z_{18})(s+z_{19})}^{\text{2nd Body-Bending Mode Zeros}}}{s^2 \underbrace{(s+p_1)(s+p_2)}_{\text{Rigid Mode Poles}} \underbrace{(s+p_3)(s+p_4)}_{\text{2nd Body-Bending Mode Poles}} \underbrace{(s+p_5)(s+p_6)}_{\text{1st Body-Bending Mode Poles}}}$$

NOTE: Accelerometer located at second body-bending displacement node

The following roots depend on flight condition:

Flight Condition	q (psf)	M	z_1 (rad/sec)	z_2 (rad/sec)	z_3 (rad/sec)	$z_{4,5}$ (rad/sec)	z_{11} (rad/sec)	z_{12} (rad/sec)	z_{13} (rad/sec)	$z_{14,15}$ (rad/sec)	$z_{16,17}$ (rad/sec)	p_1 (rad/sec)	p_2 (rad/sec)
1	5000	2.3	+0.76	-3000	+3000	+0.554j530	-0.000	-375	+000	+0.334j30	+0.034j309	+0.03+j0.3	0.03-j0.3
2	3000	1.7	+0.50	-3000	+3000	+0.34j440	-0.0135	-300	+545	+0.224j31	+0.44j439	+0.74+j0.0	+0.74-j0.0
3	1500	1.07	+0.44	-3000	+3000	+0.3j340	-0.033	-000	+543	+0.104j15	+0.334j340	+0.7+j7.0	+0.7-j7.0
4	1000	4.3	+0.135	-3329	+3079	0+j330	-0.000	-651	+330	+0.078j13	+0+j330	+3.0	-3.0
5	000	1.7	+0.101	-3329	+3000	0+j105	-0.0135	-545	+000	+0.0644j0.3	+0+j175	+0.141+j3.36	+0.141-j3.36
6	000	0.30	+0.3	-3300	+3079	0+j330	-0.0333	-547	+330	+0.107j0.3	+0+j105	+0.345+j4.1	+0.345-j4.1
7	10	0.3	+0.0011	-3010	+3330	0+j11	+0.00135	-337	+000	40.0	0+j31	0+j0.33	0-j0.33

The following roots are invariant with flight condition:

$z_{10,19} = p_{3,4} = 0.334j339.0$

$z_{8,9} = p_{5,6} = 3.71j371.0$

of the ratio $K_I/K_{\dot{z}}$ at each flight condition. (The composition of this transfer function can be determined from Figure 31.) Figure 32 shows typical loci of system zeros (or roots of the $\dot{\theta}_\epsilon/\delta$ numerator) for Flight Condition 3 with values of $K_I/K_{\dot{z}} = 2$, 3, and 4 respectively. Because the roots on these loci become zeros of the overall system, it is desirable to place them in a well damped position. The real open-loop pole, located at -2, -3, and -4 respectively in these figures, is given directly by the ratio $K_I/K_{\dot{z}}$, and indicates that system response becomes faster for higher values of $K_I/K_{\dot{z}}$. However, as shown in these figures, when $K_I/K_{\dot{z}}$ is greater than 3, the complex branch of the locus fails to progress in an arc down to the real axis, and these roots are left in a position representing less damping. This results in a lighter damped rigid mode, and therefore is undesirable. These considerations lead to the choice $K_I/K_{\dot{z}} = 3$.

Figures 33 through 37 show the roots of the $\dot{\theta}_\epsilon/\delta$ numerator for the remainder of flight conditions, except Condition 7. These root loci are based on the ratio $K_I/K_{\dot{z}} = 3$, and indicate satisfactory values for $K_{\dot{z}}$. From these plots, values for $K_{\dot{z}}$ were selected that place the quadratic pair in a well-damped position.

The total system root loci, $\dot{z}/\dot{z}_c$, for determining $K_{\dot{\theta}}$ are shown in Figures 38 through 43. The zeros appearing in these plots are those determined by the loci of Figures 32b and 33 through 37, plus the zeros introduced by compensation in the inner forward loop. At the left of each of these plots is an enlargement of the region near the first body bending pole, and on the right is an enlargement of the region about the origin showing the rigid mode details. The gain-stable requirement for the first body bending mode implies that the operating point on the locus emanating from the first body bending mode pole be at least 6-db below the gain at which the locus crosses the circle. Uncertainty in phase of the servo response at this frequency implies an uncertainty in the direction of the locus emanating from the first body bending pole. Examination of these figures shows that the critical design requirements arise from the high Mach number condition (Figure 41) where system response requirements require high gains. Limitations on high gains arise from the locus that crosses the imaginary axis in the vicinity of 140 rad/sec, and from the gain-stable requirement for the first body bending

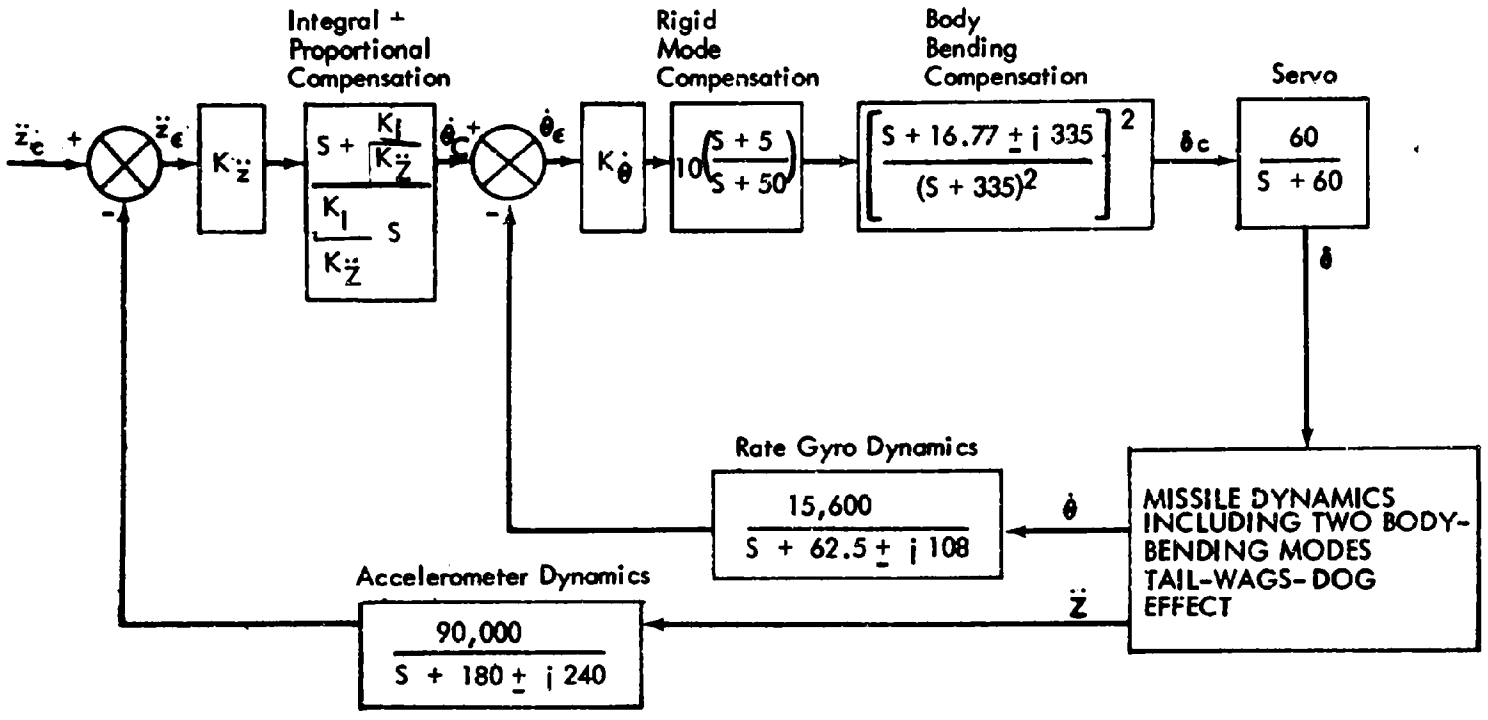

Figure 31: TYPE I AUTOPILOT BLOCK DIAGRAM

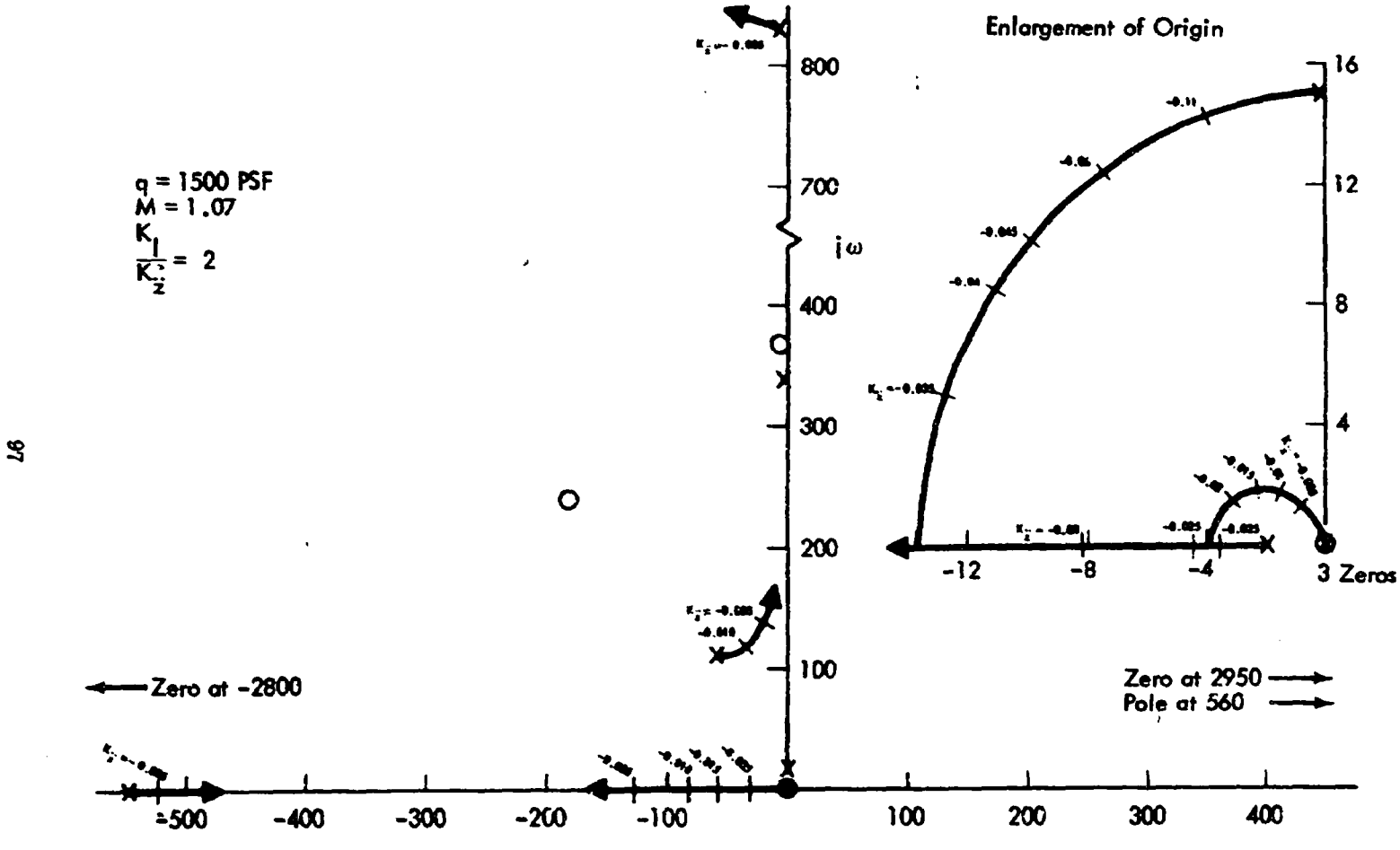

Figure 32a: LOCI OF SYSTEM ZEROS— FLIGHT CONDITION 3

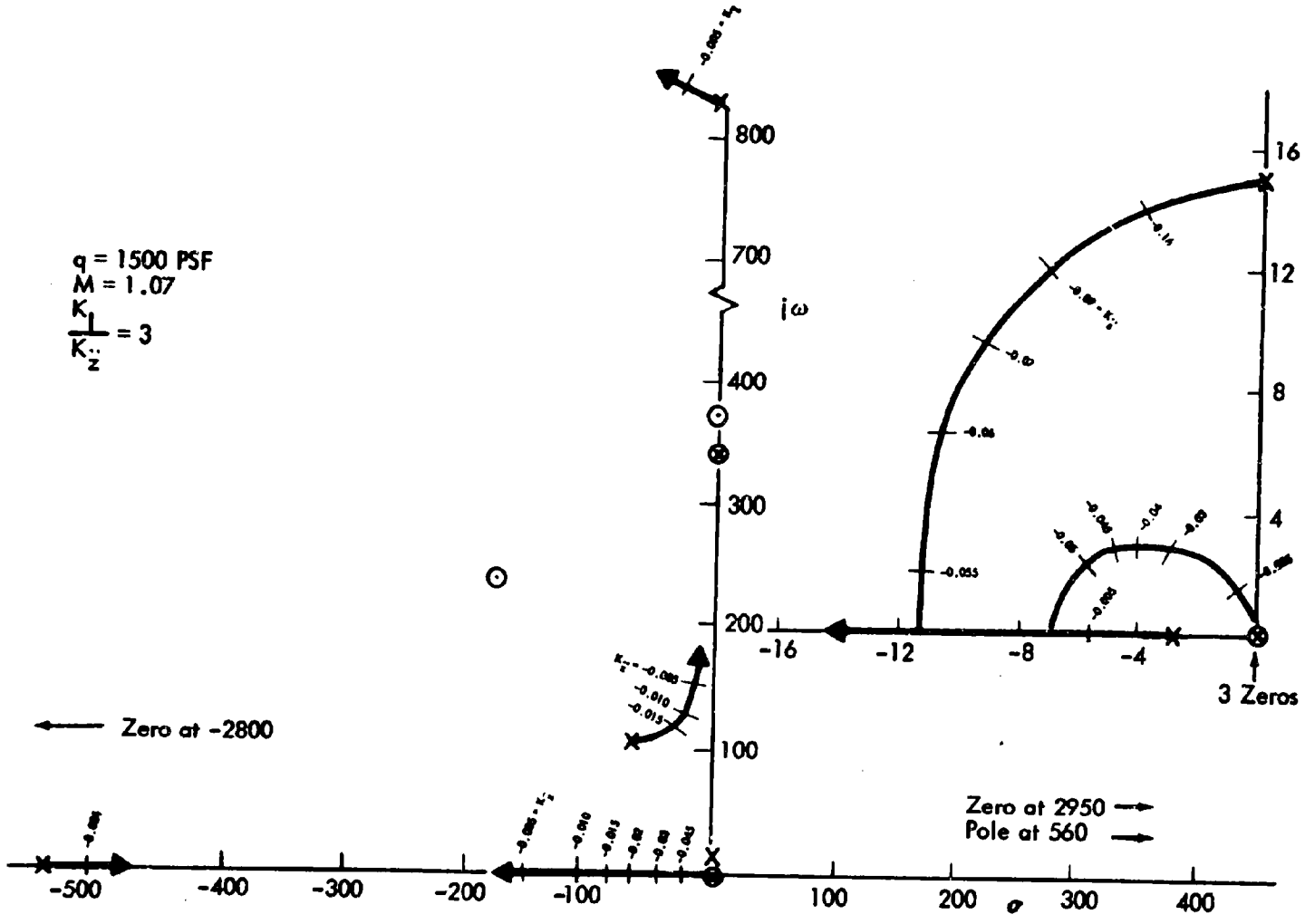

Figure 32b: LOCI OF SYSTEM ZEROS—FLIGHT CONDITION 3

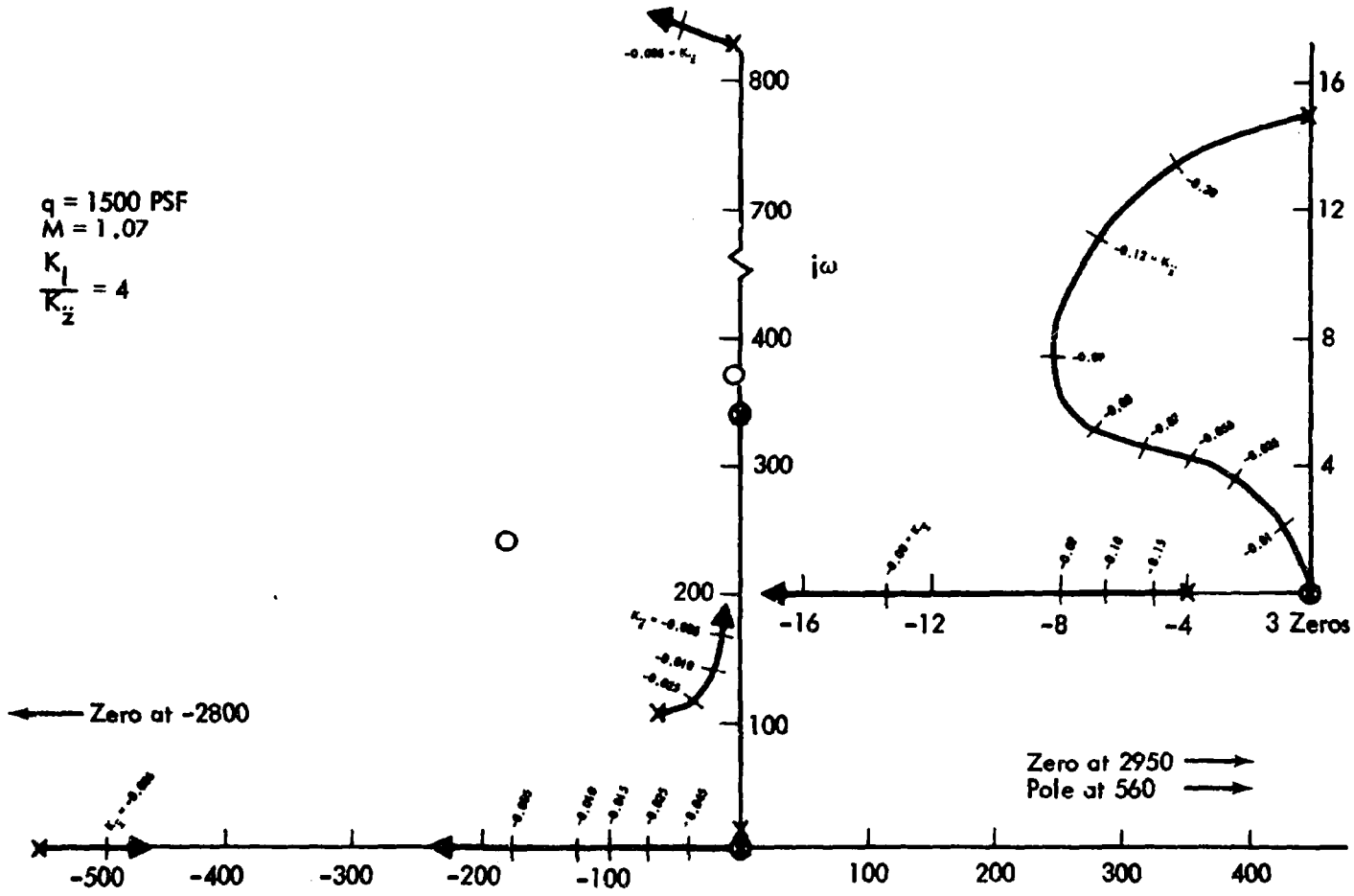

Figure 32c: LOCI OF SYSTEM ZEROS—FLIGHT CONDITION 3

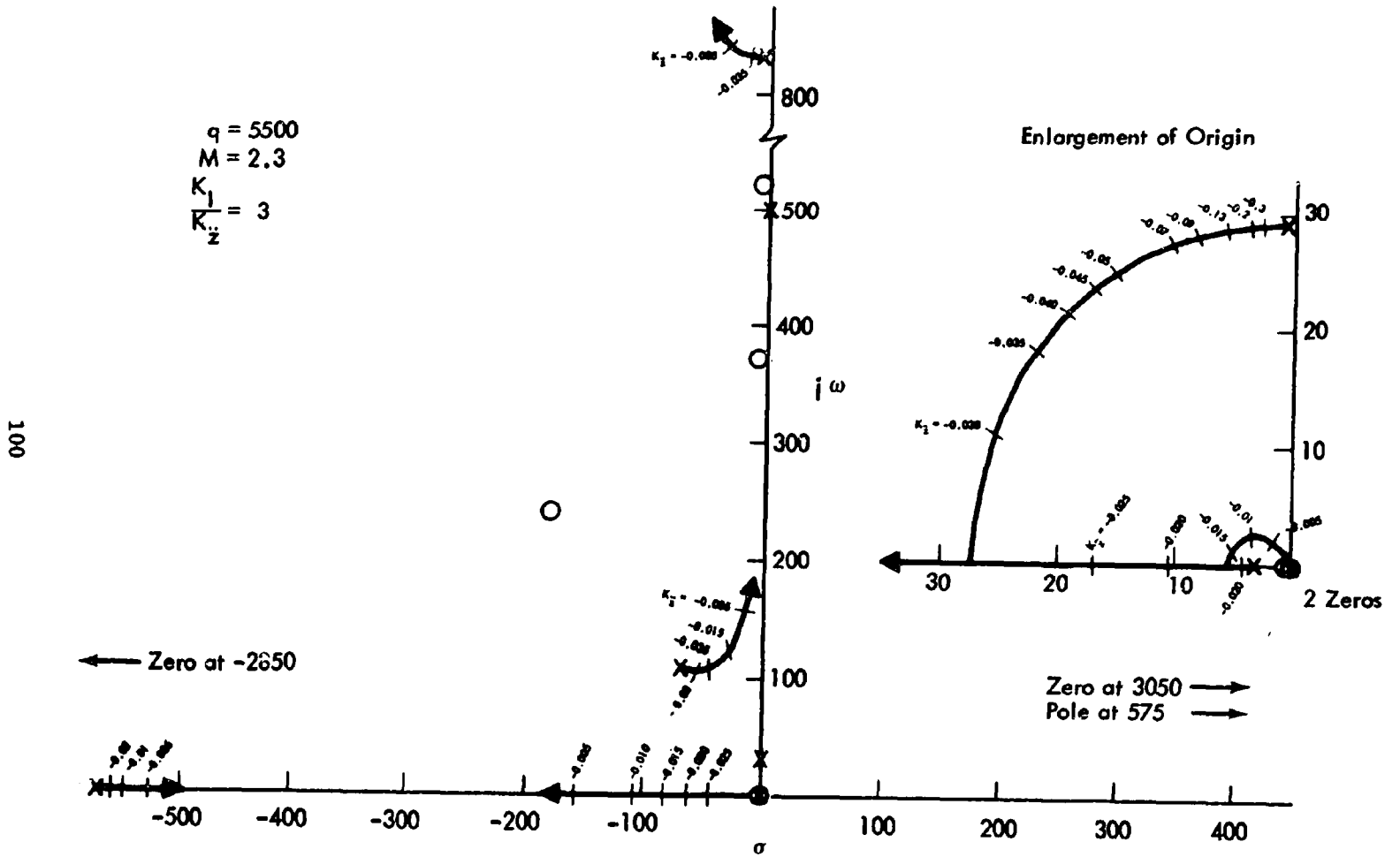

Figure 33: LOCI OF SYSTEM ZEROS - FLIGHT CONDITION 1

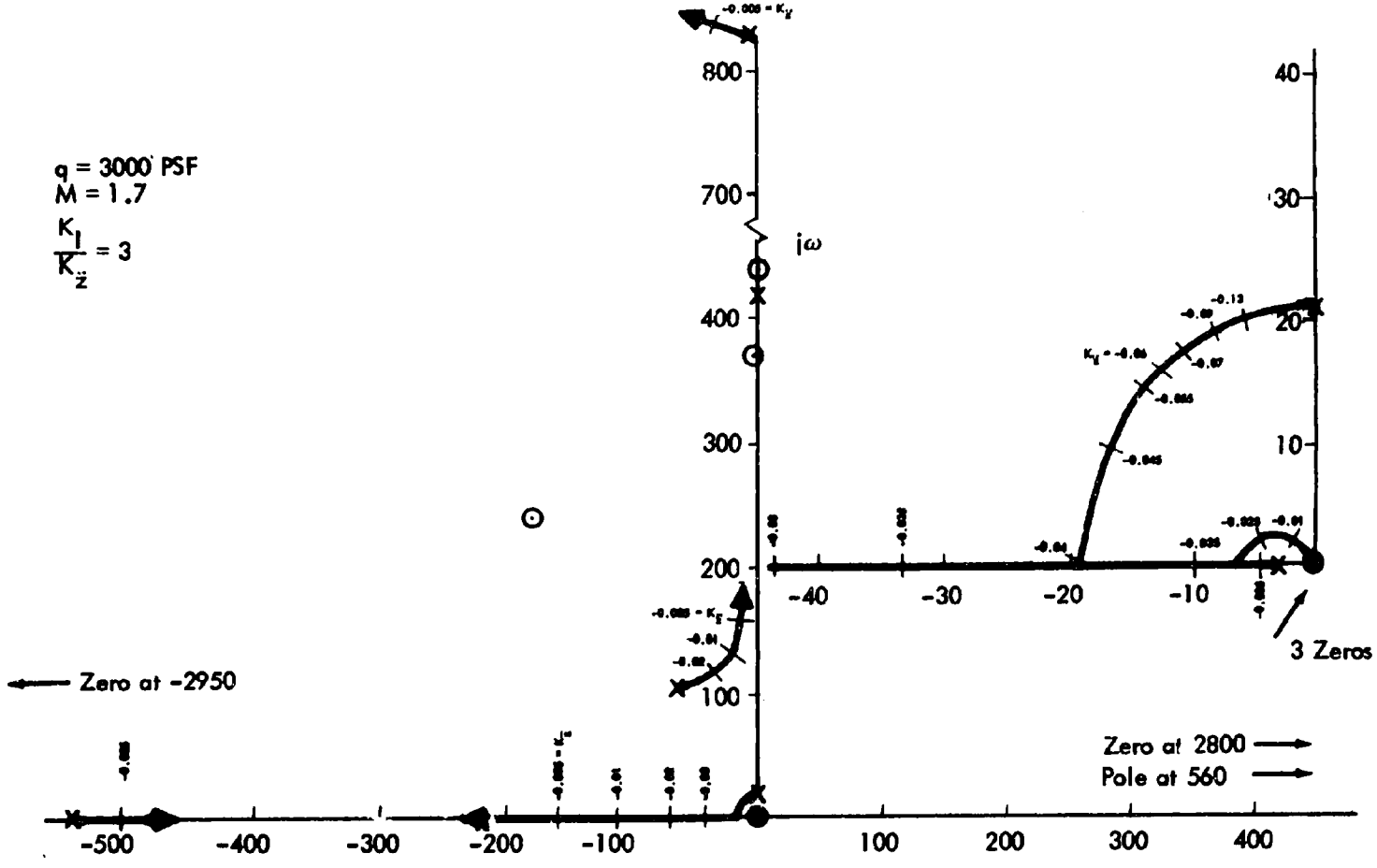

Figure 34: LOCI OF SYSTEM ZEROS —FLIGHT CONDITION 2

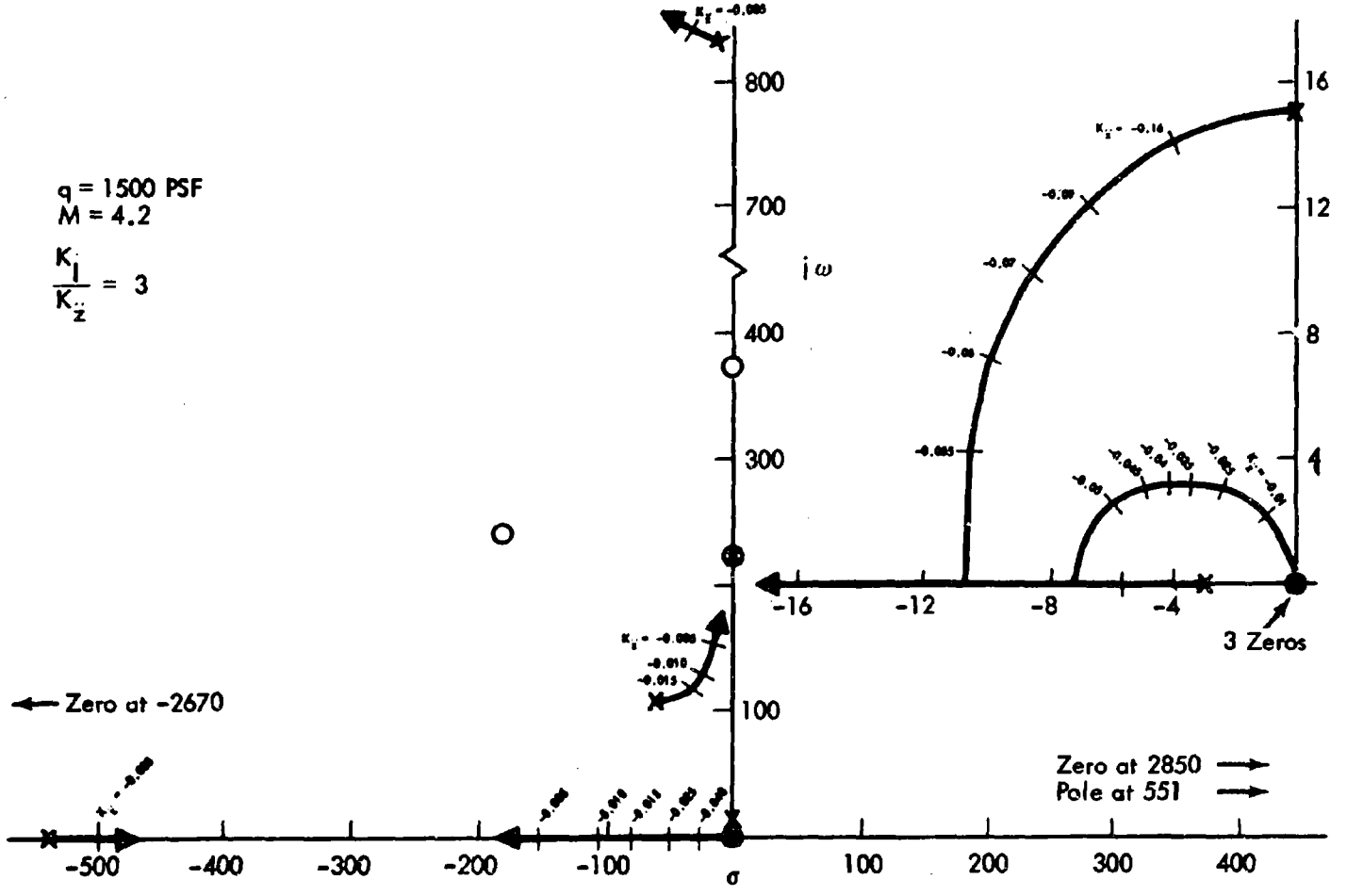

Figure 35: LOCI OF SYSTEM ZEROS — FLIGHT CONDITION 4

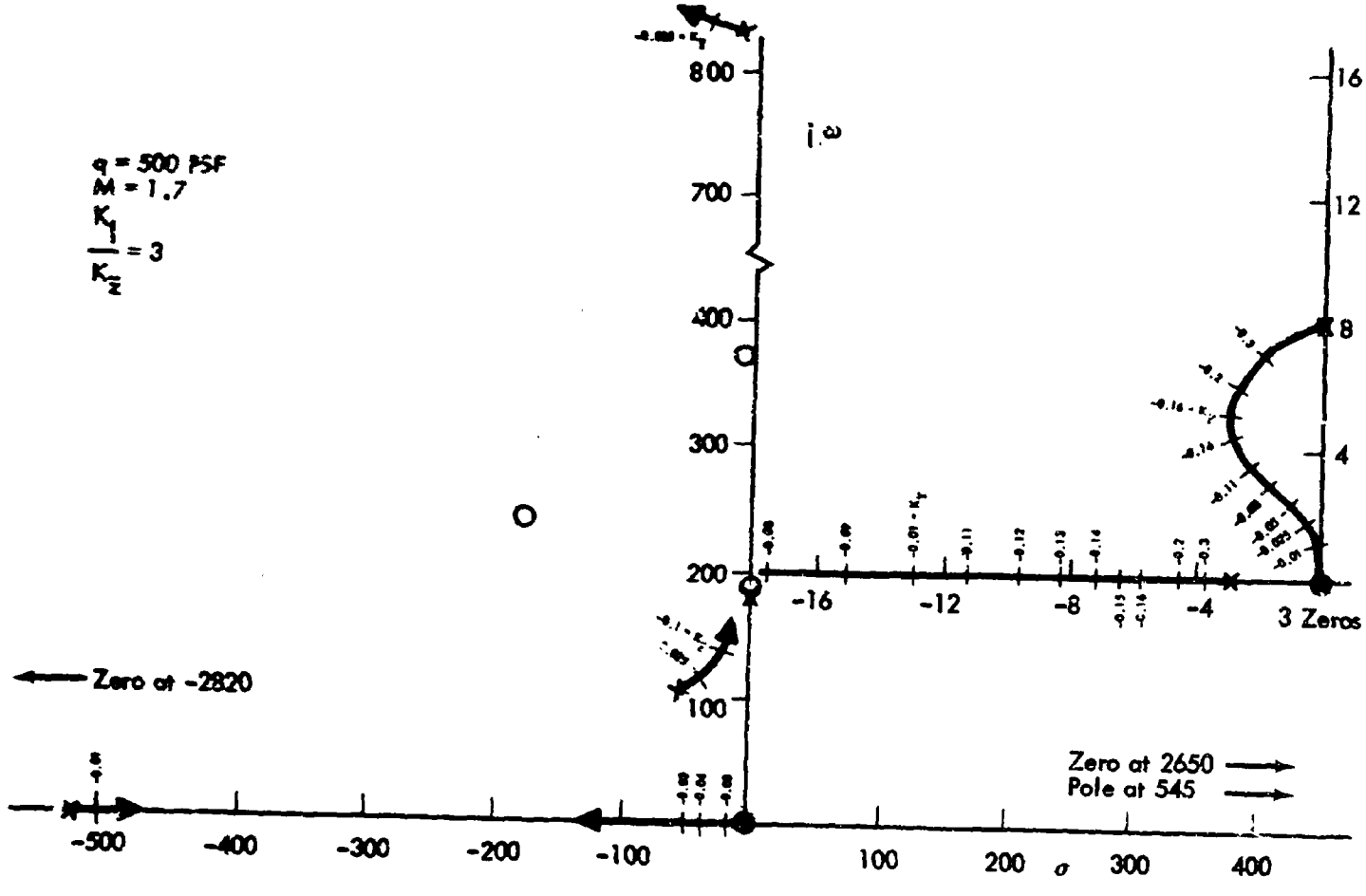

Figure 36: LOCI OF SYSTEM ZEROS — FLIGHT CONDITION 5

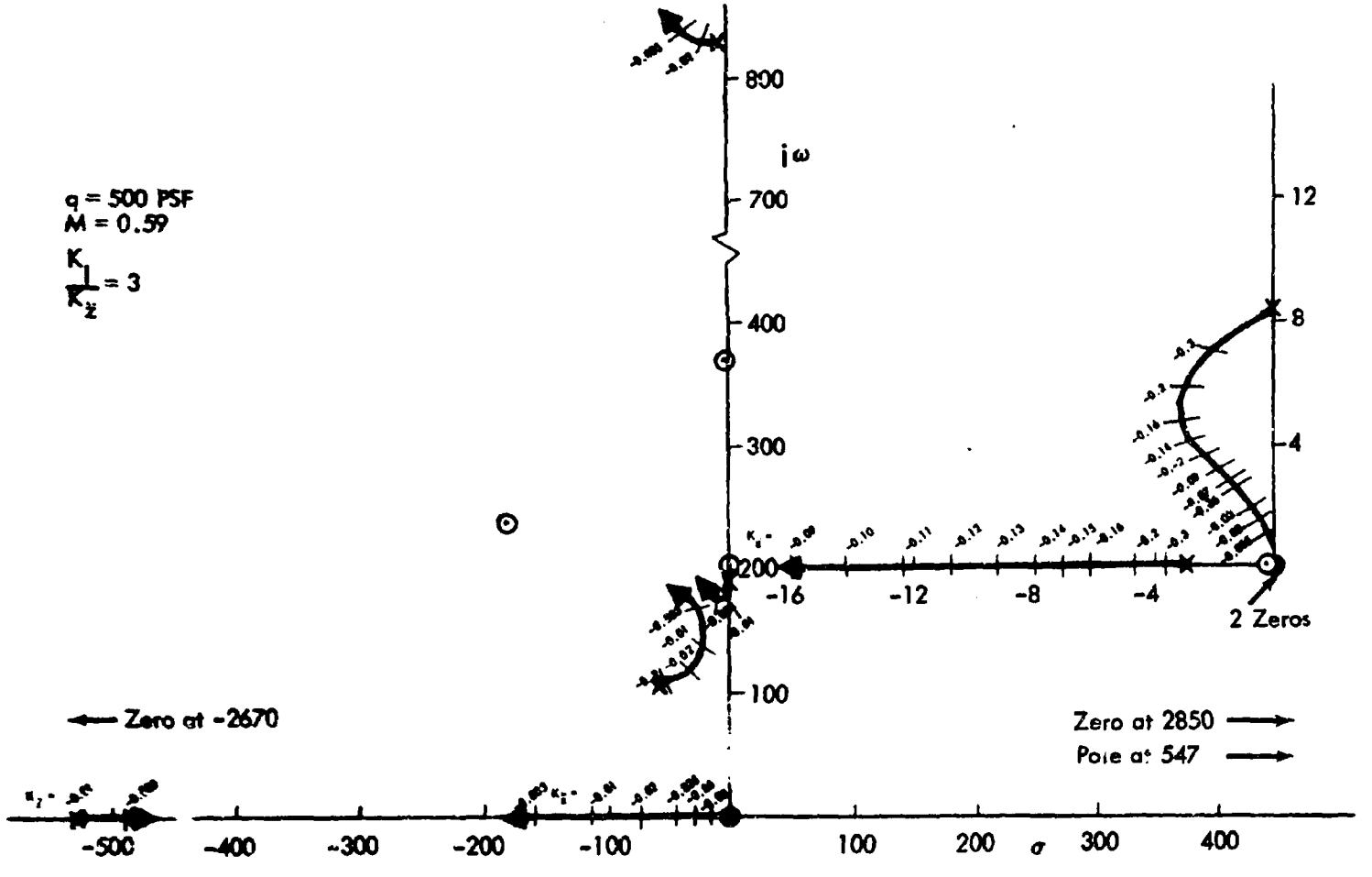

Figure 37: LOCI OF SYSTEM ZEROS—FLIGHT CONDITION 6

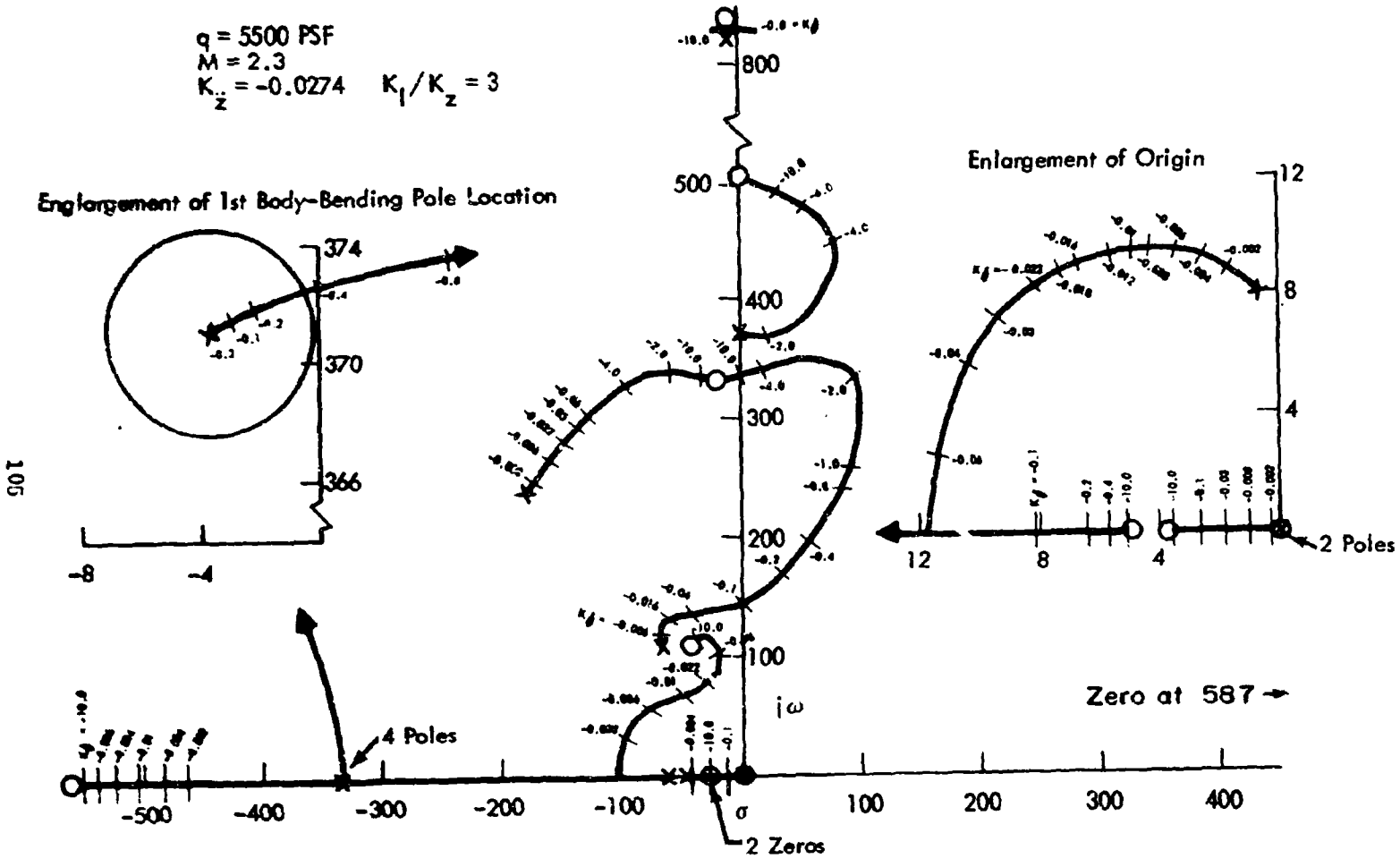

Figure 38: ROOT LOCI FOR $\ddot{z}/\ddot{z}_c$ FLIGHT CONDITION 1

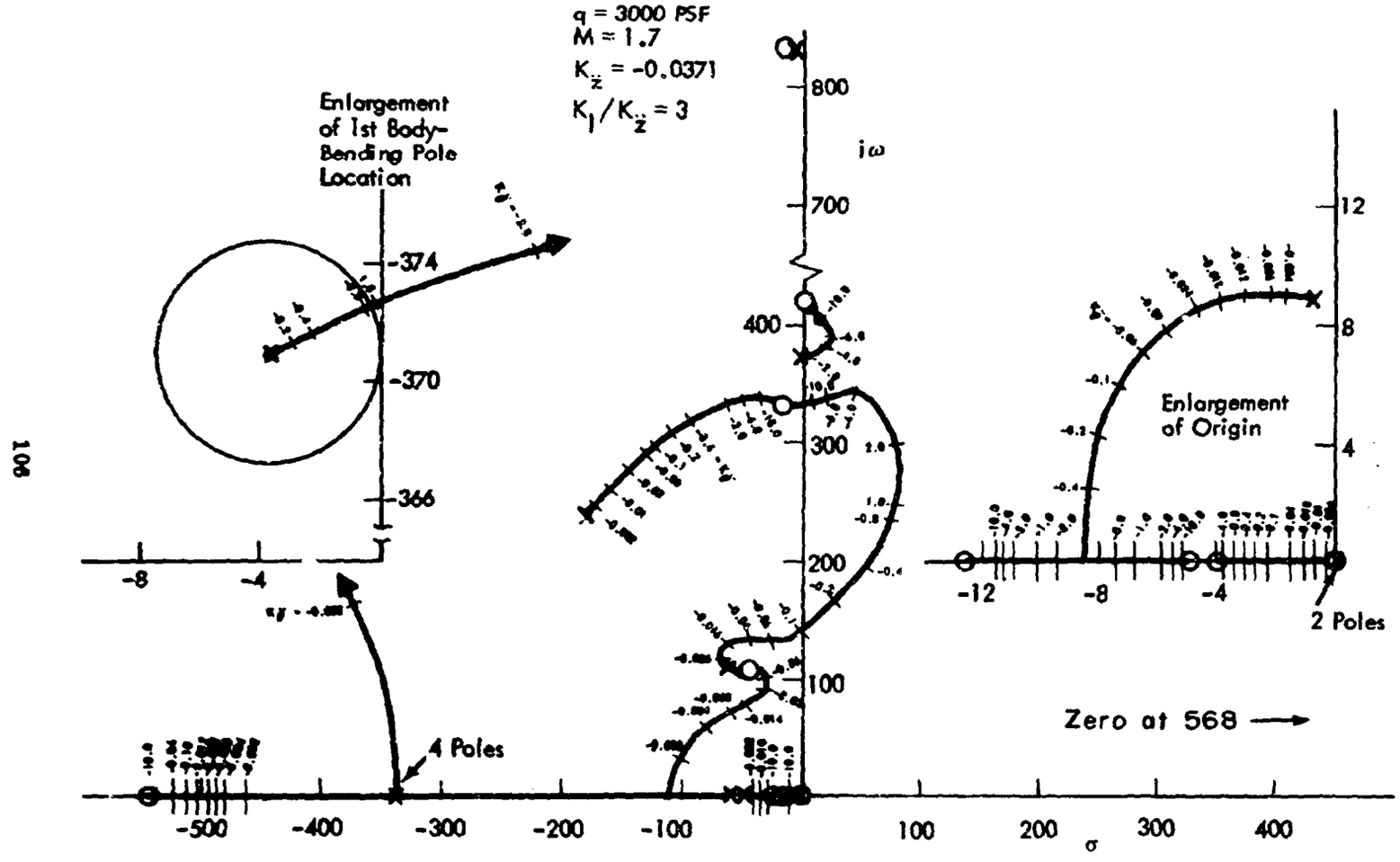

Figure 39: ROOT LOCI FOR $\ddot{z}/\ddot{z}_c$ — FLIGHT CONDITION 2

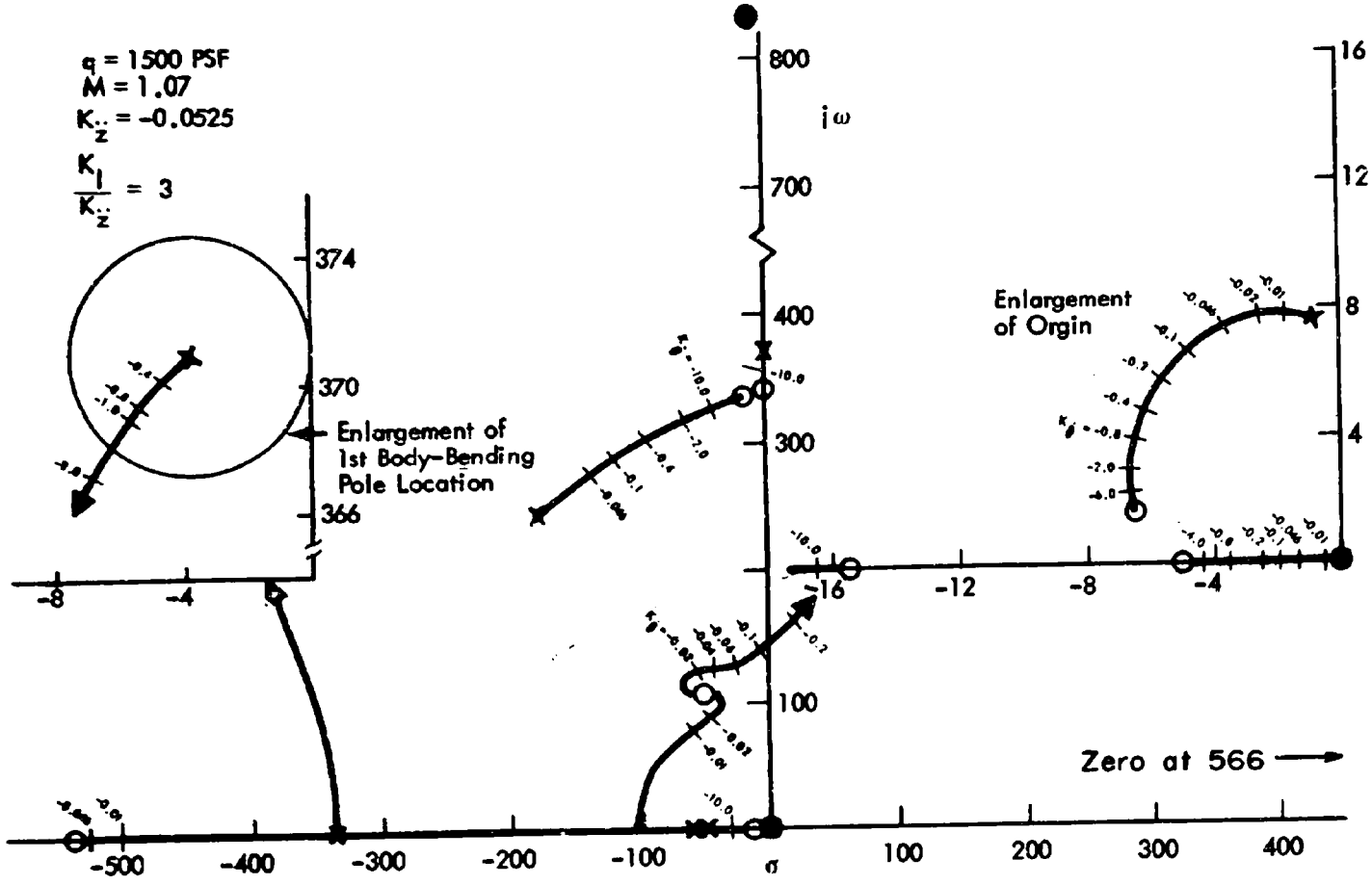

Figure 40: ROOT LOCI FOR $\ddot{z}/\ddot{z}_c$ — FLIGHT CONDITION 3

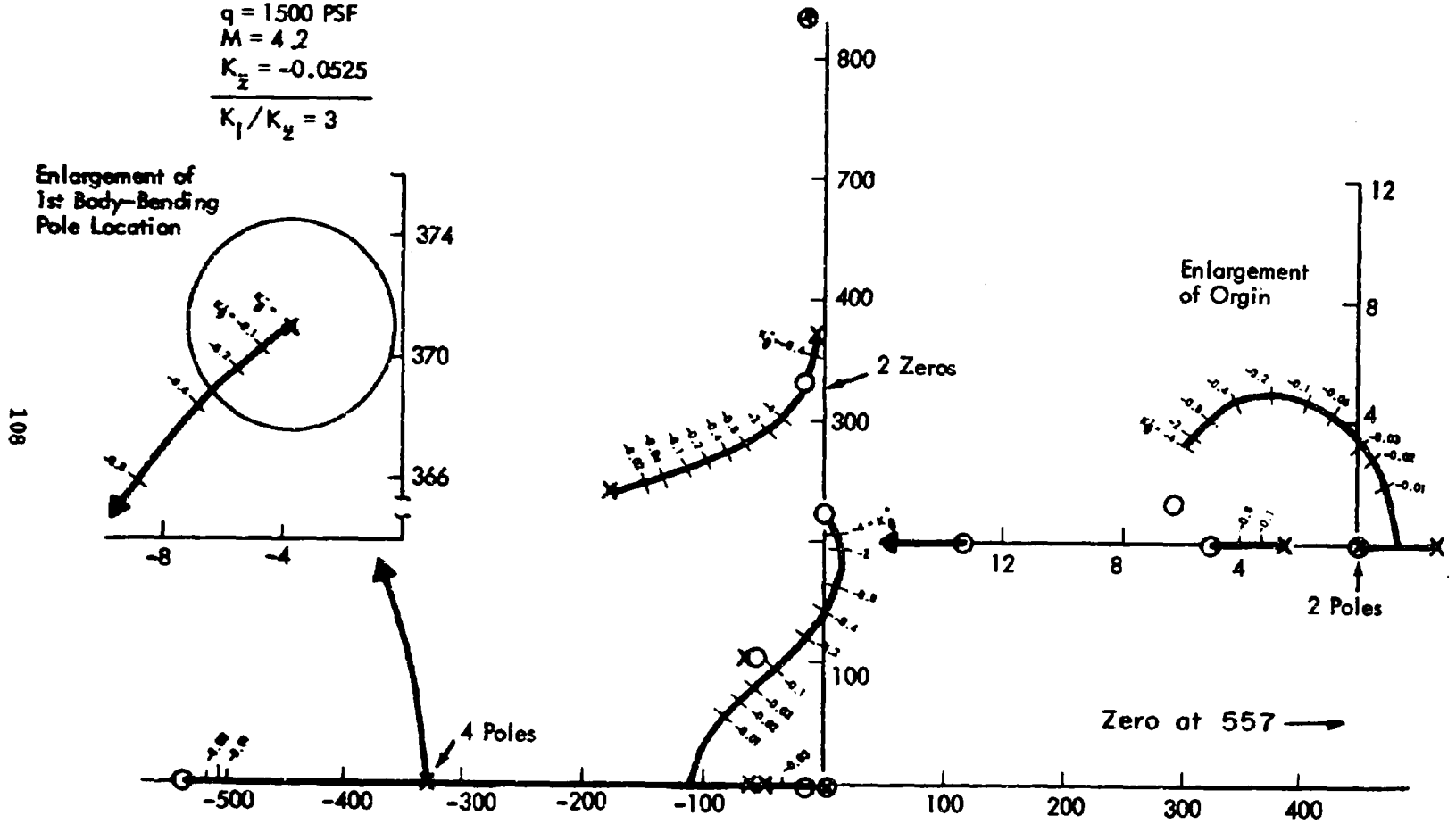

Figure 41: ROOT LOCI FOR $\ddot{z}/\ddot{z}_c$ —FLIGHT CONDITION 4

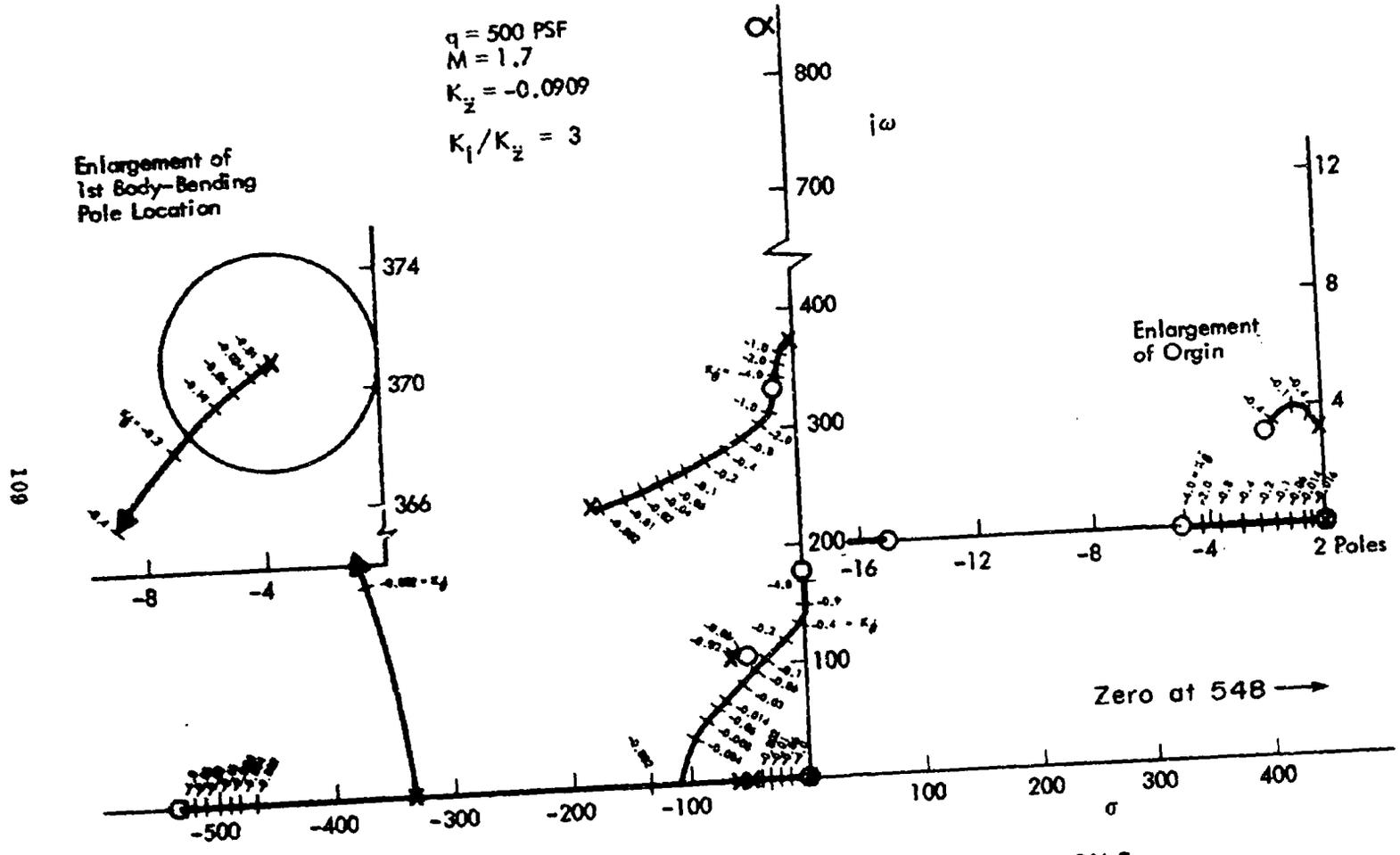

Figure 42: ROOT LOCI FOR $\ddot{z}/\ddot{z}_c$ — FLIGHT CONDITION 5

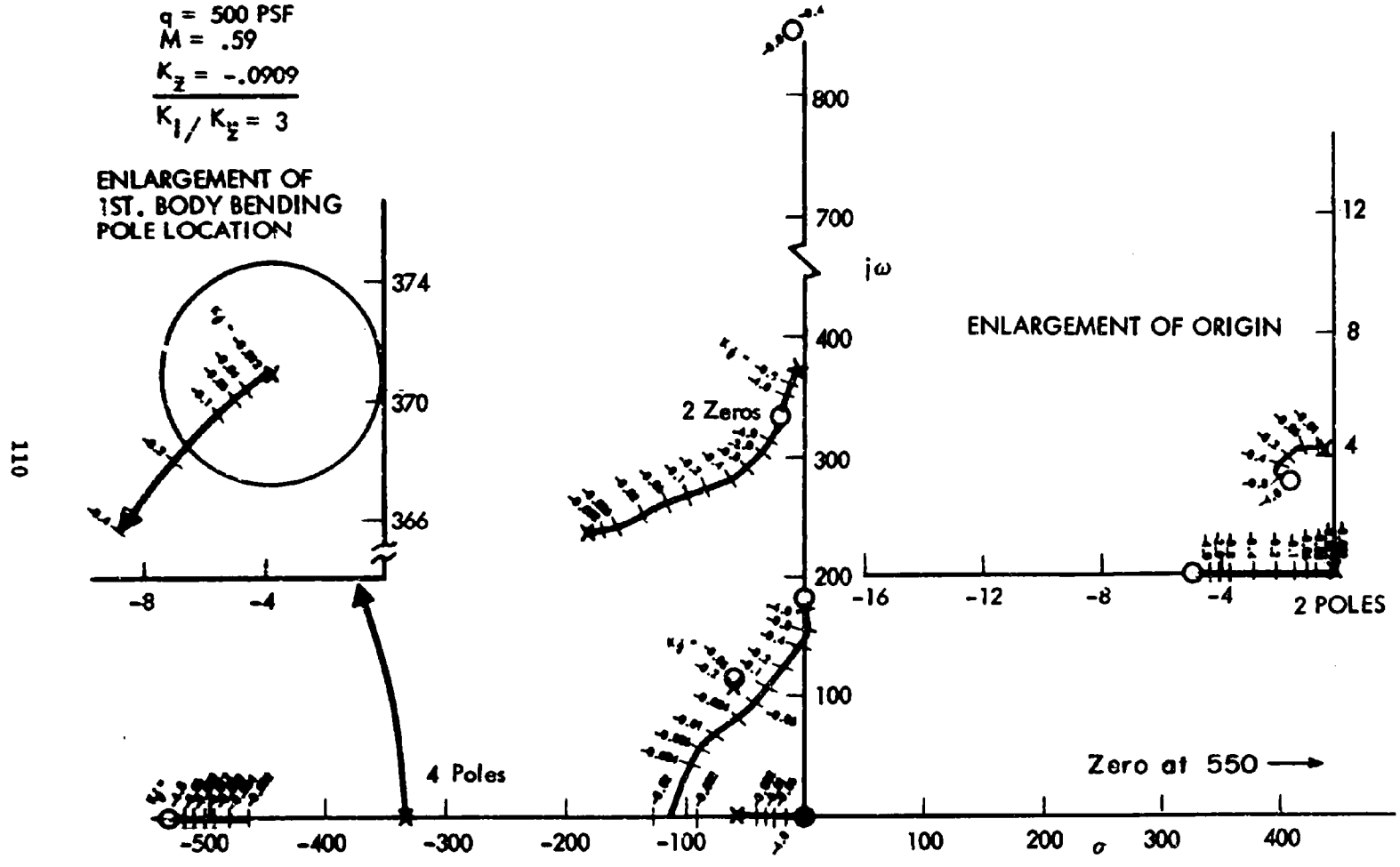

Figure 43: LOCI FOR $\ddot{z}/\ddot{z}_c$ — FLIGHT CONDITION 6

mode. For the high Mach number condition, the requirement for high gain arises in providing adequate damping of the rigid mode response, rather than from the requirement for response time. The high dynamic pressure condition (Figure 38) does not impose any critical design requirements; adequate system response can be achieved with gains that are not critical from a stability standpoint.

Amplitude versus phase plots of the system are shown in Figures 44 through 49. The stability criteria for gain and phase margins are shown in a combined form, or "vector margin" requirement, represented by the ellipse. The frequency locus in the vicinity of the first body bending mode frequency must lie 6-db or more below the 0-db point for the operating gain because its location laterally on the plot is uncertain due to phase response uncertainty of the fin servos at this frequency. These plots are useful in determining system gains that satisfy the stability criteria because a change in operating gain in effect shifts the 0-db reference point in these plots and does not alter the locus shape. In general, the chosen operating gain is different than the gain for which the plot was originally made. The location of the 0-db line, corresponding to the chosen operating gain, is indicated by the position of the horizontal axis of the vector margin ellipse.

Figure 50 shows step response characteristics for the chosen operating gains as obtained using a digital computer time response program. A first-order 0.5-second time constant step response is shown for reference. The use of integral plus proportional compensation in the outer forward loop yields zero steady state error. The initially chosen time response requirement of 0.5 second is achieved or exceeded for all cases. The high frequency oscillatory response occurring early in the response time is associated with the residues of the roots on the locus that cross the imaginary axis in the vicinity of 140 rad/sec. These responses were obtained without rate saturation in the fin servo. (When a rate limit of 150 degrees per second was added in the analog studies, this oscillatory response was essentially eliminated.) Stability limitations on upper gain margin for the high Mach number condition restrict the damping achievable for the rigid mode response; consequently, the overshoot characteristic is high compared to the response achievable for flight conditions where the missile is statically stable.

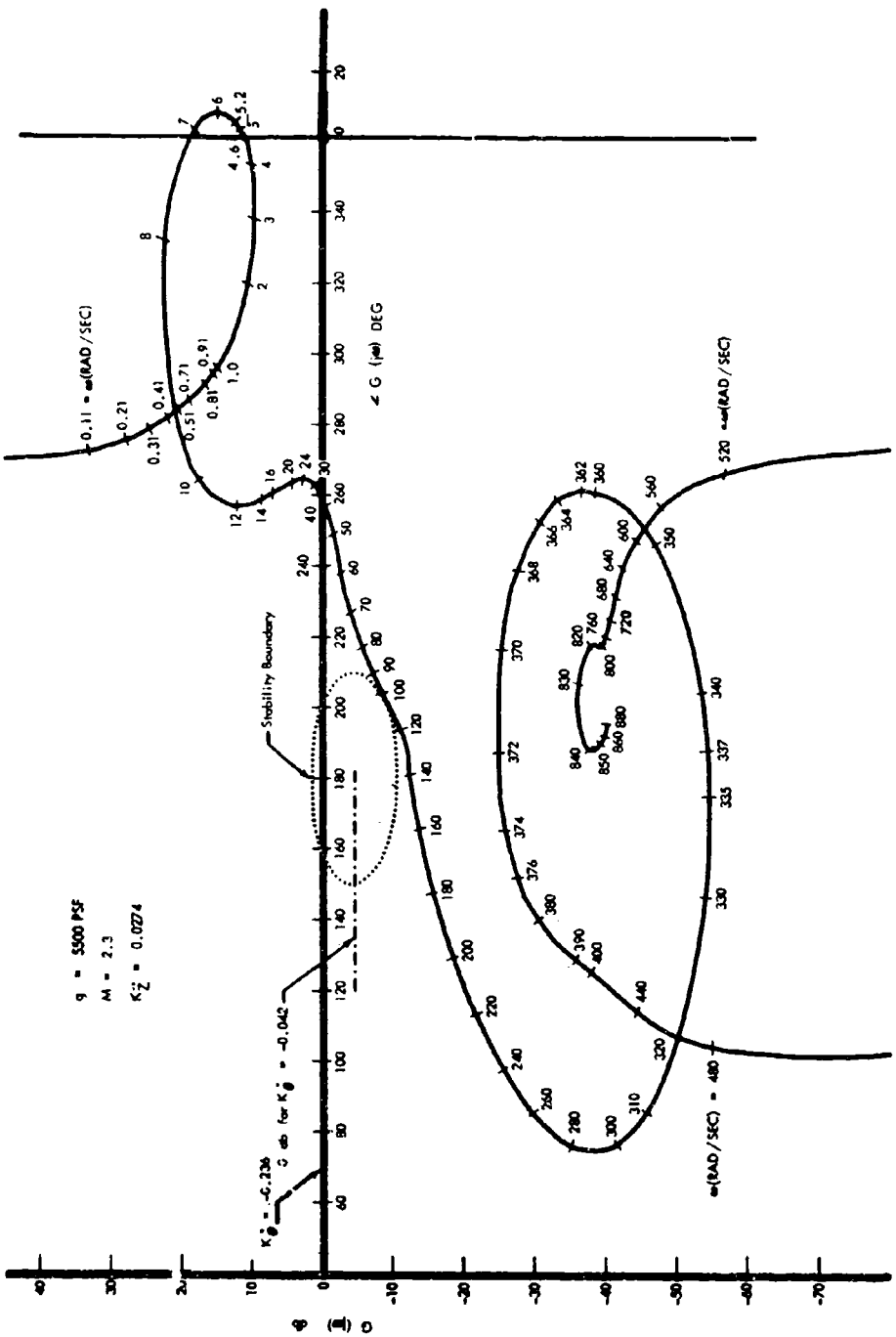

Figure 44: FREQUENCY RESPONSE - FLIGHT CONDITION 1

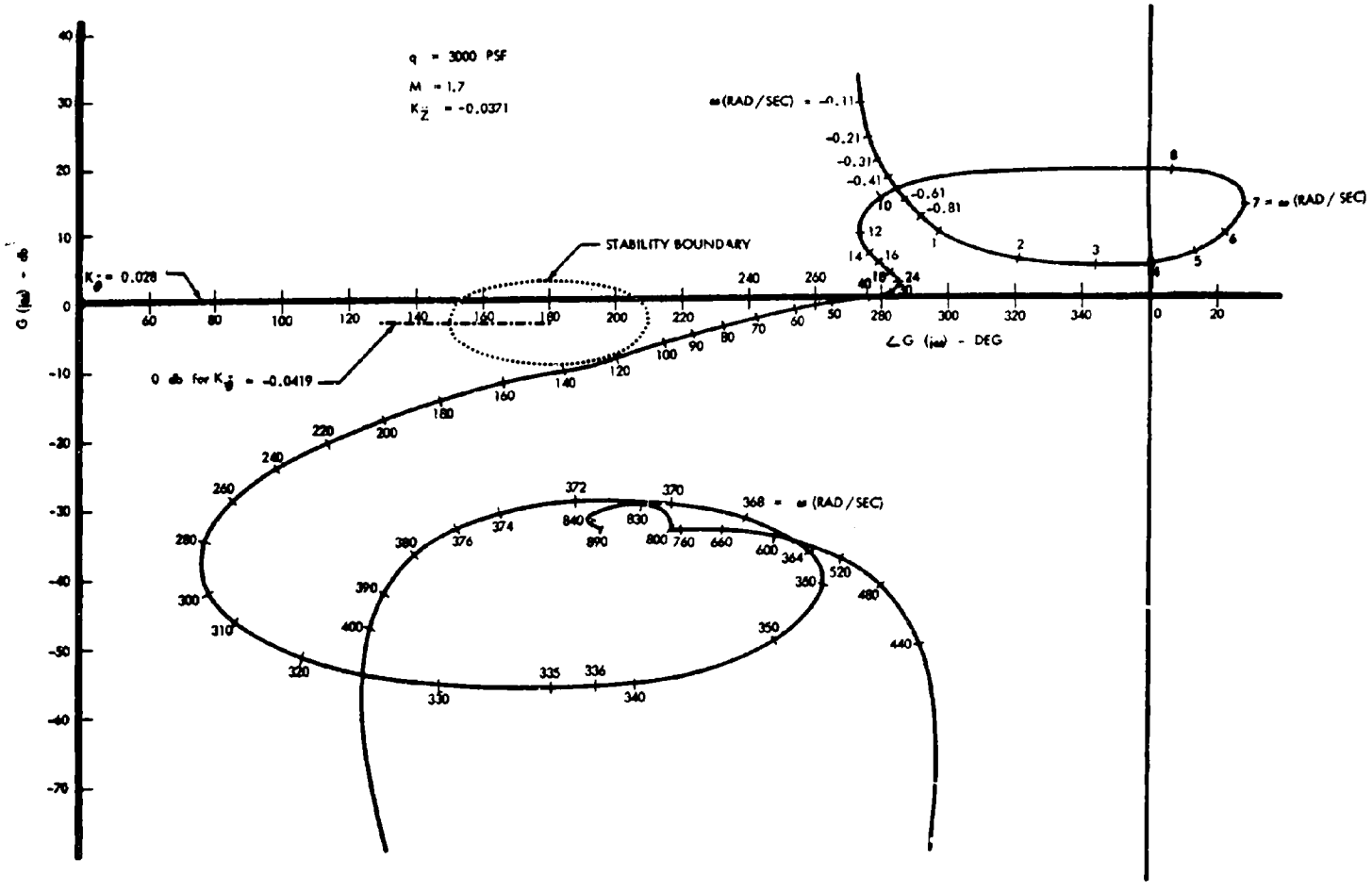

Figure 45: FREQUENCY RESPONSE - FLIGHT CONDITION 2

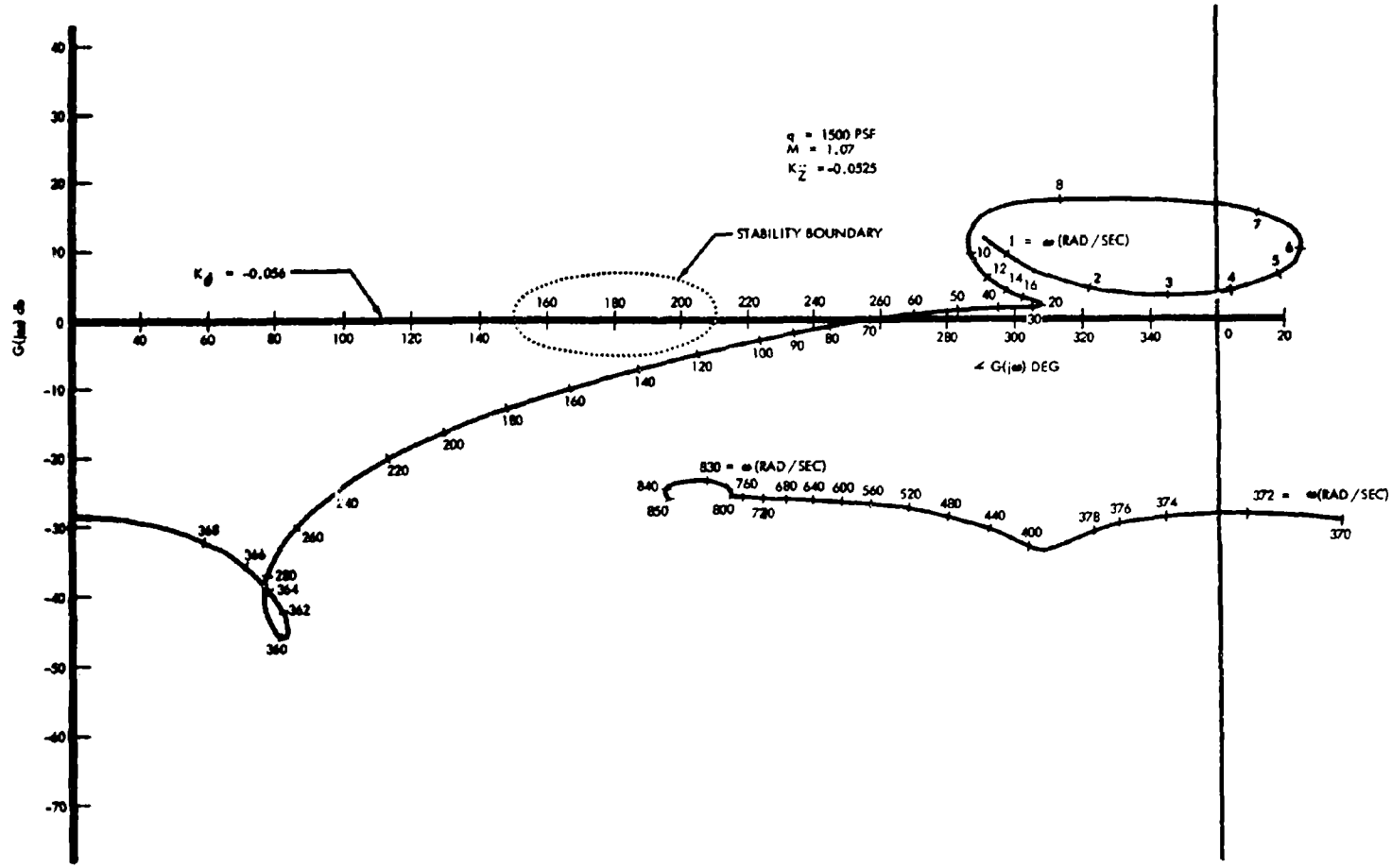

Figure 46 : FREQUENCY RESPONSE - FLIGHT CONDITION 3

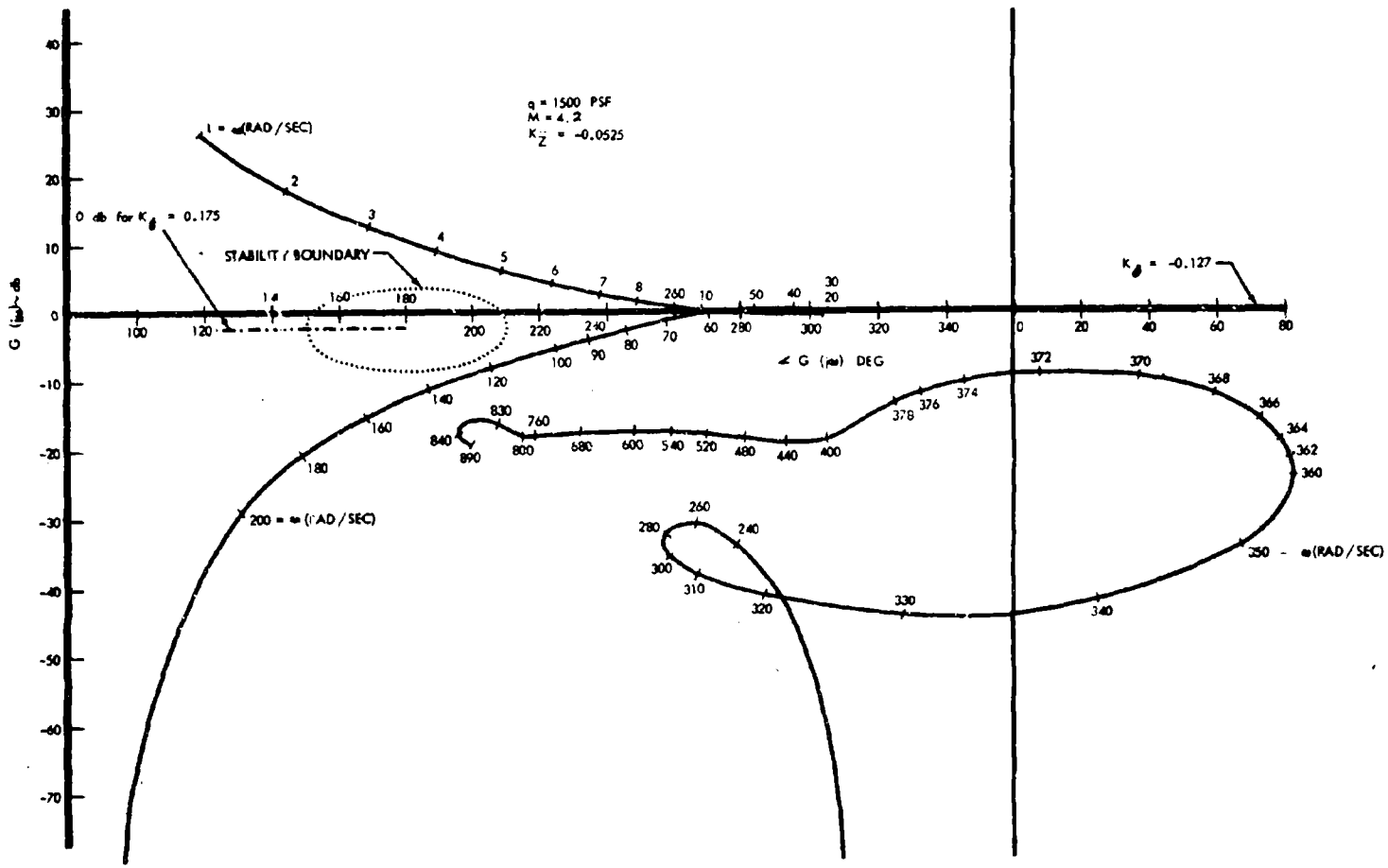

Figure 47 : FREQUENCY RESPONSE - FLIGHT CONDITION 4

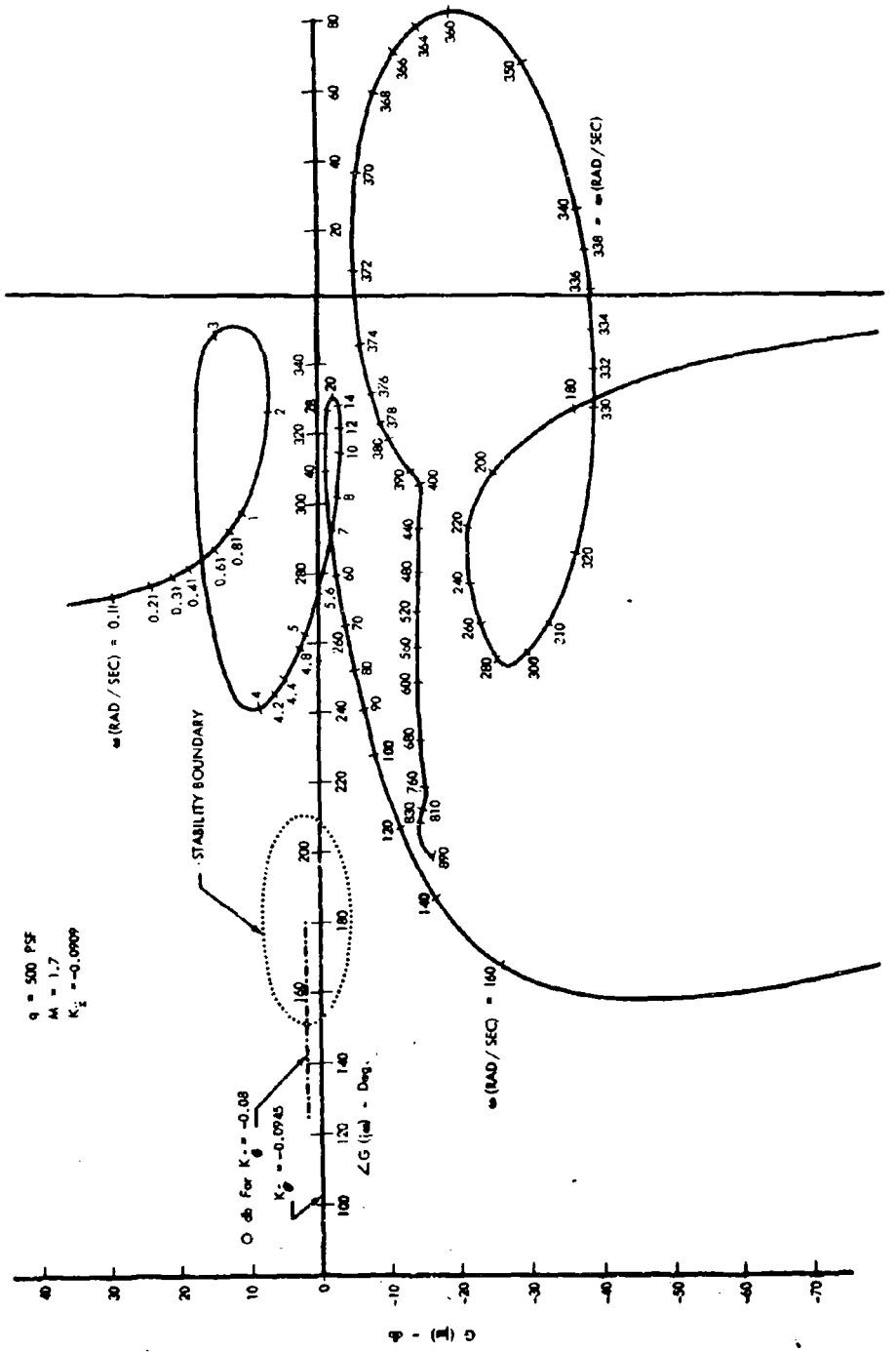

Figure 48: FREQUENCY RESPONSE - FLIGHT CONDITION 5

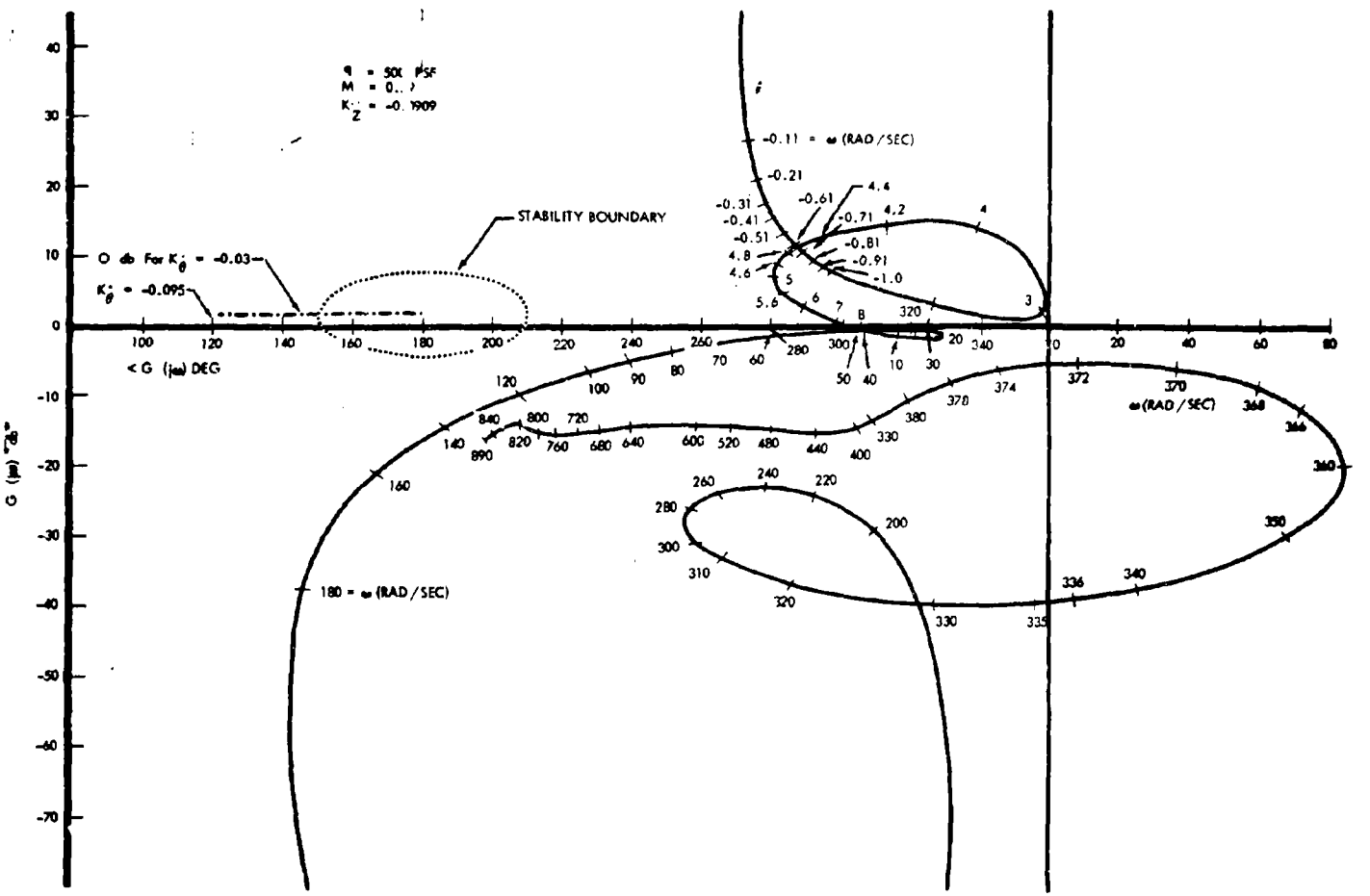

Figure 49: FREQUENCY RESPONSE - FLIGHT CONDITION 6

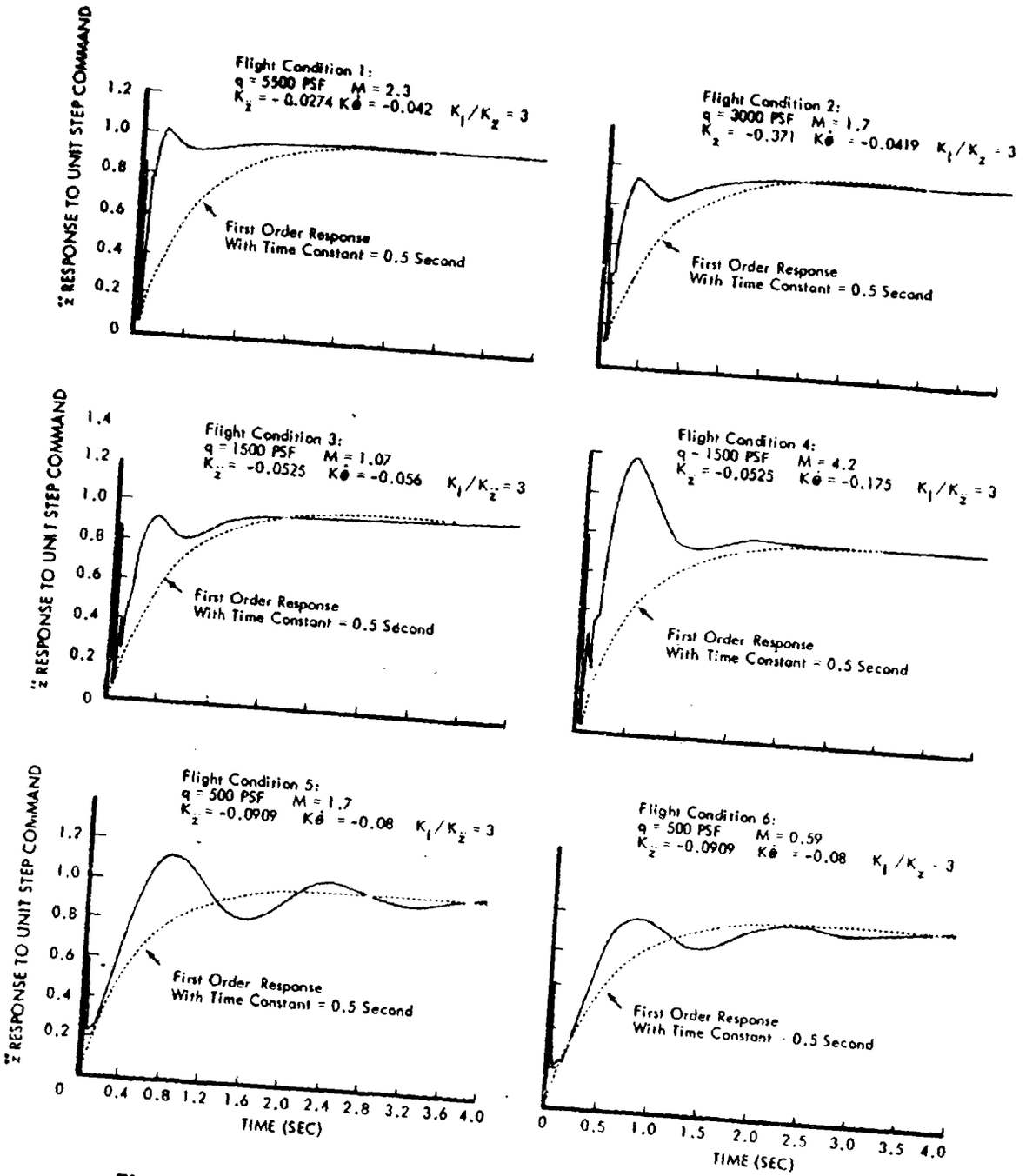

Figure 50: TIME RESPONSE FOR NOMINAL AUTOPILOT

The six major flight conditions were simulated on an analog computer to check against the digital gain margin data and time-response data and to study several nonlinear hardware characteristics. Gain margins and time responses were verified.

Fin control servomechanism rate limiting of 150 degrees/second had no degrading effect on autopilot performance and served to nearly eliminate the high-frequency oscillatory response that was shown in the digital computer time responses. The difference in response is shown for Flight Condition 5 in Figure 51. The effect of a pure time delay (such as could result from a digital autopilot and/or the fin control servo) on autopilot stability was investigated. It was found that a 0.01-second delay could be tolerated for Flight Conditions 1 through 5, and 0.015-second could be tolerated for Flight Condition 6.

The effects of aerodynamic fin masking and high fin angles of attack on autopilot stability were found to be small for this configuration.

The low dynamic pressure (10 psf) apogee condition (Flight Condition 7) presented special design problems. Inspection of the missile acceleration transfer function (shown in Table VIII) for this condition shows that the "accelerometer zeros," — those rigid mode zeros whose location is determined by the accelerometer position along the missile longitudinal axis — lie on the real axis in the left and right half planes. This situation prevents the design of a stable Type 1 normal acceleration system of the type considered. These zero locations are, in conditions of extremely low dynamic pressure, dependent not only on the accelerometer location, but also on the tail-wags-dog characteristic. If the effective tail-wags-dog frequency can be made sufficiently high, the accelerometer zeros can be made to lie on the imaginary axis as they do for the other flight conditions considered in the terminal phase of flight. The tail-wags-dog frequency can be influenced by mass balancing of the control fins, and this influences the minimal dynamic pressure for which a satisfactory normal acceleration autopilot can be designed. Study of Condition 7 was dropped during the nominal autopilot design because the primary interest was in the terminal homing phase of flight.

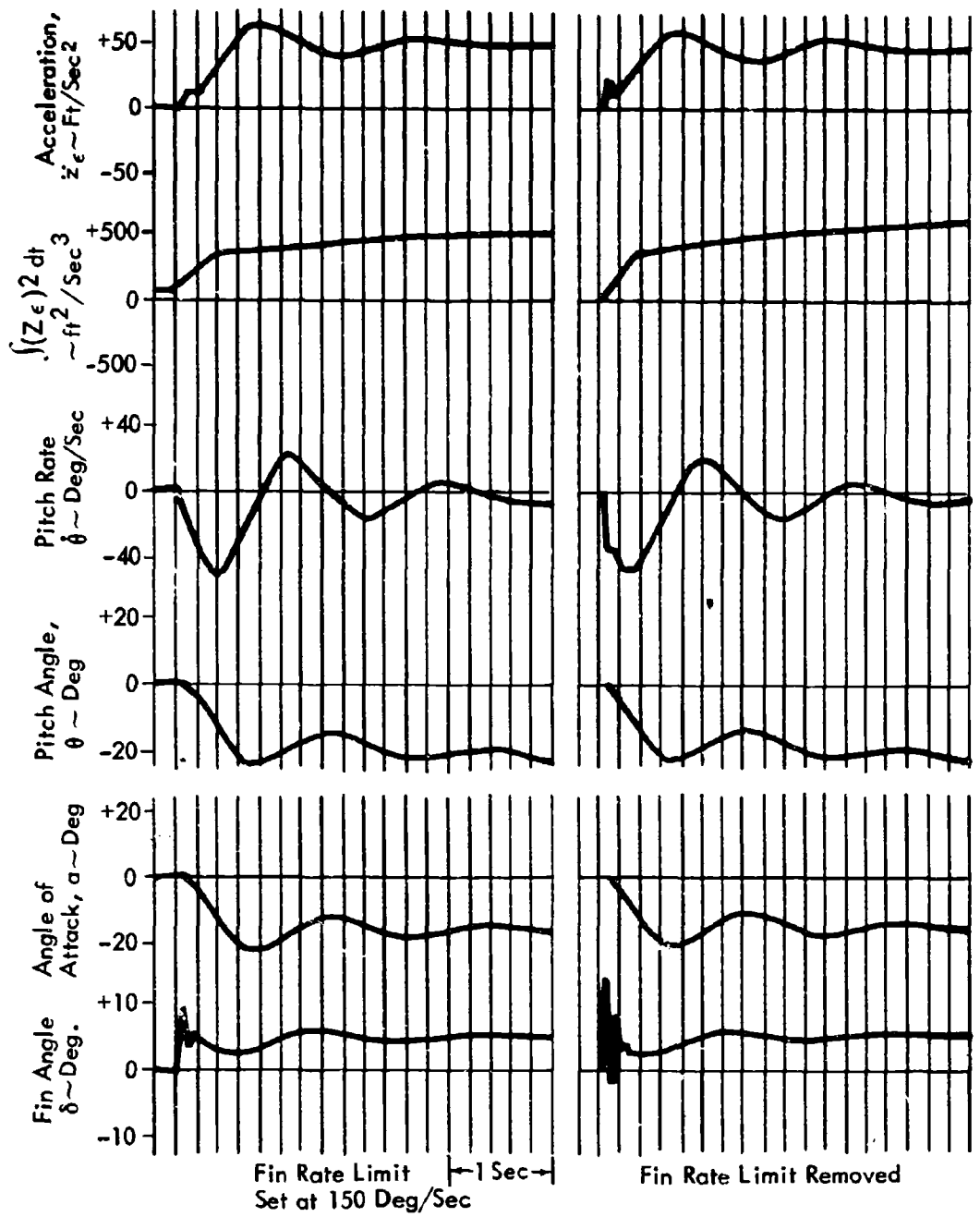

Figure 51: EFFECT OF SERVO RATE LIMIT ON TRANSIENT RESPONSE

It is significant to note the importance that body bending plays in the autopilot design. The missile is relatively stiff structurally with a ratio of rigid mode to first body bending mode frequencies of approximately 1 to 50. Yet when practical consideration is made of the phase uncertainty of high frequency fin servo response, along with the choice of integral plus proportional control to produce zero steady state error, the consideration of body bending directly influences the achievable system response and involves the designer in trades on the choice of body bending compensation. If integral plus proportional control is not used, relatively fast rigid mode response can be achieved. However, the design of such a system to keep steady state error bounded to less than 45% requires the use of high gains; these high gains conflict with requirements for body bending stability. These considerations lead to the conclusion that control analyses that neglect the effects of body bending will very likely reach invalid conclusions relative to the achievable time response and steady state error characteristics.

2. Bistable Controller. The nominal Type 1 autopilot required gain changes over the flight regime to provide satisfactory performance. As discussed in Section III, this was accomplished for the terminal (or homing) phase in the analog simulation by programming $K_{\dot{z}}$ as a function of q. It would be desirable from a simplification standpoint to avoid gain programming. A substantial in-house research program on the application of advanced control theory to autopilots for defense missiles was in progress at the time of the ASM investigation. Extensions of the bistable controller concept described by Gieseking (Reference 7), and employing Lyapunov's second method were found to be quite successful in providing constant gain autopilots with nearly invariant response for defense missile configurations. (This work is documented in Reference 8.) The bistable concepts provide a state variable dependent bias command signal to a bistable control element in the autopilot forward loop. Because of the success of the defense missile application, it appeared possible that these same concepts might have the potential for simplifying the ASM autopilot even though the ASM is a different type of missile. A block diagram of a bistable augmented autopilot resulting from the application of these concepts is shown in Figure 52. The following is a

discussion of the synthesis, simulation, and performance of this bistable controller concept for the ASM configuration used in this program.

A bistable controller was first applied to the nominal Type 1 autopilot. Results with the Type 1 autopilot were not entirely successful. The bistable controller did speed up time responses to step commands and improved the stability in Flight Condition 4. However, the system suffered from relaxation-type limit-cycle problems and was quite sensitive to the $\dot{\theta}$ gain entering the bistable command channel. Further investigations were conducted with a Type 0 system (no forward loop integrator). With this system, a bistable controller concept was synthesized which exhibited satisfactory stability and time response, and had less than 15% steady state error. The final controller concept deviated considerably from Gieseking's concept; however, his work did provide considerable insight into what was required to synthesize the final bistable controller concept.

The Type 0 autopilot was first studied without the bistable controller for performance comparison purposes. The Type 0 autopilot is identical to the Type 1 autopilot except the forward loop integration and compensation networks shown in Figure 31 are removed. Gain limits for this system were approximately the same as those found for the Type 1 system. The Type 0 system met the response requirement but required about the same gain scheduling as the Type 1 system. It also exhibited about 10% steady state acceleration error with the best gains for each condition. With the autopilot gains set for Flight Condition 1 (a terminal homing phase condition) and held constant, the system response was very poor in some flight conditions and the steady state acceleration error was as large as 45%.

A bistable controller was then added to the Type 0 system using the approach of Gieseking. As shown in Figure 52, the bistable controller adds a positive or negative acceleration command (U) in parallel with $\tilde{z}_\epsilon$. The sign of (U) is chosen by the sum of the state variables, which are: acceleration error, $\tilde{z}_\epsilon$; attitude rate, $\dot{\theta}$; and fin angle, δ. The weighting gains of these summed state variables were determined using the second method of Lyapunov. The bistable controller

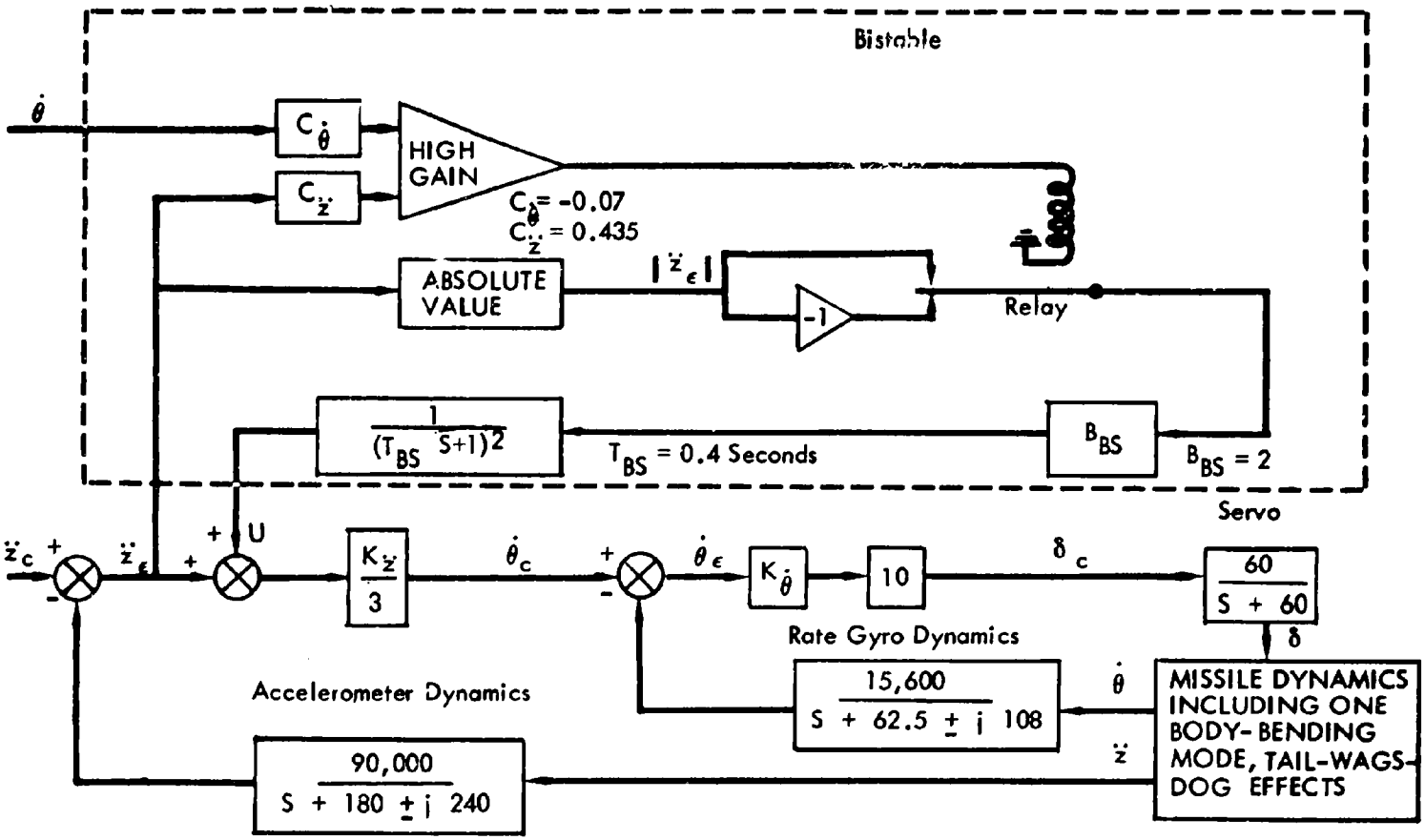

Figure 52: TYPE 0 AUTOPILOT BLOCK DIAGRAM AND MODIFIED BISTABLE CONTROLLER

shown in Figure 52 worked well and met response time requirements. It reduced steady state acceleration error to approximately one-third of that associated with a fixed gain Type 0 autopilot.

Figure 53 illustrates the time response of the bistable augmented Type 0 system and compares this response to that of an unmodified Type 0 autopilot without gain adjustment to a Type 1 autopilot that has ideally adjusted gains.

The final bistable controller represents a deviation from that described by Gieseking. The low pass filter was added to the bistable output to avoid exciting body bending modes. Without the filter, the bistable gain can not be made high enough to improve the ASM response at high q conditions. The addition of the filter induced a limit cycle. Two more modifications were necessary to eliminate this limit cycle. The bistable output magnitude was made proportional to $\bar{z}_\epsilon$ while the sign was controlled by the sum of state variable parameters $\bar{z}_\epsilon$ and $\dot{\theta}$ each weighed by a constant multiplier (see Figure 52). The gain of this $\dot{\theta}$ state variable signal was about half the magnitude and the negative of what Lyapunov's second method showed it should be. The use of the $\dot{\theta}$ state variable in this case was to stabilize a limit cycle and not to improve system response time as in the basic bistable controller design.

A 6-db tolerance was demonstrated on parameters B_{BS}, T_{BS}, and $C_{\dot{\theta}}$ with this controller. A much faster response time could have been obtained by reducing T_{BS} but, in this case, the allowable tolerance on $C_{\dot{\theta}}$ was very small. Work with this control system indicated that several bistable controllers performing differing tasks would further improve performance. One such controller would be used to improve response time and another to stabilize limit cycle oscillations with perhaps a third controller to reduce steady state errors. Further study may indicate which combination of state variables is best for switching and which is best for absolute values of (U).

The hardware necessary to implement the bistable augmented autopilot is conventional and inflight gain adjustment is not required. The absolute value functions

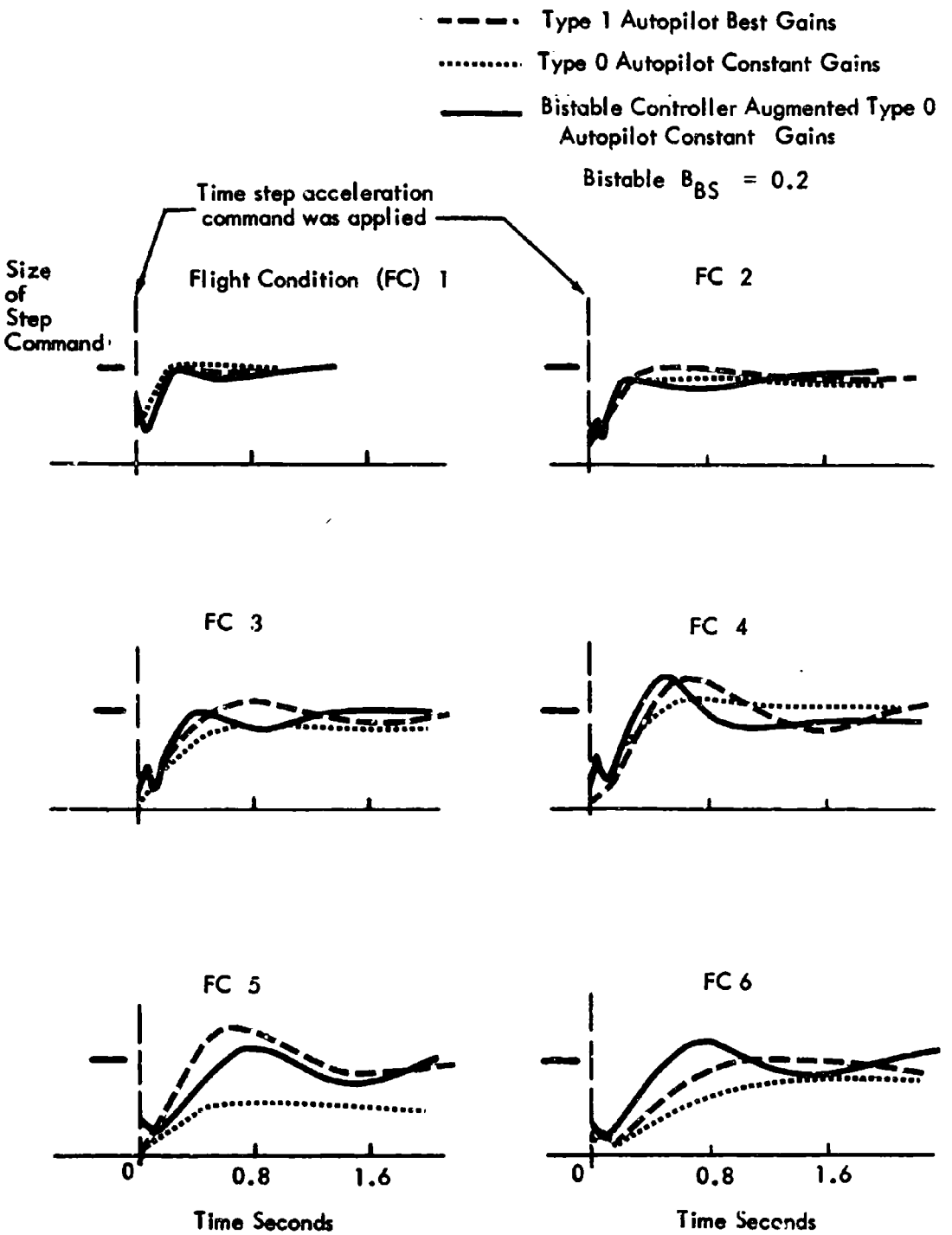

Figure 53: AUTOPILOT PERFORMANCE COMPARISON

and simple summing of signals to control the bistable output sign can be implemented using relays or solid state switches and amplifiers, or digital components.

Even though the final bistable controller is not of the same form as that studied by Gieseking, it was developed only through the insight gained through the investigation of his technique. The synthesis of the controller required a considerable amount of cut and try effort; however, analytical techniques are being developed which will make the synthesis more efficient (Reference 8).

3. Self-Adaptive Autopilots. Several adaptive control concepts were examined briefly for potential application to the ASM considered in the study. The examination was conducted in light of known characteristics of the ASM configuration (e.g., body bending, aerodynamic stability, tail-wags-dog effects, and required autopilot gains) to outline possible advantages and potential problem areas associated with implementing these systems. The adaptive concepts which were considered as likely candidates were:

- Honeywell high gain system (Reference 9)
- G. E. adaptive system (Reference 10)
- Pitch, yaw, or roll axis dither to determine control effectiveness (Reference 11)
- Calculation of M_α during flight (References 12 and 13)

The Honeywell system tends to hold the system gain to a value near the upper gain stability limit. The G. E. system can have a preselected gain margin. Both concepts utilize a pair of system poles which become unstable at gains lower than critical vehicle modes such as body bending. These poles may be inherent in the basic flight control system design or may be introduced especially to provide a dynamic characteristic for the adaptation loop design.

In the Honeywell system, a limit cycle motion results when a pair of poles are driven across the $j\omega$ axis; autopilot gain is adjusted to maintain a preselected limit cycle amplitude. The G. E. system does not permit a limit cycle of the compensation pole, and consequently, for the same compensation poles, would tend to operate at a lower gain than the Honeywell system.

The difficulty with both of these concepts lies in the selection of satisfactory poles, invariant with flight conditions both in frequency and the gain at which they become unstable, for monitoring the stability of the control system. For some vehicles, a critical vehicle mode may place a lower stability limit on the autopilot. This problem was encountered in X-20 studies and may place very close bounds on the acceptable autopilot gains. For the study vehicle, which has relatively high body bending frequencies, the complex rate gyro poles could be considered suitable for monitoring the stability of the autopilot for either of the approaches. (The gyro poles would have to be sufficiently invariant with temperature to allow their use.) For Flight Conditions 1 through 6, this pair of poles (at 140 rad/sec) become unstable prior to the first body bending mode (at 370 rad/sec). However, at Condition 7, as was previously discussed, the body bending poles become unstable first. To make either concept work on the study vehicle, it would be necessary to select different compensation poles, or make modifications (such as changes in the tail-wags-dog frequencies as was previously discussed) so that the gyro poles would become unstable first. In either case, the designer becomes involved in the entire regime of making trades between system stability, time response, sensor location, and required gains and compensation.

For the Honeywell concept, the effects of the limit cycle must be considered. First, a determination must be made of the tolerable limit-cycle amplitudes from the standpoint of structural integrity. Secondly, the effect of limit cycle amplitude on control servo power requirements must be considered. Installed power capabilities on ASM configurations tend to be marginal because space and weight are at a premium. The power required to maintain a limit cycle such as is required in the Honeywell concept can become a predominant factor in determining servo-power requirements.

The third adaptive approach is to program autopilot gain as a function of control effectiveness. A dither signal is applied to the autopilot vehicle axis. By monitoring the effect of the signal on vehicle amplitude about that axis the control effectiveness can be determined. Then if the required autopilot gains to maintain the stability margins are known as a function of control effectiveness (N_δ), the gain

can be adjusted. More vehicle parameter variation effects can be removed if the dither is applied to the axis in which the gain adjustment is required. However, if this is undesirable with some configurations, it may be possible to apply the dither signal to one axis and adjust the gain in another axis (e.g., dither roll axis and adjust pitch axis).

An acceptable pitch rate gain program ($K_{\dot{\theta}}$) as a function of control effectiveness (actually shown as N_{δ}/I), for the baseline Type 1 autopilot discussed previously is shown in Figure 54. This program provides the desired gains which were determined in the Type 1 autopilot design (Table VII) for the terminal phase conditions (1, 2, and 3). Gains for 4, 5, and 6 are acceptable. The upper and lower gain stability limits for Flight Conditions 1 through 6 are also shown. It can be seen that none of these points fall within 6 db of the programmed gain. It should be noted that only Condition 4 has a lower-gain limit. The missile is statically unstable at this condition and a minimum gain is therefore required for stability. This can be seen from the amplitude-phase plot in Figure 47. An advantage of this approach to an adaptive autopilot is the possibility of conducting all the testing and monitoring of response in the roll axis which is usually the least critical of the vehicle axes. A complicating factor is that relationships between roll-axis response and control effectiveness in pitch and yaw are not always straightforward.

The final concept involves the calculation of the autopilot gains from a single parameter, M_{α}/I. As shown in Figure 55, there is an explicit autopilot gain for given M_{α}/I. (This brings together all the effects of Mach number, dynamic pressure, angle of attack, and c.g. shift). This concept involves the calculation of M_{α} from measurements of $\ddot{\theta}$, $\dot{\theta}$, $\ddot{z}$, and δ. References 12 and 13 establish the feasibility of applying the technique to an adaptive autopilot. It has been shown to be possible to calculate the values of the stability derivatives based on a comparison of the assumed vehicle equations of motion to actually measured motions of the vehicle. Two equations are usually needed for each axis because of the requirement for measurable state variables. This computation can be carried out continuously, with values of stability derivatives being continuously updated.

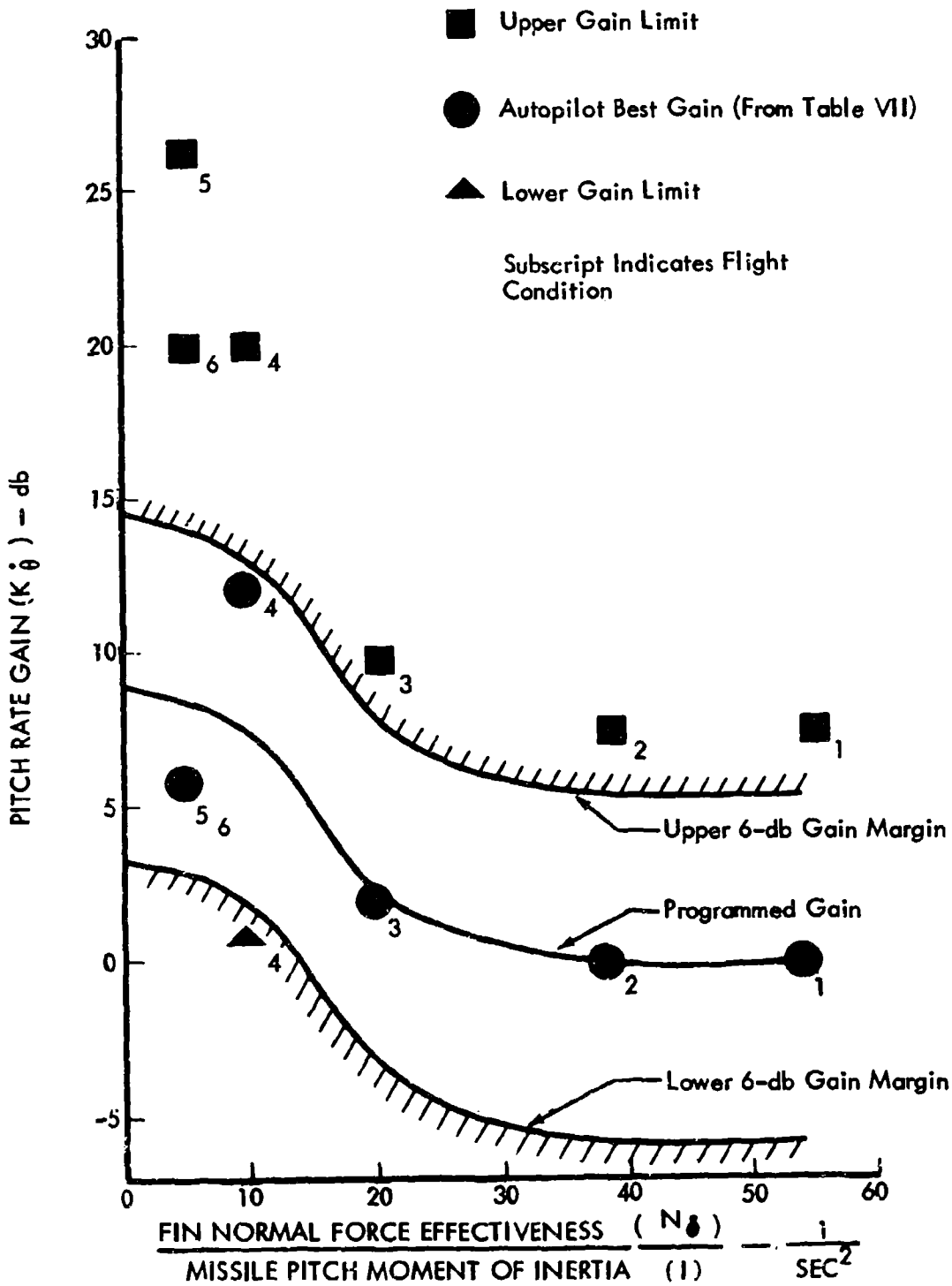

Figure 54: GAIN PROGRAM FOR NOMINAL TYPE 1 AUTOPILOT

The application of any of the above concepts to an ASM of the type being considered appears feasible but would require considerable analysis and simulation to confirm feasibility and to evaluate potential performance improvements. Performance improvements would have to be weighed against implementation complexity to determine the best approach for a given application.

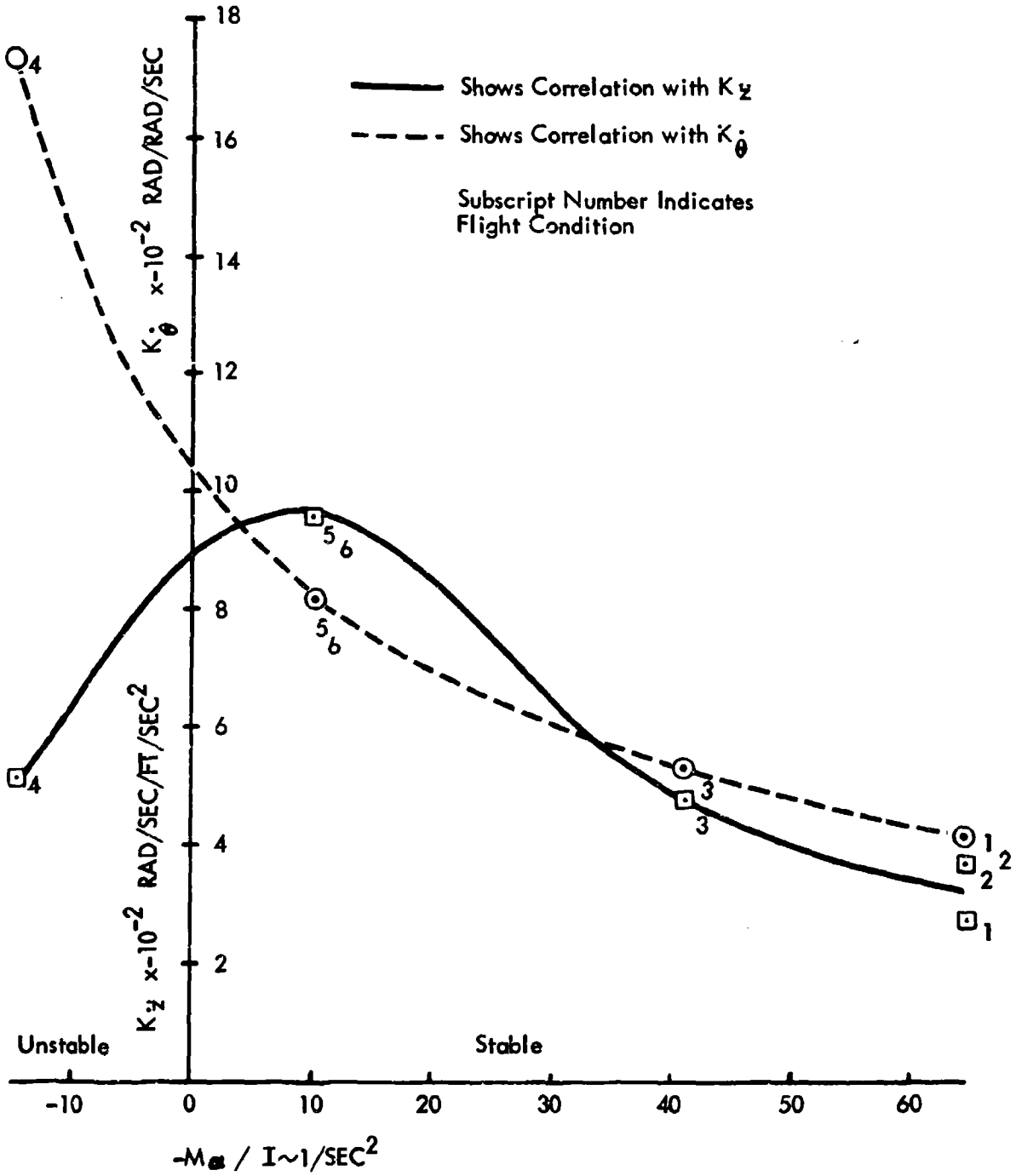

Figure 55: TYPE 1 AUTOPILOT BEST GAIN vs M_{α}/ I

SECTION VII

CONCLUSIONS AND RECOMMENDATIONS

In summary, the results of the study have shown that:

(1) Assuming that satisfactory homing sensors are available, high accuracy terminal guidance of ASM is feasible and considerable control system design flexibility is possible;

(2) An optimal guidance system can be implemented to meet practical missile requirements and characteristics, and can be implemented with state-of-the-art onboard digital computers;

(3) Nominal inertial and homing sensor characteristics, which were selected for the study, are compatible with ASM miss distances of approximately 5 feet;

(4) For the selected ASM configuration, a normal acceleration autopilot provided satisfactory inner-loop performance for the homing phase.

Based upon the effects of nominal equipment anomalies and disturbances considered, the choice of homing guidance concept should be made from the standpoint of simplicity, cost, and development time. In terms of miss distance, no really significant performance advantages or disadvantages were found for any of the concepts. The one exception is that pursuit guidance should not be used if large bias errors are present. If an inertial rate stabilized gimbaled tracker is used, proportional guidance can be implemented easily using the output of the rate gyro for sensor gimbal stabilization. Optimal guidance can be implemented with either body-fixed sensors or gimbaled sensors.

Implementation of the optimal guidance concept was shown feasible with realistic system characteristics. The preliminary digital computer sizing (Section V) shows that several state-of-the-art computers have sufficient capacity for implementation of the optimal guidance law. Based on the assumptions made for sensor performance and estimates of the increased computer requirements, use of the optimal guidance laws does not appear justified at this time. The 2600-word memory computer needed for optimal guidance is about 1500 words larger than estimates for implementing the more conventional proportional or pursuit guidance.

The optimal guidance concept showed no significant advantages over proportional and pursuit guidance for the range of sensor errors and disturbances that were investigated. Examination of optimal guidance error data shows that the main contribution to the miss distance is the error the optimal (Kalman) filter makes in estimating the position deviations normal to the trajectory. Because the miss distances for proportional and pursuit guidance were almost as small, it appears that the filtering action of the vehicle and autopilot dynamics are almost as good as the optimal filtering action of the optimal filter.

As more homing sensors are developed and performance data are obtained, it may be found that the performance of some of the sensors may not be as good as assumed in this study. However, these sensors may have tactical advantages that make consideration of them necessary.

The Kalman filter that was developed for the study was based on white noise; however, other filters can be developed for nonwhite noise if the noise can be described statistically. Thus the optimal techniques have the potential of coping with poorer sensor characteristics than the conventional techniques. Trades could then be conducted between sensor performance and cost, and optimal-guidance performance and implementation cost. The results that show the optimal filter to be the predominate source of error suggest the possibility that more simple linear guidance laws could be used with the filter with little increase in error.

There are tactical situations in which optimal guidance concepts would have advantages. If there were long blind zones such as might be encountered if the TV tracker lost the target; the ability of the optimal system to guide on position information from inertial platform measurements updated while the target seeker was still operating would allow accurate guidance. If proportional or pursuit guidance did not have enough time to get the missile accurately aimed at the target before the blind zone, or if the blind zone was long enough for the effects of wind to be appreciable, proportional or pursuit guidance would be substantially poorer.

Although investigations of equipment anomalies indicated no serious restrictions on impact accuracy, the results of the state-of-the-art surveys indicate that the homing sensor may be a major weakness in the design of an ASM. This weakness is not necessarily due to poor performance on the part of the sensor (in fact the results of the TV tracker experiment were surprisingly good) but is primarily due to the lack of adequate performance data for actual trackers. The tracker error model (bias and white noise) used in this study was based on the best available information but is nevertheless idealistic. Sensor errors are seldom this simple— rate gyros that may be used in a tracker gimbal stabilization loop are known to have output noises that may contain dominant frequencies as low as 1 to 2 cps. This type of noise, because it approaches the missile control frequency regime, makes a high accuracy control problem considerably more difficult than the white noise. Even predominantly higher frequency noise can cause difculties with a digital flight control system.

The number of general conclusions that can be made about the normal acceleration autopilot design are limited because they are very much configuration dependent. However, some precautions should be mentioned. Basic designs should not be predicated on simplified autopilot representations in determining autopilot response criteria to meet miss distance requirements. In the configuration investigated, the actual autopilot response was well above that required to make response effects negligible. Details such as body bending and guidance gains must also be considered in the autopilot design because of their interrelationship with overall system stability and time response. Some type of programmed gain or adaptive configurations will be required for the normal acceleration autopilot because of the wide range of flight conditions to which the homing ASM is subjected and the rather stringent response requirements during the terminal phase. As discussed in Section VI, a programmed gain autopilot would not be easy to implement. The bistable controller concept that was investigated appears to have considerable promise. It can be implemented with available components and it provides good response and steady-state error characteristics.

To provide additional information necessary to the design of satisfactory homing ASM's, the following areas of investigation are recommended:

(1) Better definition, under realistic operating conditions, of the performance characteristics of homing sensors that are potentially useful from a tactical standpoint is necessary. Information is required on acquisition capability, response characteristics, and the statistical and real-time characteristics of the output errors. The output error data should provide bias error distribution and noise power spectral density characteristics. Power spectral density information should cover the very low frequency range (less than 1 cps) to include bias shift effects. Tape recordings of tracker noise would be useful in simulation studies. Acquisition range capability is needed to define midcourse guidance accuracy requirements; more detailed blind range information is necessary to select blind range guidance concepts.

(2) More complete hybrid computer simulations of optimal control concepts should be conducted in which its impact on the autopilot can be determined (and vice versa) and effects of items such as autopilot response, command limiting, and servo limiting can be evaluated. Control power requirements should be compared with those for proportional and pursuit guidance.

(3) Additional autopilot studies in which cross-coupling effects are included should be conducted to compare relative merits of the bistable controller and other adaptive concepts. This effort should include an investigation of the use of bistable controllers with more than one bistable signal. Compatibility of the homing phase and midcourse phase autopilots with the boost phase control requirements should be investigated.

REFERENCES

1. Hart, J. E., Adkins, L. A., and Lacau, L. L., Stochastic Disturbance Data for Flight Control System Analysis, ASD-TDR-62-347, Lockheed-Georgia Co., Marietta, Georgia, 1962.

2. Montgomery, J. M., Homing Air to Ground Missile Flight Simulation, D2-36515-1, The Boeing Company, 1966 (Available through DDC).

3. Wonham, W. M., Stochastic Problems in Optimal Control, Research Institute for Advanced Study (RIAS) Report 63-14, May 1963.

4. Kalman, R. E., New Methods and Results in Linear Prediction and Filtering Theory, Research Institute for Advanced Study (RIAS) Report 61-1, January 1961.

5. Bryson, A. E., and Johansen, D. E., "Linear Filtering for Time Varying Systems Using Measurements Containing Colored Noise," IEEE Transactions on Automatic Control, January 1965.

6. Laning, J. H., and Battin, R. H., Random Processes in Automatic Control, McGraw-Hill, New York, 1956.

7. Gieseking, Darrel, "An Optimum Bistable Controller for Increased Missile Autopilot Performance," IEEE Transactions on Automatic Control, October 1963.

8. Bakken, O. A., et al, Application of Modern Control Theory to Defense Missiles, D2-125095-1, The Boeing Company.

9. Rang, E. R., and Stone, C. R., "Adaptive State Vector Control Adaptive Controllers Derived by Stability Considerations," Military Products Group Report 1529-TR-9, Minneapolis-Honeywell Regulator Company, 15 March 1962.

10. Self Adaptive Control System Evaluation on X-15 Simulator, LMEJ 4465, G.E. Light Military Electronics Dept. Armament and Control Section, Johnson City, N.Y.

11. Stallard, D. V., A Missile Adaptive Roll Autopilot with a Small Amplitude Limit Cycle, Raytheon Co. Missile Systems Division, Session 18, Paper 3, IREEJACC Conference, 1965.

12. Zaborsky, J., Luedde, W., Berger, R., Berger, J., and Madonna, M., Development of an Advanced Digital Adaptive Flight Control System, FDL-TDR-64-115, McDonnell Aircraft Corp., St. Louis 66, Missouri, 1964.

13. Clingman, W. Dean, Aerodynamic Stability Derivations from Flight Test Data — Wing II, D2-14731-1, The Boeing Company, Confidential.

14. Stein, Lawrence H., Matthews, Malcolm M., and Frenk, Joel W., STOP — A Computer Program for Supersonic Transport Trajectory Optimization, to be released as a low number series NASA contractor report, The Boeing Company, 1967.

APPENDIX I

STATE-OF-THE-ART SURVEY

1. Introduction. State-of-the-art surveys were conducted in the areas of inertial guidance sensors, optical homing guidance sensors, and radar-type active and passive homing sensors. Original intentions to include current ASM control concepts, terminal accuracy, and effects of disturbances on terminal accuracy in the survey were frustrated by the inaccessibility of classified material.

Three basic inertial navigation sensor schemes were studied: strapdown, floated ball (MIT "flimbal" concept), and the gimbaled platform. The survey resulted in the selection of the conventional gimbaled platform type inertial measurement unit as a baseline sensor for the study. An analysis of the errors generated during midcourse prior to target acquisition, intrinsic to this system, for three representative air-to-ground trajectories and three cost level instrumentations was accomplished. The error data generated from this analysis were used as initial position and velocity error data for the miss distance analyses.

The results of the survey of optical sensors indicated that all such systems (TV or infrared), both current and projected for the 1970 period, employ manual target acquisition. In some systems the target is acquired before launch from the carrier aircraft; in others the sensor output is telemetered to the carrier aircraft and the necessary signals for manual target acquisition and lockon are transmitted back to the missile. Once acquisition is achieved the system is no longer dependent on a man in the loop and the terminal phase of the flight is completed automatically. Because this study was concerned primarily with the terminal homing phase of flight, studies performed for optical homing sensors did not include investigation of the dynamics and pecularities of manual target acquisition.

A gimbaled TV tracker using centroid tracking logic was chosen as the baseline sensor because insufficient data was available to evaluate the correlation type tracker. To get quantitative effects of target and background characteristics and range to target on tracker errors, an experiment was performed using the

centroid tracking concept and photographs of various targets taken from different altitudes. Simulated homing flights yielded the effect of range-to-target on tracker error. The effect of target contrast was not determined.

The study results showed that radar cannot provide an operationally useful system against any wide variety of targets, due to target scintillation characteristics and background reflection characteristics of nearby objects. Because active radar sensors appear applicable only to very restricted target situations, radar sensors were not considered in the system studies.

2. Inertial Measurement Unit. The baseline inertial guidance sensor chosen for further study was the conventional gimbaled type of inertial platform, for which information was available on cost and accuracy. Equipment variations for this type of inertial measurement unit, relating cost to sensor accuracy, were exercised with an upper limit on cost of the platform and associated electronics of $40,000 (excluding airborne computer).

The primary function of the inertial guidance system is to furnish boost and midcourse navigation information for guidance purposes, and also in some instances to provide information on missile motion during the homing phase.

To perform these functions the inertial navigation system and its associated navigation and guidance computer must have the following characteristics: (1) unlimited azimuth freedom to handle missile launch in any direction; (2) information outputs of missile acceleration, velocity, and attitude; (3) guidance and navigation accuracy sufficient to ensure target acquisition at the end of the midcourse phase of flight; (4) compatibility with the weapon carrier's master navigation system; and (5) be simple, reliable, inexpensive, light, small, and have a short starting time.

The three basic inertial navigation schemes studied were strapdown, floated ball, and gimbaled platform.

In the strapdown or analytic system, the inertial sensors, consisting of rate gyros and accelerometers, are mounted directly to the missile structure. The inertial attitude of the missile is determined by integrating the rate gyro output;

missile position and velocity in inertial coordinates are computed from the accelerometer outputs, taking into account the time varying orientation of the accelerometer input axis with respect to inertial space. The advantages of the strapdown system include: small size, weight, and power requirement, all of which result from the absence of the gimbal structure, angular resolvers, torquers, and slip ring of gimbaled systems. The system is all-attitude and certain instrument error coefficients can be minimized by properly orienting the instruments with respect to the missile nominal acceleration vector.

The disadvantages of the strapdown system reside in the large, high-speed computer to conduct the coordinate transformation necessitated by the non-commutivity of angular displacement; the stringent demands on range and resolution of the inertial instruments, particularly the gyros; the susceptibility of the platform to base motion coupling, coning induced errors, misalignment introduced by thermal base motion coupling, and complexity of the airplane navigation interface.

The floated ball platform consists of displacement gyros and accelerometers mounted in a spherical ball, neutrally buoyant in a fluid filled cavity. External communication with the ball is provided by a set of brush contacts to the ball, multiplexed communication signals being modulated on the d.c. power supply. The platform is all-attitude, compact, light, and with moderate power consumption. The stabilized ball isolates the inertial instrument from the base vibration and coning motion.

The disadvantages of the floated ball include the complex signal connection to the ball, non-Euler angle attitude sensing, and inability to achieve preferential orientation of inertial sensor with respect to the missile acceleration vector. The floated ball platform was regarded as high risk, because it had not yet been flown.

The advantages of the conventional gimbaled platform are low risk, absence of extreme requirements on the inertial sensory compatibility with airplane navigator. Euler angle-attitude readout, minimum computational requirements (spatial integrations performed mechanically by gimbals), and high degree of base

motion isolation. By use of a four-gimbal arrangement, the platform can be made all-attitude.

Its disadvantages included: size, weight, and power consumption; cooling requirement; and inability to achieve optimal orientation of sensors.

Three systems were compared in a somewhat arbitrary quantitative manner in the "Opinion Table," Table IX. Each performance parameter — risk, weight, volume, and power consumption — is assigned a weighting factor of up to 10 (the "maximum weight" column) based on its considered importance. Each of the candidate systems is assigned a "relative weight" of up to 10 that represents its merit for each of the performance parameters. The product of the "maximum weight" and the "relative weight" represents the score. Total score is the sum of the scores for the performance parameters. As shown in Table IX, the conventional gimbaled platform received the highest score. It was selected as the baseline inertial navigation system.

The system selected for this study consists of an external, three-gimbal, roll-limited stabilized platform on which are mounted an orthogonal triad of accelerometers. (A roll-stabilized missile is assumed.) The outputs of these accelerometers are singly and doubly integrated to determine the components of missile position and velocity. There are a number of methods of mechanizing this system. Because the system will probably be tracking the local vertical before launch, it may be well to continue this type of operation during missile guidance to eliminate starting transients, due to the step change at launch, from one type of mechanization to another. However, other mechanizations such as a "space fixed" platform coordinate system, with a coordinate transformation in the navigation computer, may prove to be worth its cost, because the use of inaccurate torquing components (intrinsic to the low-cost grade platform considered here) can be eliminated. Final selection of mechanization should include the trade between errors and cost to mechanize and compute the data for sensor pointing from the platform coordinates.

Table IX: OPINION TABLE

Parameter	Maximum Weight	Strapdown Relative Weight	Strapdown Score	Floated Ball Relative Weight	Floated Ball Score	Gimbaled Relative Weight	Gimbaled Score
Risk	10	5	50	3	30	10	100
Weight, volume, power consumption	3	10	30	8	24	4	12
Extreme sensor requirements	5	3	15	10	50	10	50
Computer requirements	10	3	30	7	70	10	100
Cooling requirements	2	10	20	7	14	4	8
Airplane system interface	5	4	20	8	40	10	50
Signal path equipment	8	10	80	4	32	8	64
Base motion isolation	8	5	40	10	80	10	80
Preferential instrument alignment	5	10	50	5	25	5	25
Cost	10	10	100	5	50	7	70
TOTAL			435		415		559

NOTE:
- The higher the score the more favorable the characteristic.
- Greatest possible weight = 10.
- Product of maximum weight for each parameter and relative weight equals the score.

Three different trajectories were considered in the analysis: a long-range semiballistic trajectory, a medium-range low-altitude skip trajectory, and a short-range semiballistic trajectory.

Three cost levels of IMU were considered in the error analysis for each of the trajectories. Table X presents the cost breakdown for each of the IMU's.

Table X: IMU COST BREAKDOWN

Three Gyros	$ 600	$ 3,000	$ 9,000
Three Accelerometers	1,200	3,000	9,000
Platform Navigation Computer	9,200	16,000	18,000
Electronics	2,000	3,000	4,000
TOTAL	$13,000	$25,000	$40,000

The two main sources of error in this system are initial condition errors and instrumentation errors. One representative set of data for initial condition errors at launch was used. There are two independent sources of initial heading error; the heading error introduced by the weapon carrier, and the error from the slaving misalignment of the inertial platform. These errors were assumed uncorrelated. Their effect was to produce a cross-range error. Initial misalignment of the platform vertical, though considered in the detailed analysis of errors, produced negligible errors. The mapping error was considered to be 1 foot per nautical mile. To study instrumentation error propagation in the inertial navigation system and assess the overall accuracy of the weapon system, a previously developed digital computer inertial navigation error analysis program was used. The inertial components and their characteristics are tabulated in Table XI. Briefly, the system gyro and acceleration analysis error models included were: 1σ uncertainty in accelerometer bias, (b); the 1σ uncertainty in accelerometer scale factor, (SF); the 1σ uncertainty in accelerometer cross-axis sensitivity, (NL); the 1σ uncertainty in gyro random drift, (RD); the 1σ uncertainty in mass unbalance, (MU); and the 1σ uncertainty in gyro aniso elasticity, (Aniso). Each term of the gyro error model was integrated separately

Table XI: VARIOUS COST LEVEL IMU COMPONENTS

Approximate System Cost		Gyro	Accelerometer	b	SF	NL	RD	MU	Aniso
	$13,000	M. H. GG-384	Donner 4G10	6×10^{-5}g	2.4×10^{-4}	3×10^{-6}	10°/M	10°/M/g	
	$25,000	G. P. I. 9567	G. P. I. 2414	6×10^{-5}g	2.5×10^{-4}	3×10^{-6}	1°/M	2°/M/g	0.5°/M/g^2
	$40,000	M. H. GG-8001	M. H. GG-177	1.4×10^{-5}g	1×10^{-5}	3×10^{-6}	2°/M	0.4°/M/g	

b ~ 1σ uncertainty in scale factor

SF ~ scale factor

NL ~ 1σ uncertainty in accelerometer cross-axis sensitivity

RD ~ 1σ uncertainty in gyro random drift

MU ~ 1σ uncertainty in mass balance

Aniso ~ 1σ uncertainty in gyro aniso elasticity

to give the components of 1σ uncertainty in the platform tilt angle, and these were then introduced into the net acceleration model. Each term was singly and doubly integrated to yield the influence of each error source on the overall system velocity and position accuracy. Further, the program determined the square root of the expected value of the sum of squares of these errors. It was assumed that there were no correlated uncertainties in the error sources; hence, the result was the root square sum (RSS) of the errors. The hand-calculated initial condition errors were combined with the computer-determined IMU errors and the total error-at-acquisition budgets that resulted are tabulated in Tables XII, XIII, and XIV. Note that in the cost range of $13,000 to $40,000, the accuracy of the inertial navigation system is not substantially increased for cost levels beyond $25,000.

3. TV Homing Sensors. Vendor data on optical homing sensors showing the effect of range to target, and target versus background characteristics were required as a basic input to the formulation of the optimal guidance filter, but the state-of-the-art survey did not yield these data. However, sufficient descriptive information on TV-type centroid trackers was obtained to enable such accuracy characteristics to be evaluated on a semi-idealized basis. No information was found that would allow a credible prediction of accuracy for correlation-type trackers; therefore, the TV-type tracker using centroid-tracking logic was selected as the baseline sensor to be considered. Tracker output errors were assumed to consist of bias error and white noise. From all available data, the standard deviation of white noise was from 1 to 3 milliradians. The nominal value was chosen to be 1 milliradian. The nominal value of bias error was assumed to be 1.74 milliradians.

The literature search on TV sensors revealed data for only narrow-field-of-view devices that were intended for use with an inertial attitude or attitude rate stabilized gimbaled mount. The wide field of view devices, for which data was obtained, provided the wide field of view capability during the acquisition phase only, and had only a narrow field of view capability in the tracking mode. Due to lack of information on the characteristics of wide field of view trackers, and

Table XII: 1σ ERRORS FOR SHORT-RANGE SEMIBALLISTIC TRAJECTORY

	Cost of IMU			$13,000	$25,000	$40,000
			Slant Range Acquisition (~ft)	Total Error at Acquisition		
1σ Errors	Position (~ft)	x	15,000	1065	1010	1010
			30,000	1060	1010	1009
			60,000	1050	1009	1005
		y	15,000	1091	1015	1015
			30,000	1091	1015	1013
			60,000	1091	1010	1009
		z	15,000	670	285	252
			30,000	630	280	248
			60,000	560	265	240
	Velocity (ft/sec)	$\dot{x}$	15,000	5.90	4.02	1.27
			30,000	5.74	3.98	1.27
			60,000	5.42	3.91	1.25
		$\dot{y}$	15,000	19.9	15.0	16.8
			30,000	18.5	15.0	16.3
			60,000	15.8	15.0	15.2
		$\dot{z}$	15,000	12.70	1.69	2.75
			30,000	10.90	1.71	2.21
			60,000	7.40	1.74	1.14
	Table Tilt Angle (~degree)	θ_x	15,000	3.030	0.073	0.060
			30,000	2.820	0.070	0.056
			60,000	2.400	0.064	0.048
		θ_y	15,000	3.030	0.074	0.063
			30,000	2.820	0.084	0.058
			60,000	2.400	0.104	0.049
		θ_z	15,000	3.030	0.068	0.047
			30,000	2.820	0.080	0.047
			60,000	2.400	0.102	0.049

Table XIII: 1σ ERRORS FOR LOW-ALTITUDE SKIP TRAJECTORY

Cost of IMU				$13,000	$25,000	$40,000
			Slant Range Acquisition (~ft)	Total Error at Acquisition		
1σ Errors	Position (~ft)	x	15,000	6100	1390	1300
			30,000	4900	1250	1210
			60,000	2500	1150	1100
		y	15,000	5000	1940	1900
			30,000	4500	1820	1720
			60,000	4000	1600	1350
		z	15,000	560	450	348
			30,000	525	420	347
			60,000	430	380	347
	Velocity (ft/sec)	$\dot{x}$	15,000	72.0	11.3	10.8
			30,000	64.0	10.0	9.5
			60,000	55.0	8.5	8.0
		$\dot{y}$	15,000	72.0	13.6	13.2
			30,000	64.0	12.5	12.2
			60,000	57.0	10.7	10.5
		$\dot{z}$	15,000	10.0	2.6	1.1
			30,000	3.6	1.5	1.0
			60,000	0.3	0.2	0.1
	Table Tilt Angle (~degree)	θ_x	15,000	7.460	0.430	0.144
			30,000	7.110	0.410	0.139
			60,000	6.620	0.370	0.132
		θ_y	15,000	7.460	0.430	0.144
			30,000	7.110	0.410	0.139
			60,000	6.620	0.370	0.132
		θ_z	15,000	7.150	0.430	0.144
			30,000	6.840	0.410	0.139
			60,000	6.450	0.370	0.132

Table XIV: 1σ ERRORS FOR LONG-RANGE SEMIBALLISTIC TRAJECTORY

Cost of IMU				$13,000	$25,000	$40,000
			Slant Range Acquisition (~ ft)	Total Error at Acquisition		
1σ Errors	Position (~ ft)	x	15,000	3790	1200	1082
			30,000	3640	1190	1075
			60,000	3330	1160	1060
		y	15,000	2990	2520	2480
			30,000	2890	2460	2410
			60,000	2700	2320	2300
		z	15,000	1950	530	339
			30,000	1930	525	334
			60,000	1890	500	240
	Velocity (ft/sec)	$\dot{x}$	15,000	32.0	5.3	4.4
			30,000	29.0	4.7	3.9
			60,000	23.3	3.6	2.8
		$\dot{y}$	15,000	32.4	12.7	11.8
			30,000	29.6	12.4	11.7
			60,000	24.0	12.0	11.6
		$\dot{z}$	15,000	15.7	2.7	3.4
			30,000	13.3	2.6	3.1
			60,000	8.7	2.5	2.6
	Table Tilt Angle (~degree)	θ_x	15,000	6.39	0.30	0.13
			30,000	6.28	0.28	0.13
			60,000	6.06	0.26	0.12
		θ_y	15,000	6.39	0.30	0.13
			30,000	6.28	0.29	0.13
			60,000	6.06	0.27	0.12
		θ_z	15,000	6.24	0.30	0.13
			30,000	6.14	0.29	0.13
			60,000	5.93	0.27	0.12

also the apparent equivalence of body-fixed and gimbaled sensors as conceptually applied to the optimal guidance task, the studies were based on the characteristics of narrow-field-of-view gimbaled TV trackers only. A simplified block diagram of a single axis implementation of this type of tracker is shown in Figure 56.

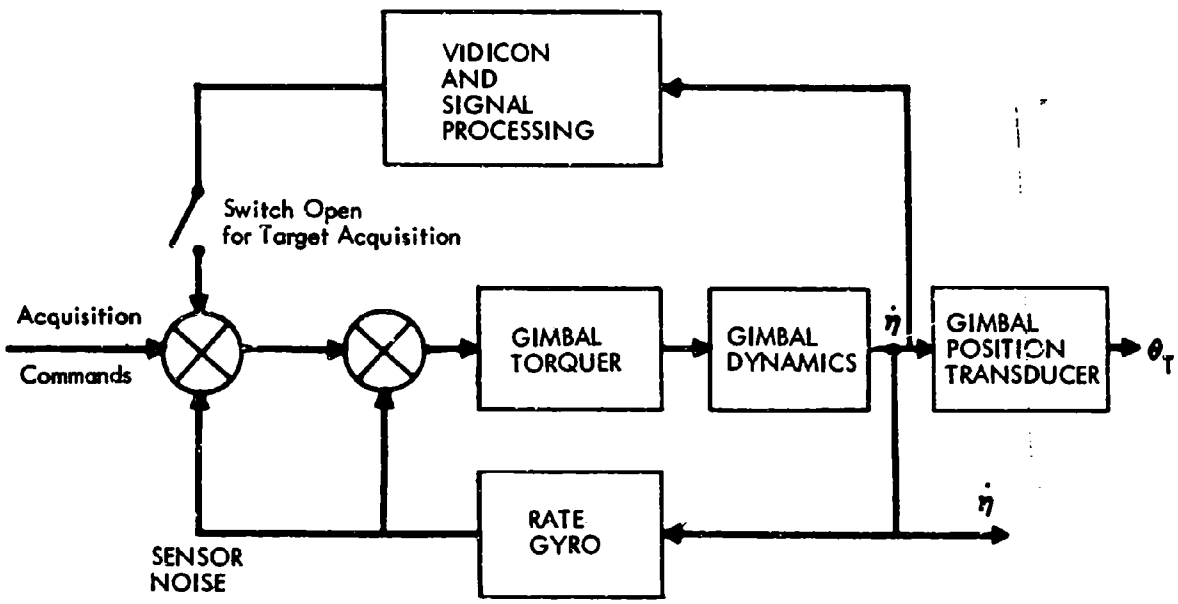

Figure 56: TV TRACKER BLOCK DIAGRAM

An experimental program was undertaken to generate accuracy characteristics for a centroid tracking sensor with scan resolution typical of the Walleye/Condor trackers. To get quantitative effects of target and background characteristics and range to target on tracker errors, simulated homing flights were made using photographs of various representative targets taken from five different altitudes. Results of the range-to-target effect on tracker error were obtained, but the effect of target contrast was not determined.

a. TV Tracker Survey Summary. The optical sensors considered included imaging and nonimaging systems. The general shortcomings of nonimaging systems tend to eliminate them quickly from further consideration. Mechanical complexity is one major drawback. In order to achieve substantial background rejection capability with a nonimaging system, complex modulation and demodulation techniques are necessary in the electronic signal processing, including the use of reticles and/or nutating devices. Reticle systems are fixed to one set of operating parameters — such as field of view, target size, modulation frequencies, and scan pattern. Reticles and reticle drive systems with their attendant bulkiness and moving parts can be eliminated by use of the vidicon. Imaging tubes with electronic scan allow the use of some rather straightforward signal processing to determine target size, number of targets, and spatial position in a given raster configuration. Independent horizontal and vertical deflection systems permit wide variation in programming scan rates and raster patterns to optimize tracking capabilities. A literature search produced a great number of references to TV trackers and related systems. Examination of the available material was begun with a study of the Navy's Walleye missile guidance scheme (an edge-type tracker), the Norden proposal on a similar device for the Condor missile, centroid-type trackers by Southern Research Institute, Barnes Engineering Company, and a few others.

A typical TV tracker includes a camera, tracker circuits, monitor, and a servo gimbal drive system to mechanically close the loop. For special applications, accessories such as image intensifiers, telescopic lenses, optical filters, automatic iris, and electronic exposure controls can be added to the system. Target position information is derived by locating video information relative to the raster scanned. Because the beginning of each horizontal and vertical scan is known, the position of the target can be determined by measuring the period of time from the start of a frame and line until the appearance of the video pulse indicating target presence. Video pulses are located relative to reference generator outputs that are synchronized with the horizontal and vertical sweep waveforms of the camera. The reference generator outputs are used to create x and y

tracking gate crosshairs that can be positioned anywhere within the field of view by adjusting a delay in the sync information.

Background discrimination is accomplished through the use of gating, to blank out a large portion of the raster. This allows a primary target to be tracked while other targets, decoys, and background details in the field of view are ignored. Blanking is synchronized with target video so that the video gate automatically tracks the target as it moves within the field of view. Video processing consists of amplification, clipping, smoothing, and removal of undesired background signal. In contrast systems, the target video is selected on the basis of amplitude relative to the background by clipping away the lower amplitude information. Video peaks are then amplified and used to trigger a position detector flip-flop circuit. Target position is determined from the output pulse width of the position detector that has been triggered by the target video pulse and the delayed sync pulse. This information is then integrated and amplified to provide a d.c. voltage output proportional to the position of the target.

The Walleye tracker, being well along in development, is probably most representative of the edge tracker state of the art. One large drawback of tracker systems that operate on the edge or point features of a target is the tendency to track the corners of targets or to shift to a false target, such as a bright point. This may make them highly susceptible to decoying and ineffective against a target-background complex containing many points of equal reflectance. The edge tracking philosophy is such that a target will be tracked by the edge that is scanned earliest, rather than as a whole. Therefore, at close range, the edge or corner of the target becomes the aim point, and central hits are of low probability.

There are two concepts of centroid-type tracking. One uses the spatial distribution of the target center. When used as the aimpoint, this pseudocentroid should produce central hits. This concept is known as "contrast tracking" as it is based on an area-gated scheme that computes the location of the centroid of the weighted video information lying inside the gate. The area-gated devices

do not track the center of the target proper as the contrast-contour trackers are able to do.

The Ford-Aeronutronics Multiple Edge Adaptive Tracking (MEAT) tracker and the Southern Research Institute (SRI) tracker are most representative of the state of the art in contrast-contour trackers. The MEAT tracker uses an asterisk-shaped scan pattern that can be generated from the center to outside edges of the target, or, as a result of recent development, a reverse outside to edge asterisk pattern can be used. Thus, the tracker operator has the option of choosing scan patterns to accommodate different target-background situations. The MEAT tracker logic can locate an apparent centroid with as little as 120 degrees of target periphery defined by a workable contrast edge. The SRI tracker has evolved through a number of gating schemes, including a manually set gate, a self-fitting rectangular gate, and the most recently developed contour-following gate with shape memory that offers the best immunity from momentary loss of contrast on any edge of the target.

Correlation-type trackers are the least known. This method has the potential of being best for use against poorly defined targets, because information from the entire scene is used. On the other hand, a correlation tracker with a large field of view would be ineffective against a target in a uniform background. Two correlation tracking schemes were encountered during the survey. One, by General Electric, had a field of view smaller than the target and a memory logic capable of updating itself once per second. The other was a system being developed by General Precision Labs and Sperry. This system had a 25-degree field of view and used a preinstalled photo transparency of the target scene as the reference. The reference photo transparency is rotated back and forth and, as the image of the scene on the ground aligns with the photo, a bright correlation spot is observed. The correlation spot represents the condition in which maximum correlation appears between the bright points on the ground and transparent portions of the phototransparency. At present, correlation devices have been developed mainly as a target acquisition aid for the pilot. A great deal more complexity must be added to convert it into a tracker. At the time of this survey, no company had

implemented a tracker from this concept as yet, although Emerson Electric is reported to have solved the problem with a more complex unit using magnetic drum storage and a mechanical scanning detector.

A summary of some of the tracking techniques known is shown in Table XV.

Table XV: SURVEY OF OPTICAL TRACKING SYSTEMS

System	Military Agency	Tracking Discipline	Tracking Characteristics	Sensor	Gimbaled Sensor	Field of View	Remarks
Walleye							
Condor							
MEAT (Philco)							
Occs I (Philco)							
Southern Research Institute							
Occs II (G. E.)							
"Hogs" (LTV)							

Classified Data — See Classified Supplement, Figure 8

This represents information gathered through reports and visits to vendors. In general, the majority of equipment being developed is not beyond the breadboard stage. Little effort has been placed on the mechanics and servo system involved for gimbaled use in a missile.

b. TV Tracker Experiment. Almost no testing has been done that would produce usable performance or accuracy data. The material surveyed for the subject contract, and visits with vendors, yielded no quantitative information on the effects of target and background characteristics (i.e., target detail, contrast, range, etc.) on tracker errors. Because this information was required as a basic input to the optimal guidance filter synthesis, a program was initiated to obtain a

reasonable estimate of tracker errors due to target and background characteristics through the simulation of the information processing characteristics of a target centroid tracker.

Aerial transpositive photographs were obtained for 12 selected ground targets at five different altitudes. A reference mask was photographically incorporated around each target, or group of targets, to be scanned by the simulator. Targets selected varied from sharply defined high-contrast targets to poorly defined low-contrast targets approaching the marginal limits of manual target acquisition capability. These are shown in Figures 57 and 58.

The experimental equipment consisted of a flying spot scanner arrangement, shown in Figures 59 and 60. Each aerial photograph was scanned by a 250-line, 1-inch by 1-inch raster, representing a 25-milliradian square field of view that gives a scan resolution typical of the Walleye/Condor trackers. A wide-band FM tape recorder was used to record the scanner video outputs, the sweep generator output, and the mask reference pulses. The analog data was then digitally encoded for processing by a digital analysis program that analyzed the data using centroid-tracker logic.

The contour centroid of each target was precisely measured with a Vanguard motion analyzer having an accuracy of 0.026% of the 25-milliradian field-of-view dimension. The deviation of the computed centroid from the actual centroid was determined for each target, based on the difference between the centroid as computed using the digital analysis of video scan data, and the centroid as measured by the Vanguard motion analyzer.

Analysis of the resulting data determined the effect of altitude on the rms tracker error as shown in Figure 61. Each data point represents tracking errors for a minimum of 10 different targets. Two results should be noted. First, the range of rms error is below the 1.74 milliradians selected as a 1σ error for the study. Second, the error increases significantly as altitude is decreased. No significant correlation was obtained between target contrast and tracker accuracy.

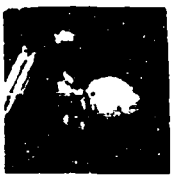

1. SILO LID COVER

2. CRANE

3. EQUIPMENT TRAILER

4. MAINTENANCE BUILDING

5. MINUTEMAN SILO

6. CUBICLE

7. AEROSTAND

8. AUTOMOBILE

9. GUARD SHACK

10. STORAGE SHED VENT

11. CONSTRUCTION BARRICADE

12. MISSILE TRANSPORTER/ERECTOR TIE-DOWN PLATE

Figure 57: TWELVE TEST TARGETS FROM 1000 FEET ALTITUDE

1000 FEET

2000 FEET

5000 FEET

7500 FEET

10,000 FEET

Figure 58: MINUTEMAN SILO TARGET AT FIVE DIFFERENT ALTITUDES

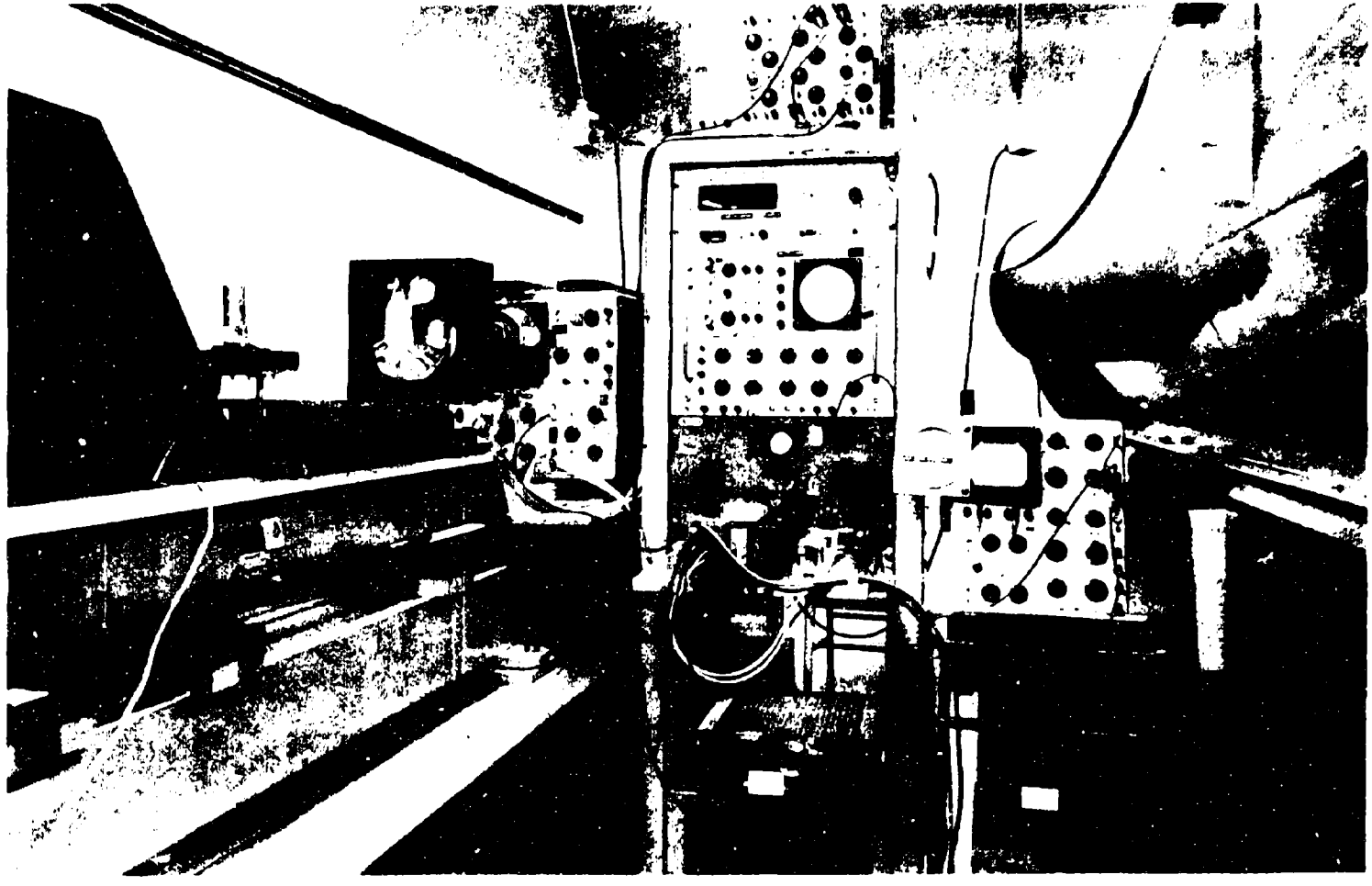

Figure 59: TV TRACKER SCANNER SIMULATION EQUIPMENT

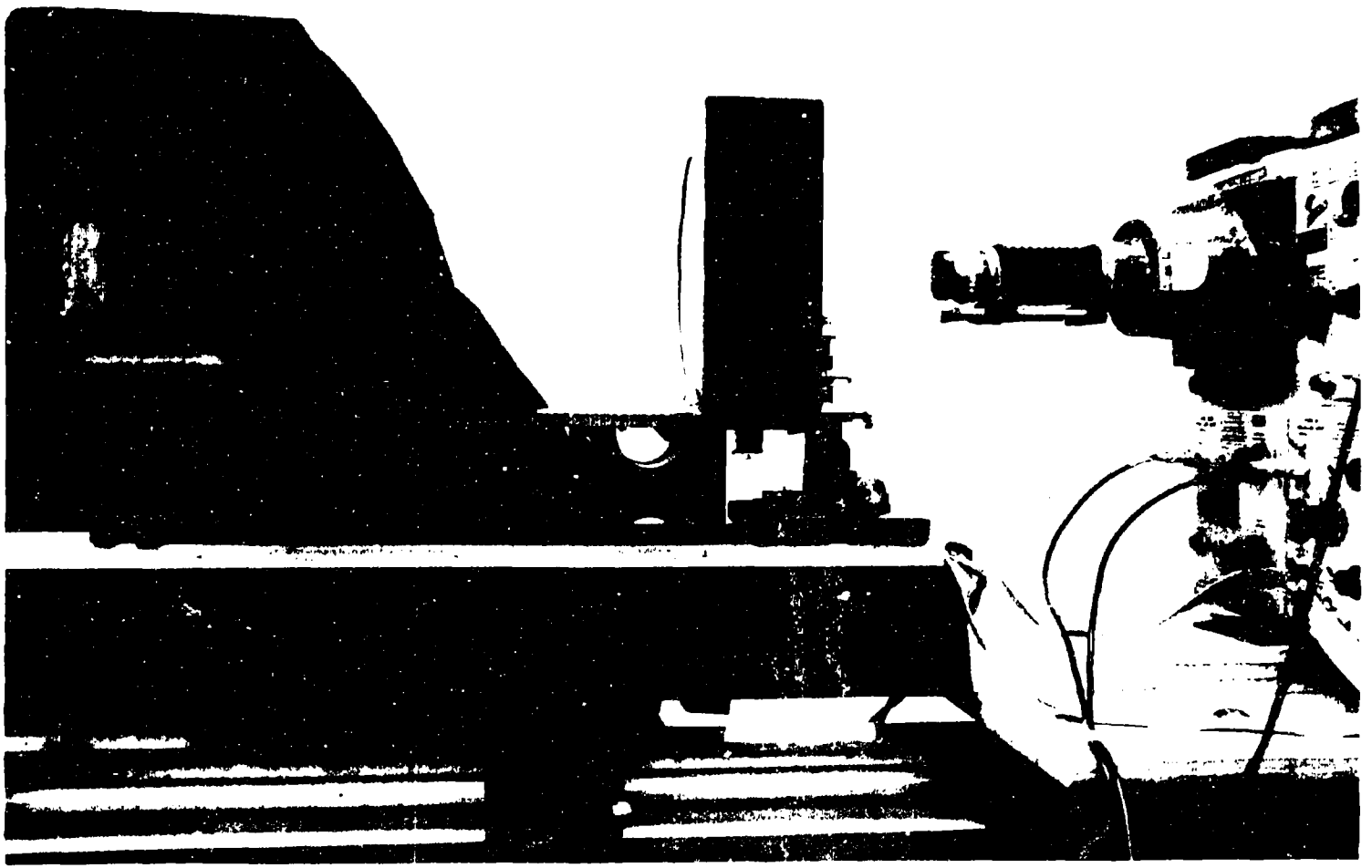

Figure 60: TV TRACKER SCANNER SIMULATION EQUIPMENT

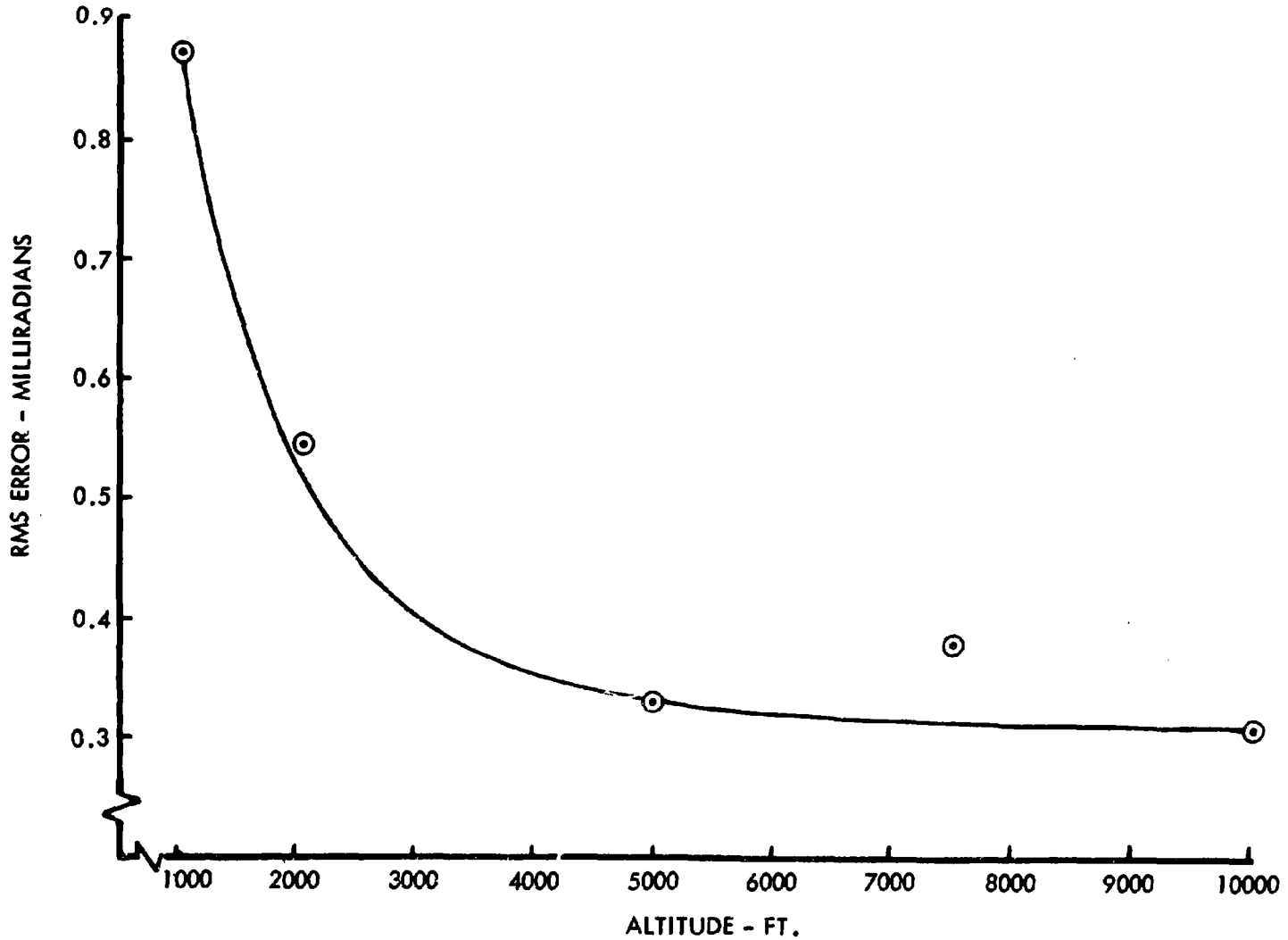

Figure 61: TV TRACKER ACCURACY

4. Radar Homing Sensors. Several possible means for using active radar trackers for terminal guidance of homing ASM's were examined, and it was concluded that the types of targets for which radar would make a useful tracking device were severely restricted as to proximity of adjacent targets and target size. The target acquisition problem also imposes operationally undesirable requirements on the flight of the carrier aircraft.

Airborne acquisition radars are limited as to the targets they can acquire and track by the size of the antenna, the carrier wavelength, range to the target, and clutter background. The mode of operation is such that the operator in an airplane watches a radar image of the ground until the intended target comes into view, lines up crosshairs so as to lock a tracking system to the target, and then allows radar information to be available to a missile that will use it to home in on the ground target. The slow reaction time of the human operator coupled with the great speed of the missile and the small space available on the missile for a tracking antenna, dictate that the only targets that can be tracked must have a radar cross section of greater than 1800 square feet. A metal sphere, 50 feet in diameter, has such a cross section. Such a large target has its compensations however, because the tracking radar needs only a 3-watt average radiated power output.

The tracking and acquisition problems are quite different, the latter being much more difficult to solve. Three acquisition systems were considered: missile-mounted search and track; airplane-mounted synthetic aperture search and missile-mounted track; and airplane-mounted illumination and search and missile-mounted track. The most promising is the one in which the missile tracks a patch on the ground illuminated by the airplane until the missile gets close enough to convert to active target seeker operation. For a target with a radar cross section larger than other objects within a 600-foot-diameter circle, an airplane-mounted forward-looking radar that makes use of antenna beamwidth for azimuth resolution and time delay for range resolution requires the aircraft to fly within 10 miles of the target. (This assumes a 5-foot-diameter scanning antenna that operates on

X-band.) When the target is located by the observer, he will switch the antenna to an automatic tracking mode that always illuminates the target. The missile is then launched, acquires the illuminated patch, and continues toward the target until its resolution capability as an active radar becomes better than as a passive radar. This occurs at about 12,000 feet slant range for an antenna diameter of 1 foot at X-band (10 GHz). This system has not previously been proposed or constructed. However, the techniques involved are straightforward and do not push the state of the art far with respect to individual components.

If it is necessary to launch the missile while the aircraft is 100 miles from the target, a 50-foot antenna is required on the aircraft. This may be implemented by making a fixed array out of the wing and using an electronic scanning method, such as a butler matrix discrete scan, to obtain azimuth resolution. This system does not limit the maneuvers of the aircraft.

In any of the acquisition modes, the tracking system would have a capability of homing in on jamming or homing in on a radar installation. However, the option would have to be selected before missile launch.

For target tracking, the resolution capabilities of the radar system are restricted by the electrical antenna length, range to the target, and operating frequency. The electrical length can be made no larger than the physical length unless special techniques such as synthetic aperture antennas are employed. These special techniques are, in general, side-looking and depend on the vehicle carrying the radar to fly in a straight line. A radar contained in a terminal guidance missile would have to use a conventional antenna due to its anomalous flight characteristics. The largest antenna likely to be installed in an ASM is 1 foot in diameter. The smallest possible operating wavelength is 0.1 foot or X-band. Therefore, due to diffraction limitations, the smallest target that can be identified at a range of 20,000 feet would have an average linear dimension of 1000 feet. This would not present a problem in tracking if the target was isolated and had a sky background, because the resolution continues to improve as the radar approaches the target. However, with a surface background, it is quite unlikely that a situation could be

found whereby only one target would be found in a 1000-foot circle, and that the integrated surface reflectivity would be less than that of the target. It is expected that the only missions that would use a radar for terminal guidance would be those where visibility is restricted, because an optical system would be capable of operating in the presence of electronic countermeasures and dense target configuration. The types of targets for which a radar tracker could be used must be isolated and of high contrast — such as bridges, trains, aircraft, ground vehicles, or metal buildings.

The radar cross section of the background is a function of the type of terrain, rf frequency, and the angle of incidence, which is the angle between local vertical and the line of sight to the target. Multilobe radars, such as monopulse or conical scan, become confused as to the exact position of a target that is distributed over several rf wavelengths. Large amounts of position error can be obtained at almost any angle of incidence. However, if the targets are small, or the target has a very rough jagged surface, large errors are more likely at small angles of incidence.

The noise and error sources are numerous. Ten of the most significant error sources are: receiver thermal noise spectrum; special emission from hot microwave sources; multipath noise; dynamic lag in the tracking servo loop; glint; scintillation; friction-backlash-stiction noise; propagation noise error; radome error; and change in position of antenna beam center as a function of transmitter frequency change.

In conclusion, target acquisition presents difficulties that make the use of active radar impractical for air-to-surface missile systems of the type being considered, except for isolated high cross-section targets. For specially selected targets where radar is practical, it is less susceptible to weather than a TV tracking system. The noise sources in a tracking radar are a function of the approach angle and nature of the target, so that specific missions must be considered when applying the Kalman optimal filtering technique to a system with a radar tracker.

APPENDIX II

GUIDANCE COMPARISON TECHNIQUES

The effectiveness of proportional, pursuit, and optimal guidance are compared in Tables III and IV by giving the standard (1σ) deviation of the position deviation normal to the nominal trajectory at the time the nominal trajectory hits the target. In these tables this quantity is called the 1σ miss distance. The use of this quantity as the index for comparison is motivated by the discussion in Section V.3.b. To compute this quantity for each of the guidance laws, the ASM equations of motion for each guidance law are linearized about the nominal trajectory. Then the differential equations for the covariance matrices of the deviations in position and velocity from nominal values are written in terms of the coefficients of these linearized equations. For each of the guidance laws, the matrix differential equation for the covariance matrix is solved to obtain the covariance matrix at the time the nominal trajectory hits the target. A simple formula relates this quantity and the 1σ miss distance.

To reduce the complexity of the guidance comparison computation for proportional and pursuit guidance, the ASM motion was restricted to the plane of the nominal trajectory. For the optimal guidance law, the computation has been carried out for the full 6-degree-of-freedom system.

1. Computation of Proportional Guidance Covariance Matrix. The equations of a proportionally guided ASM moving in a plane are given in Equations 84 through 91. Proportional guidance attempts to make the total normal force on the missile proportional to the target tracker rate. The coefficient of proportionality is a negative constant times the nominal velocity. The normal force on the vehicle consists of the aerodynamic normal force, C_N, plus the gravitational normal force. In instrumenting the proportional guidance, the aerodynamic normal force is directly measured by an accelerometer. The normal gravitational force is equal to the weight times the cosine of the angle the missile axis makes with a horizontal plane. This angle is known except for a random bias, b, from an inertial platform measurement. Hence, the normal force which is commanded,

F_N, is given by Equation 90. The target tracker is assumed to be a second-order linear tracker.

$$\dot{x} = -V \cos \gamma \tag{84}$$

$$\dot{z} = -V \sin \gamma \tag{85}$$

$$\dot{V} = -\frac{D(\alpha + \Delta\alpha_w,\ V + \Delta V_w,\ z)}{m} - g \sin \gamma \tag{86}$$

$$\dot{\gamma} = \frac{L(\alpha + \Delta\alpha_w,\ V + \Delta V_w,\ z)}{m V} - \frac{g}{V} \cos \gamma \tag{87}$$

$$\ddot{\eta} + C_1 \dot{\eta} = C_2 \left(\tan^{-1} \frac{z}{x} + N - \eta \right) \tag{88}$$

$$C_N(\alpha + \Delta\alpha_w,\ V + \Delta V_w,\ z) = D(\alpha + \Delta\alpha_w,\ V + \Delta V_w,\ z) \sin \alpha + L(\alpha + \Delta\alpha_w,\ V + \Delta V_w,\ z) \cos \alpha \tag{89}$$

$$F_N = C_N(\alpha + \Delta\alpha_w,\ V + \Delta V_w,\ z) - m g \cos (\alpha + \gamma + b) \tag{90}$$

$$F_N = -3 m \bar{V} \dot{\eta} \tag{91}$$

When the ASM nears the target, the target fills the TV sensor screen and the target tracker is unable to track the target. For proportional and pursuit guidance the acceleration normal to the missile was held equal to zero during this blind zone.

When Equations 84 through 91 are linearized about the nominal trajectory, the system

$$\begin{pmatrix} \delta\dot{x} \\ \delta\dot{z} \\ \delta\dot{V} \\ \delta\dot{\gamma} \\ \delta\dot{\eta} \\ \delta\dot{\dot{\eta}} \\ \delta\dot{b} \end{pmatrix} = A(t) \begin{pmatrix} \delta x \\ \delta z \\ \delta V \\ \delta\gamma \\ \delta\eta \\ \delta\dot{\eta} \\ \delta b \end{pmatrix} + B(t) \begin{pmatrix} W_x \\ W_z \\ N \end{pmatrix} \tag{92}$$

is obtained.

The matrices A(t) and B(t) are indicated in Figures 62 and 63. In Figure 62 the expression

$$\frac{\partial C_N}{\partial \alpha} + m\ g\ \sin\ (\alpha + \gamma) \tag{93}$$

is abbreviated by "Den."

In Equation 92 and Figure 63 the change in angle of attack, $\Delta\alpha_w$, and speed, ΔV_w, due to winds have been related to the components of wind velocity, W_x and W_z, in the horizontal and vertical directions by the formulas

$$\Delta\alpha_w = -\frac{W_\gamma}{V} \qquad \Delta V_w = W_V \tag{94}$$

$$\begin{pmatrix} W_V \\ W_\gamma \end{pmatrix} = \begin{pmatrix} \cos\ \gamma & \sin\ \gamma \\ -\sin\ \gamma & \cos\ \gamma \end{pmatrix} \begin{pmatrix} W_x \\ W_z \end{pmatrix} \tag{95}$$

Let P(t) denote the covariance matrix of the state variables of Equation 92. The winds, W_x and W_z, and the sensor noise, N, are considered as independent white noise processes. It follows from Reference 4, Page 250, that the covariance matrix P(t) satisfies the differential equation

$$\dot{P} = A(t)\ P + P\ A(t)^T + B(t)\ Q\ B(t)^T \tag{96}$$

in which Q is the covariance matrix of the noise vector, W_x, W_z, N.

2. Computation of Pursuit Guidance Covariance Matrix. For pursuit guidance the equation

$$F_N = -\ 3\ m\ \bar{V}\ \dot{\eta} \tag{97}$$

of the proportionally guided system is replaced by the equation

$$F_N = -\ C_3\ (\gamma + \eta + b). \tag{98}$$

Hence, the computation of miss distance for pursuit guidance is carried out in a similar manner to that of proportional guidance. Equation 92 holds for pursuit guidance, if the elements in the 4th, 5th, 6th, and 7th columns of the 3rd and 4th

$$
\begin{bmatrix}
0 & 0 & \cos\gamma & -V\sin\gamma & 0 & 0 & 0 \\
0 & 0 & \sin\gamma & V\cos\gamma & 0 & 0 & 0 \\
0 & -\frac{1}{m}\left(\frac{\partial D}{\partial z}-\frac{1}{Den}\frac{\partial D}{\partial \alpha}\frac{\partial C_N}{\partial z}\right) & -\frac{1}{m}\left(\frac{\partial D}{\partial V}-\frac{1}{Den}\frac{\partial D}{\partial \alpha}\frac{\partial C_N}{\partial V}\right) & -g\cos\alpha+\frac{g\sin(\alpha+\gamma)}{Den}\frac{\partial D}{\partial \alpha} & 0 & -\frac{3V\frac{\partial D}{\partial \alpha}}{Den} & \frac{g\sin(\alpha+\gamma)\frac{\partial D}{\partial \alpha}}{Den} \\
0 & \frac{1}{mV}\left(\frac{\partial L}{\partial z}-\frac{1}{Den}\frac{\partial L}{\partial \alpha}\frac{\partial C_N}{\partial z}\right) & \left[\frac{1}{mV}\left(\frac{\partial L}{\partial V}-\frac{1}{Den}\frac{\partial L}{\partial \alpha}\frac{\partial C_N}{\partial V}\right)-\frac{L}{mV^2}+\frac{g\cos\gamma}{V^2}\right] & \frac{g}{V}\sin\gamma-\frac{g\sin(\alpha+\gamma)}{V\,Den}\frac{\partial L}{\partial \alpha} & 0 & -3\frac{\partial L}{\partial \alpha} & -\frac{g}{V}\frac{\sin(\alpha+\gamma)}{Den}\frac{\partial D}{\partial \alpha} \\
0 & 0 & 0 & 0 & 1 & 0 & 0 \\
-\frac{C_{2z}}{x^2+z^2} & \frac{C_{2x}}{x^2+z^2} & 0 & 0 & -C_2 & -C_1 & 0 \\
0 & 0 & 0 & 0 & 0 & 0 & 0
\end{bmatrix}
$$

Figure 62: MATRIX A (t) OF INFLUENCE COEFFICIENTS OF THE STATE VARIABLES IN THE PROPORTIONALLY GUIDED STATE

$$
\begin{bmatrix}
0 & 0 & 0 \\
0 & 0 & 0 \\
-\frac{\cos\gamma}{m}\frac{\partial D}{\partial V} - \frac{\sin\gamma}{m}\frac{\partial D}{\partial \alpha}\left[D\cos\alpha - L\sin\alpha - mg\sin(\alpha+\gamma)\right] & -\frac{\sin\gamma}{m}\frac{\partial D}{\partial V} - \frac{\cos\gamma}{mV}\frac{\partial L}{\partial \alpha}\left[D\cos\alpha + L\sin\alpha + mg\sin(\alpha+\gamma)\right] & 0 \\
\frac{\cos\gamma}{mV}\frac{\partial L}{\partial V} + \frac{1}{mV}\frac{\partial L}{\partial \alpha}\left[D\cos\alpha - L\sin\alpha - mg\sin(\alpha+\gamma)\right] & \frac{\sin\gamma}{mV}\frac{\partial L}{\partial V} - \frac{\cos\gamma}{mV}\frac{\partial L}{\partial \alpha}\left[D\cos\alpha - L\sin\alpha - mg\sin(\alpha+\gamma)\right] & 0 \\
0 & 0 & 0 \\
0 & 0 & C_2 \\
0 & 0 & 0
\end{bmatrix}
$$

Figure 63: MATRIX B (t) OF INFLUENCE COEFFICIENTS OF WINDS AND SENSOR NOISE IN THE PROPORTIONALLY OR PURSUIT GUIDED ASM

rows of the matrix A(t) are replaced by the elements of the submatrix indicated in Figure 64.

3. Computation of the Optimal Guidance Covariance Matrix. Let S_1 denote the state vector of Equation 49, Section V, expressed in rectangular coordinates and S_2 the state vector expressed in flight path coordinates, that is:

$$S_1 = \begin{pmatrix} \delta x \\ \delta y \\ \delta z \\ \delta u \\ \delta v \\ \delta w \end{pmatrix} \qquad S_2 = \begin{pmatrix} \delta x \\ \delta y \\ \delta z \\ \delta V \\ \delta \chi \\ \delta \gamma \end{pmatrix} \tag{99}$$

Equation 49, Section V, implies S_1 and S_2 are related by the matrix

$$S_1 = \begin{pmatrix} I & 0 \\ 0 & F_{12}(t) \end{pmatrix} S_2 = \Xi S_2 \tag{100}$$

in which Ξ has a 3 x 3 identity matrix in the upper left corner and the matrix, $F_{12}(t)$, in the lower right corner is the 3 x 3 submatrix in the upper right-hand corner of F(t) of Figure 18.

$$F(t) = \begin{bmatrix} 0 & F_{12}(t) \\ F_{21}(t) & F_{22}(t) \end{bmatrix}$$

From the theory of Kalman filtering:

$$E\left\{(S_1 - \hat{S}_1)\,\hat{S}_1^T\right\} = 0. \tag{101}$$

and the upper left 6 x 6 submatrix of 8 x 8 matrix Σ of Equation 77 is equal to $E\left\{(S_1 - \hat{S}_1)\,(S_1 - \hat{S}_1)^T\right\}$. In the remainder of this section Σ denotes this 6 x 6 submatrix.

Define estimates of δV, $\delta\gamma$, $\delta\chi$ by:

$$\begin{pmatrix} \hat{\delta V} \\ \hat{\delta\gamma} \\ \hat{\delta\chi} \end{pmatrix} = F_{12}^{-1}(t) \begin{pmatrix} \hat{\delta u} \\ \hat{\delta v} \\ \hat{\delta w} \end{pmatrix} \tag{102}$$

$$
\begin{bmatrix}
-g\cos\gamma + \dfrac{mg\sin(\alpha+\gamma)+C_3}{mDen}\dfrac{\partial D}{\partial \alpha} & \dfrac{C_3}{mDen}\dfrac{\partial D}{\partial \alpha} & 0 & \dfrac{\left(mg\sin(\alpha+\gamma)+C_3\right)}{mDen}\dfrac{\partial D}{\partial \alpha} \\
\dfrac{g}{V}\sin\gamma - \dfrac{mg\sin(\alpha+\gamma)+C_3}{mV\,Den}\dfrac{\partial L}{\partial \alpha} & -\dfrac{C_3}{mV\,Den}\dfrac{\partial L}{\partial \alpha} & 0 & -\dfrac{\left(mg\sin(\alpha+\gamma)+C_3\right)}{mV}\dfrac{\partial L}{\partial \alpha}
\end{bmatrix}
$$

Figure 64: SUBMATRIX OF ELEMENTS WHICH REPLACE ELEMENTS IN A(t) FOR PURSUIT GUIDANCE

Now compute $E\{S_2\ S_2^T\}$

$$E\{S_2\ S_2^T\} = E\{\Xi^{-1}\ S_1\ S_1^T\ (\Xi^{-1})^T\} = \Xi^{-1}\ E\{S_1\ S_1^T\}\ (\Xi^{-1})^T$$

Let $S_1 = (S_1 - \hat{S}_1) + \hat{S}_1$, substitute into the above equation nd simplify using Equation 101

$$E\{S_2\ S_2^T\} = \Xi^{-1}\ E\{(S_1 - \hat{S}_1)(S_1 - \hat{S}_1)^T\}\ (\Xi^{-1})^T + \Xi^{-1}\ E\{\hat{S}_1\ \hat{S}_1^T\}\ (\Xi^{-1})^T$$

From the definition of Σ given below Equation 101

$$E\{S_2\ S_2^T\} = \Xi^{-1}\ \Sigma\ (\Xi^{-1})^T + E\{\hat{S}_2\ \hat{S}_2^T\} \tag{103}$$

Equation 79 of Section V may be rewritten as:

$$\dot{\hat{S}}_1 = \begin{pmatrix} 0 & 0 \\ 0 & I \end{pmatrix} \dot{S}_1 + \begin{pmatrix} 0 & I \\ 0 & 0 \end{pmatrix} \hat{S}_1 + K_6(t) \left[H(t) \begin{pmatrix} S_1 - \hat{S}_1 \\ - - - - \\ b - \hat{b} \end{pmatrix} + N \right] \tag{104}$$

where b is the bias vector $\begin{pmatrix} b_1 \\ b_2 \end{pmatrix}$, $\hat{b}$ is its estimate,

N is the noise vector $\begin{pmatrix} N_1 \\ N_2 \end{pmatrix}$,

and $K_6(t)$ is the upper 6 x 2 submatrix of 8 x 2 matrix $K(t)$ in Equation 76 of Section V.

Substitute for S_1 using Equation 100 noting that

$$\dot{\Xi} = \left(\begin{array}{c|c} 0 & 0 \\ - - & - - - - \\ 0 & \dot{F}_{12}(t) \end{array}\right)$$

$$\dot{\Xi}\,\hat{S}_2 + \Xi\,\dot{\hat{S}}_2 = \begin{pmatrix} 0 & 0 \\ 0 & I \end{pmatrix}\left[\dot{\Xi}\,S_2 + \Xi\,\dot{S}_2\right] + \begin{pmatrix} 0 & I \\ 0 & 0 \end{pmatrix}\Xi\,\hat{S}_2$$

$$+ K_6(t)\left[H(t)\begin{pmatrix} \Xi\,(S_2 - \hat{S}_2) \\ \hline b - \hat{b} \end{pmatrix} + N\right] \qquad (105)$$

Solve this for $\dot{\hat{S}}_2$

$$\dot{\hat{S}}_2 = \Xi^{-1}\,\dot{\Xi}\,(S_2 - \hat{S}_2) + \begin{pmatrix} 0 & 0 \\ 0 & I \end{pmatrix}\dot{S}_2 + \begin{pmatrix} 0 & F_{12}(t) \\ 0 & 0 \end{pmatrix}\hat{S}_2$$

$$+ \Xi^{-1}\,K_6(t)\left[H(t)\begin{pmatrix} \Xi\,(S_2 - \hat{S}_2) \\ \hline b - \hat{b} \end{pmatrix} + N\right]$$

Substitute from Equation 53 into Equation 49 remembering that the optimal control results when the optimal estimate, $\hat{S}_2$, is substituted for the state, S_2.

$$\dot{S}_2 = F(t)\,S_2 - G(t)\,M^{-1}\,G(t)^T\,U(t)\,\hat{S}_2 + D(t)\,W$$

Now use this to help solve for $\dot{\hat{S}}$

$$\dot{\hat{S}}_2 = \Xi^{-1}\,\dot{\Xi}\,(S_2 - \hat{S}_2) + \begin{pmatrix} 0 & 0 \\ 0 & I \end{pmatrix}\left[F(t)\,S_2 - G(t)\,M^{-1}\,G(t)^T\,U(t)\,\hat{S}_2 + D(t)\,W\right] + \begin{pmatrix} 0 & F_{12}(t) \\ 0 & 0 \end{pmatrix}\hat{S}_2 + \Xi^{-1}\,K_6(t)\left[H(t)\begin{pmatrix} \Xi\,(S_2 - \hat{S}_2) \\ \hline b - \hat{b} \end{pmatrix} + N\right]$$

To put this in terms of $\hat{S}_2$ and $(S_2 - \hat{S}_2)$, add and subtract $F(t)\,\hat{S}_2$ in the second term. Remember that $F(t) = \begin{pmatrix} 0 & F_{12}(t) \\ F_{21}(t) & F_{22}(t) \end{pmatrix}$ and partition G and D into 3 x 2 submatrices $G(t) = \begin{pmatrix} 0 \\ G_2(t) \end{pmatrix}$, $D(t) = \begin{pmatrix} 0 \\ D_2(t) \end{pmatrix}$

$$\dot{\hat{S}}_2 = \Xi^{-1}\,\dot{\Xi}\,(S_2 - \hat{S}_2) + \begin{pmatrix} 0 & 0 \\ F_{21}(t) & F_{22}(t) \end{pmatrix}(S_2 - \hat{S}_2) + \begin{pmatrix} 0 & 0 \\ F_{21}(t) & F_{22}(t) \end{pmatrix}\hat{S}_2 \qquad (106)$$

$$- G(t)\,M^{-1}\,G(t)^T\,U(t)\,\hat{S}_2 + D(t)\,W + \begin{pmatrix} 0 & F_{12}(t) \\ 0 & 0 \end{pmatrix}\hat{S}_2 + \Xi^{-1}\,K_6(t)\left[H(t)\begin{pmatrix} \Xi(S_2 - \hat{S}_2) \\ \hline b - \hat{b} \end{pmatrix} + N\right]$$

Now collect terms to give:

$$\dot{\hat{S}}_2 = \left[F(t) - G(t)\, M^{-1}(t)\, G(t)^T\, U(t)\right] \hat{S}_2 + D(t)\, W$$

$$+ \begin{pmatrix} 0 & 0 \\ F_{21}(t) & \left(F_{12}^{-1}(t)\, \dot{F}_{12}(t) + F_{22}(t)\right) \end{pmatrix} (S_2 - \hat{S}_2)$$

$$+ \Xi^{-1}(t)\, K_6(t) \left[H(t) \begin{pmatrix} \Xi(t)\, (S_2 - \hat{S}_2) \\ b - \hat{b} \end{pmatrix} + N \right]. \qquad (107)$$

Denote the covariance matrix of $\hat{S}_2$ by $P(t)$. The quantity $P(t)$ is given by $P(t) = E\left\{\hat{S}_2(t)\, \hat{S}_2{}^T(t)\right\}$ in which E denotes the expected value operation. Suppose the winds are given by a white noise process.

By computing

$$E\left[\hat{S}_2(t)\, \dot{\hat{S}}_2(t)^T + \dot{\hat{S}}_2(t)\, \hat{S}_2(t)^T\right] \qquad (108)$$

and using the relationship that

$$E\left[\left(S_2(t) - \hat{S}_2(t)\right) \hat{}_2(t)^T\right] = 0 \qquad \text{and} \qquad E\left[\left(b(t) - \hat{b}(t)\right) \hat{S}_2(t)^T\right] = 0, \qquad (109)$$

the equation

$$\dot{P}(t) = \left[F(t) - G(t)\, M^{-1}(t)\, G^T(t)\, U(t)\right] P(t)$$

$$+ P(t) \left(F(t) - G(t)\, M^{-1}(t)\, G(t)^T\, U(t)\right)^T$$

$$+ \Xi^{-1}(t)\, K_6(t)\, R\, K_6(t)^T\, \Xi^{-1}(t)^T + D(t)\, E\left[W\, W^T\right] D(t)^T \qquad (110)$$

may be obtained. This equation may be solved with the initial condition $P(t_0) = 0$ to obtain $E\left\{\hat{S}_2(t_1)\, \hat{S}_2(t_1)^T\right\}$.

When this has been done, the covariance matrix $E\left\{S_2(t)\, S_2(t)^T\right\}$ is expressed in terms of previously computed quantities by Equation 103.

4. Miss Distance. The formula for the mean square deviation normal to the trajectory is given by

$$E\left[\left(\delta y(t_1) \sin \bar{\gamma}(t_1) - \delta z(t_1) \cos \bar{\gamma}(t_1)\right)^2\right]. \qquad (111)$$

This formula may be written in terms of the variances and covariances of the position variables as

$$\sin^2 \bar{\gamma}(t_1)\ E\left[\delta x(t_1)^2\right] - 2 \sin \bar{\gamma}(t_1) \cos \bar{\gamma}(t_1)\ E\left[\delta x(t_1)\ \delta z(t_1)\right] + \cos^2 \bar{\gamma}(t_1)\ E\left[\delta z(t_1)^2\right]. \quad (112)$$

Hence, the miss distance for proportional, pursuit, and optimal guidance may be computed from Equation 112 by substituting corresponding elements of the covariance matrices computed in Sections 1, 2, and 3 of this appendix for the corresponding covariances in Equation 112.

Let N(t) denote the column vector whose components are zero except for the first and third components that are $\sin \bar{\gamma}(t)$ and $-\cos \bar{\gamma}(t)$, respectively. Equation 112 may be written in matrix notation by

$$N(t_1)^T\ E\left\{ S_2(t_1)\ S_2(t_1)^T \right\} N(t_1). \quad (113)$$

Equation 103 implies, that for optimal guidance,

$$N(t)^T\ E\left\{ S_2(t)\ S_2(t)^T \right\} N(t) = N(t)^T\ \Xi(t)^{-1} \Sigma(t)\ \Xi(t)^{-1^T}\ N(t) + N(t)^T\ P(t)\ N(t). \quad (114)$$

Because N(t) is zero except for the first and third elements, and the upper right-hand 3 x 3 submatrix of $\Xi(t_1)$ is the identity matrix, the right side of this equation simplifies to:

$$N(t)^T\ \Sigma(t)\ N(t) + N(t)^T\ P(t)\ N(t) \quad (115)$$

The matrix Σ is the covariance matrix of the difference between the ASM state variables and their estimates. This matrix is the solution[1] of Equation 77 that was solved numerically to determine the weighting coefficients of the optimal filter that are given by Equation 76. Notice that Equation 77 does not depend on the coefficient matrix $M^{-1}\ G^T U$ of the optimal feedback controller. The covariance matrix Σ is an indicator of how well the optimal filter is estimating the ASM state variables. Thus the first term of Equation 115 can be considered as the contribution of the error in estimating the ASM state variables to miss distance. This term of Equation 115 will be called filter error.

(1) Modified as described on page 170.

Equation 110 for the matrix P(t) of the second term of Equation 115 does involve the coefficients of the matrix $M^{-1} G^T U$ of the optimal feedback controller. Note that if the optimal feedback controller $M^{-1} G^T U \hat{S}_2$ was replaced by a linear controller of the form, $\Lambda \hat{S}_2$, the discussion of Section 3 of this appendix would be unchanged except that the matrix Λ would replace $M^{-1} G^T U$ in the formulas. Thus the second term in Equation 115 may be considered as the contribution of the feedback controller to the impact error. This term will be called controller error.

These two types of error have been plotted as functions of time in Figure 27 as discussed previously to show relative size of these errors at various times from target acquisition to the time the nominal trajectory hits the target.

5. Computation Techniques. To compute the coefficients of the optimal filter and optimal feedback control law and to compare miss distances for optimal, proportional, and pursuit guidance, the matrix differential Equations 54, 77, 96, and 110 were solved numerically. Nominal trajectories and the influence coefficient matrices, F(t) and G(t), defined in Equation 39 were computed using existing Boeing computer programs. The matrices, F(t) and G(t), which are used as coefficients in Equations 54, 96, and 110, were fed as punched input to the programs for solving these equations. In solving Equation 110, the solution matrices, U(t) and $\Sigma(t)$, of Equations 54 and 77 were also punched inputs to the computer program.

Equations 54, 77, 96, and 110 were solved on a Univac 1107 computer. Fortran IV was used as a computing language in coding the program. Each of the programs was coded using less than two hundred instructions. A Romberg integration technique was used in integrating the equations. This integration technique uses a global integrator and has an adaptive method for varying integration step size based on accuracy estimates of the components of the matrix being computed. These accuracy estimates were printed out to check integration accuracy and to aid in monitoring the program. Several of the computations were also carried out using a Runge-Kutta variable step integration technique. The results of the

computations with the two different methods were compared as a check on the integration techniques.

Equations 54, 77, 96, and 110 are matrix differential equations of dimensions 6 x 6, 8 x 8, 7 x 7, and 6 x 6 respectively. Thus in each of the computations either 36, 49, or 64 quantities are being computed as functions of time. Integration times for these equations on the 1107 computer varied between 3 and 12 minutes.

APPENDIX III

OBSERVABILITY PROBLEMS IN THE OPTIMAL-GUIDANCE FILTER

Because Figures 28 and 29 show that the component of position deviation normal to the nominal trajectory is estimated very accurately while the vertical and horizontal components of position derivation are estimated much less accurately, it is necessary to analyze the observation process to understand the reasons for this phenomena and to make sure it does not cause poor system performance.

Insight about the measurement process may be gained by examining the effect of linearizing the line-of-sight angle measurement equations. If the random biases, b_1 and b_2, and the noise, N_1 and N_2, were set equal to their mean values of zero, the measurement, Equations 18 and 19, become

$$\psi = \tan^{-1} \frac{y}{x} \tag{116}$$

$$\Phi = \tan^{-1}\left(\frac{z}{\sqrt{x^2 + y^2}}\right) \tag{117}$$

Linearizing these equations it is seen that

$$\delta\psi = A_1(t)\ \delta x + A_2(t)\ \delta y \tag{118}$$

$$\delta\Phi = B_1(t)\ \delta x + B_2(t)\ \delta y + B_3(t)\ \delta z \tag{119}$$

in which $A_1(t)$, etc., are the partial derivatives of the respective expressions on the right side of the above equations evaluated on the nominal trajectory.

Now

$$A_1(t) = -\frac{\bar{y}}{(\bar{x}^2 + \bar{y}^2)}, \qquad A_2(t) = \frac{\bar{x}}{\bar{x}^2 + \bar{y}^2}$$

$$B_1(t) = \frac{-\bar{z}\ \bar{x}}{(\bar{x}^2 + \bar{y}^2)^{1/2}\ (\bar{x}^2 + \bar{y}^2 + \bar{z}^2)}, \qquad B_2(t) = \frac{-\bar{z}\ \bar{y}}{(\bar{x}^2 + \bar{y}^2)^{1/2}\ (\bar{x}^2 + \bar{y}^2 + \bar{z}^2)} \tag{120}$$

$$B_3(t) = \frac{\sqrt{\bar{x}^2 + \bar{y}^2}}{\bar{x}^2 + \bar{y}^2 + \bar{z}^2}$$

Now defining

$$\cos\bar{\psi} = \frac{\bar{x}}{\sqrt{\bar{x}^2 + \bar{y}^2}} \qquad \sin\bar{\psi} = \frac{\bar{y}}{\sqrt{\bar{x}^2 + \bar{y}^2}}$$

$$\cos\bar{\Phi} = \frac{\sqrt{\bar{x}^2 + \bar{y}^2}}{\sqrt{\bar{x}^2 + \bar{y}^2 + \bar{z}^2}} \qquad \sin\bar{\Phi} = \frac{\bar{z}}{\sqrt{\bar{x}^2 + \bar{y}^2 + \bar{z}^2}} \tag{121}$$

$$\bar{r} = \sqrt{\bar{x}^2 + \bar{y}^2 + \bar{z}^2}$$

these formulas become

$$A_1(t) = -\frac{\sin\bar{\psi}}{\bar{r}\cos\bar{\Phi}} \qquad A_2(t) = \frac{\cos\bar{\psi}}{\bar{r}\cos\bar{\Phi}}$$

$$B_1(t) = -\frac{1}{\bar{r}}\cos\bar{\psi}\sin\bar{\Phi}, \quad B_2(t) = -\frac{1}{\bar{r}}\sin\bar{\psi}\sin\bar{\Phi} \tag{122}$$

$$B_3(t) = \frac{1}{\bar{r}}\cos\bar{\Phi}.$$

The vectors

$$(-\sin\bar{\psi},\ \cos\bar{\psi},\ 0)$$

$$(-\cos\bar{\psi}\sin\bar{\Phi},\ -\sin\bar{\psi}\sin\bar{\Phi},\ \cos\bar{\Phi}) \tag{123}$$

are mutually perpendicular and are perpendicular to the vector

$$(\cos\bar{\psi}\cos\bar{\Phi},\ \sin\bar{\psi}\cos\bar{\Phi},\ \sin\bar{\Phi}) \tag{124}$$

that points along the line of sight of the nominal trajectory. The linearized measurement equations imply that the variations of missile positions in these two perpendicular directions times the respective weightings $1/(\bar{r}\cos\bar{\Phi})$ and $1/\bar{r}$ are being measured. The component of position along the nominal trajectory is not being measured. Hence, the only way in which the filter can correct errors in the estimate of position along the nominal trajectory is through the information given by these two perpendicular measurements on position along the trajectory. If there is bending of the nominal trajectory, the three directions expressed by the above vectors will change along the nominal trajectory. From this it should be expected that the perpendicular measurements will furnish a small amount of

information on position along the nominal. It should be expected that the correction by the filter of the estimate of this component of position will be slow. Fortunately, the components of position deviation perpendicular to the nominal trajectory are the important ones in defining miss distance.

In the discussion given below, it will be shown that if the nominal trajectory is a straight line, the system is not completely observable according to the criteria defined by Kalman (Reference 4, Page 36). For simplicity of exposition, suppose the nominal trajectory is a straight line to the target making a 45-degree angle with the ground, given by the equations:

$$\begin{aligned} \bar{x}(t) &= t - t_i \\ \bar{y}(t) &= 0 \\ \bar{z}(t) &= t_1 - t \end{aligned} \tag{125}$$

Evaluating the Equations 120 for $A_1(t)$, etc., in this case gives

$$\begin{aligned} A_1(t) &= 0 & B_1(t) &= \frac{-1}{2\,(t_1 - t)} \\ A_2(t) &= \frac{-1}{(t_1 - t)} & B_2(t) &= 0 \\ & & B_3(t) &= \frac{-1}{2\,(t_1 - t)} \end{aligned} \tag{126}$$

The optimal filter, Equation 79, is based on the consideration of Equations 74 as state equations and a modification of Equations 59 as the measurement equations. The system (Equation 74) with measurements (Equation 59) would be completely observable in the terminology of Reference 4, Page 36, if the matrix

$$M(0, s) = \int_0^s \Phi^T(t, t_1)\, H^T(t)\, R^{-1}(t)\, H(t)\, \Phi(t, t_1)\, dt \tag{127}$$

is nonsingular for some value of s between 0 and t_1. The quantity $\Phi(t, \tau)$ is the impulse response of the system (Equation 74). Equation 74 may be integrated to show that:

$$\Phi(t,\tau) = \begin{pmatrix} 1 & 0 & 0 & t-\tau & 0 & 0 & 0 & 0 \\ 0 & 1 & 0 & 0 & t-\tau & 0 & 0 & 0 \\ 0 & 0 & 1 & 0 & 0 & t-\tau & 0 & 0 \\ 0 & 0 & 0 & 1 & 0 & 0 & 0 & 0 \\ 0 & 0 & 0 & 0 & 1 & 0 & 0 & 0 \\ 0 & 0 & 0 & 0 & 0 & 1 & 0 & 0 \\ 0 & 0 & 0 & 0 & 0 & 0 & 1 & 0 \\ 0 & 0 & 0 & 0 & 0 & 0 & 0 & 1 \end{pmatrix} \tag{128}$$

Consider the case when the covariance matrix, $R(t)$, is a scalar times the identity matrix. Then R^{-1} is a scalar times the identity matrix and it may be factored out of the expression for $M(0,s)$.

Now,

$$\Phi^T(t, t_1)\, H^T(t) = \begin{pmatrix} 1 & 0 & 0 & 0 & 0 & 0 & 0 & 0 \\ 0 & 1 & 0 & 0 & 0 & 0 & 0 & 0 \\ 0 & 0 & 1 & 0 & 0 & 0 & 0 & 0 \\ t-t_1 & 0 & 0 & 1 & 0 & 0 & 0 & 0 \\ 0 & t-t_1 & 0 & 0 & 1 & 0 & 0 & 0 \\ 0 & 0 & t-t_1 & 0 & 0 & 1 & 0 & 0 \\ 0 & 0 & 0 & 0 & 0 & 0 & 1 & 0 \\ 0 & 0 & 0 & 0 & 0 & 0 & 0 & 1 \end{pmatrix} \begin{pmatrix} 0 & \frac{1}{2}(t-t_1)^{-1} \\ (t-t_1)^{-1} & 0 \\ 0 & \frac{1}{2}(t-t_1)^{-1} \\ 0 & 0 \\ 0 & 0 \\ 0 & 0 \\ 1 & 0 \\ 0 & 1 \end{pmatrix} \tag{129}$$

or

$$\Phi^T(t, t_1)\ H^T(t) = \begin{pmatrix} 0 & \frac{1}{2}(t-t_1)^{-1} \\ (t-t_1)^{-1} & 0 \\ 0 & \frac{1}{2}(t-t_1)^{-1} \\ 0 & \frac{1}{2} \\ 1 & 0 \\ 0 & \frac{1}{2} \\ 1 & 0 \\ 0 & 1 \end{pmatrix} \tag{130}$$

For brevity, denote $\frac{1}{2}(t-t_1)$ by τ. Now

$$\Phi^T(t, t_1)\ H^T(t)\ H(t)\ \Phi(t, t_1) = \begin{pmatrix} \tau^2 & 0 & \tau^2 & \frac{1}{2}\tau & 0 & \frac{1}{2}\tau & 0 & \tau \\ 0 & 4\tau^2 & 0 & 0 & 2\tau & 0 & 2\tau & 0 \\ \tau^2 & 0 & \tau^2 & \frac{1}{2}\tau & 0 & \frac{1}{2}\tau & 0 & \tau \\ \frac{1}{2}\tau & 0 & \frac{1}{2}\tau & \frac{1}{4} & 0 & \frac{1}{4} & 0 & \frac{1}{2} \\ 0 & 2\tau & 0 & 0 & 1 & 0 & 1 & 0 \\ \frac{1}{2}\tau & 0 & \frac{1}{2}\tau & \frac{1}{4} & 0 & \frac{1}{4} & 0 & \frac{1}{2} \\ 0 & 2\tau & 0 & 0 & 1 & 0 & 1 & 0 \\ \tau & 0 & \tau & \frac{1}{2} & 0 & \frac{1}{2} & 0 & 1 \end{pmatrix} \tag{131}$$

From Equation 131 it is easily seen that M(0, s) is singular. Hence, the system is not completely observable.

Unclassified
Security Classification

DOCUMENT CONTROL DATA - R&D

(Security classification of title, body of abstract and indexing annotation must be entered when the overall report is classified)

1. ORIGINATING ACTIVITY (Corporate author) The Boeing Company, Aero-Space Group P. O. Box 3707 Seattle, Wash. 98124	2a. REPORT SECURITY CLASSIFICATION Unclassified 2b. GROUP N/A

3. REPORT TITLE

OPTIMUM CONTROL OF AIR-TO-SURFACE MISSILES

4. DESCRIPTIVE NOTES (Type of report and inclusive dates)

Final Report March 1965 - March 1966

5. AUTHOR(S) (Last name, first name, initial)

Leistikow, L. Hall, J. M.
McCorkel, R. D. Clingman, W. D.
Rishel, R. W.

6. REPORT DATE	7a. TOTAL NO. OF PAGES	7b. NO. OF REFS
March 1967	183	14

8a. CONTRACT OR GRANT NO.	9a. ORIGINATOR'S REPORT NUMBER(S)
AF33(615)-2409 b. PROJECT NO. 8219 c. Task No. 821904 d.	9b. OTHER REPORT NO(S) (Any other numbers that may be assigned this report) AFFDL-TR-66-64

10. AVAILABILITY/LIMITATION NOTICES This document is subject to special export controls and each transmittal to foreign governments or foreign nationals may be made only with prior approval of the Air Force Flight Dynamics Laboratory (FDCC), Wright-Patterson Air Force Base, Ohio 45433

11. SUPPLEMENTARY NOTES	12. SPONSORING MILITARY ACTIVITY
None	AFFDL (FDCC) RTD, AFSC Wright-Patterson AFB, Ohio 45433

13. ABSTRACT

Design guidelines were developed to provide a basis for conducting design trades for a homing type air-to-surface missile with high terminal accuracy. Three basic homing guidance concepts, proportional, pursuit, and optimal guidance were evaluated on the basis of impact error. Two nominal trajectories were investigated. An optimal guidance law was developed for an ASM with realistic aerodynamic and sensor characteristics. This guidance law was based upon the use of a Kalman filter to obtain best estimates of the ASM state variable errors, and a control concept which minimizes the sum of the mean square impact error and the integral of a quadratic form of the autopilot control variables. A linearized differential equation program which computed the mean square impact error in the form of a covariance matrix deviation perpendicular to the nominal trajectory, was used for comparison of the guidance laws. A normal acceleration autopilot was designed to meet the mission requirements, and advanced bistable controller techniques were applied to obtain a quasi-adaptive autopilot which required no gain changes throughout the ASM midcourse and terminal phases. A limited state-of-the-art survey was conducted of homing and inertial sensors, and on-board digital computers suitable for a homing ASM.

DD FORM 1 JAN 64 1473

Unclassified
Security Classification

Unclassified

Security Classification

14. KEY WORDS	LINK A		LINK B		LINK C	
	ROLE	WT	ROLE	WT	ROLE	WT
Optimum control						
Guidance and control						
Air-to-surface missiles						

INSTRUCTIONS

1. ORIGINATING ACTIVITY: Enter the name and address of the contractor, subcontractor, grantee, Department of Defense activity or other organization *(corporate author)* issuing the report.

2a. REPORT SECURITY CLASSIFICATION: Enter the overall security classification of the report. Indicate whether "Restricted Data" is included. Marking is to be in accordance with appropriate security regulations.

2b. GROUP: Automatic downgrading is specified in DoD Directive 5200.10 and Armed Forces Industrial Manual. Enter the group number. Also, when applicable, show that optional markings have been used for Group 3 and Group 4 as authorized.

3. REPORT TITLE: Enter the complete report title in all capital letters. Titles in all cases should be unclassified. If a meaningful title cannot be selected without classification, show title classification in all capitals in parenthesis immediately following the title.

4. DESCRIPTIVE NOTES: If appropriate, enter the type of report, e.g., interim, progress, summary, annual, or final. Give the inclusive dates when a specific reporting period is covered.

5. AUTHOR(S): Enter the name(s) of author(s) as shown on or in the report. Enter last name, first name, middle initial. If military, show rank and branch of service. The name of the principal author is an absolute minimum requirement.

6. REPORT DATE: Enter the date of the report as day, month, year; or month, year. If more than one date appears on the report, use date of publication.

7a. TOTAL NUMBER OF PAGES: The total page count should follow normal pagination procedures, i.e., enter the number of pages containing information.

7b. NUMBER OF REFERENCES: Enter the total number of references cited in the report.

8a. CONTRACT OR GRANT NUMBER: If appropriate, enter the applicable number of the contract or grant under which the report was written.

8b, 8c, & 8d. PROJECT NUMBER: Enter the appropriate military department identification, such as project number, subproject number, system numbers, task number, etc.

9a. ORIGINATOR'S REPORT NUMBER(S): Enter the official report number by which the document will be identified and controlled by the originating activity. This number must be unique to this report.

9b. OTHER REPORT NUMBER(S): If the report has been assigned any other report numbers *(either by the originator or by the sponsor)*, also enter this number(s).

10. AVAILABILITY/LIMITATION NOTICES: Enter any limitations on further dissemination of the report, other than those imposed by security classification, using standard statements such as:

(1) "Qualified requesters may obtain copies of this report from DDC."

(2) "Foreign announcement and dissemination of this report by DDC is not authorized."

(3) "U. S. Government agencies may obtain copies of this report directly from DDC. Other qualified DDC users shall request through _____."

(4) "U. S. military agencies may obtain copies of this report directly from DDC. Other qualified users shall request through _____."

(5) "All distribution of this report is controlled. Qualified DDC users shall request through _____."

If the report has been furnished to the Office of Technical Services, Department of Commerce, for sale to the public, indicate this fact and enter the price, if known.

11. SUPPLEMENTARY NOTES: Use for additional explanatory notes.

12. SPONSORING MILITARY ACTIVITY: Enter the name of the departmental project office or laboratory sponsoring *(paying for)* the research and development. Include address.

13. ABSTRACT: Enter an abstract giving a brief and factual summary of the document indicative of the report, even though it may also appear elsewhere in the body of the technical report. If additional space is required, a continuation sheet shall be attached.

It is highly desirable that the abstract of classified reports be unclassified. Each paragraph of the abstract shall end with an indication of the military security classification of the information in the paragraph, represented as *(TS), (S), (C), or (U)*.

There is no limitation on the length of the abstract. However, the suggested length is from 150 to 225 words.

14. KEY WORDS: Key words are technically meaningful terms or short phrases that characterize a report and may be used as index entries for cataloging the report. Key words must be selected so that no security classification is required. Identifiers, such as equipment model designation, trade name, military project code name, geographic location, may be used as key words but will be followed by an indication of technical context. The assignment of links, rules, and weights is optional.

Unclassified

Security Classification